ELUCIDATING THE CHEMICAL AND THERMAL UNFOLDING PROFILES OF ORGANOPHOSPHORUS HYDROLASE AND INCREASING ITS OPERATIONAL STABILITY

A Dissertation

by

CHARLES DAVID ARMSTRONG

Submitted to the Office of Graduate Studies of
Texas A&M University
in partial fulfillment of the requirements for the degree of

DOCTOR OF PHILOSOPHY

May 2007

Major Subject: Biochemistry

ELUCIDATING THE CHEMICAL AND THERMAL UNFOLDING PROFILES OF ORGANOPHOSPHORUS HYDROLASE AND INCREASING ITS OPERATIONAL STABILITY

A Dissertation

by

CHARLES DAVID ARMSTRONG

Submitted to the Office of Graduate Studies of
Texas A&M University
in partial fulfillment of the requirements for the degree of

DOCTOR OF PHILOSOPHY

Approved by:

Chair of Committee,	James R. Wild
Committee Members,	K. C. Donnelly
	Frank M. Raushel
	J. Martin Scholtz
Head of Department,	Gregory D. Reinhart

May 2007

Major Subject: Biochemistry

ABSTRACT

Elucidating the Chemical and Thermal Unfolding Profiles of Organophosphorus Hydrolase and Increasing Its Operational Stability. (May 2007)

Charles David Armstrong, B.S., Texas A&M University;

M.S., University of Houston Clear Lake

Chair of Advisory Committee: Dr. James R. Wild

Organophosphorus hydrolase (OPH, EC 3.1.8.1) is a homodimeric enzyme that has been observed to unfold via a three-state unfolding pathway ($N_2^* \leftrightarrow I_2 \leftrightarrow 2U$) under chemical denaturing conditions. The dimeric intermediate (I_2) is catalytically inactive and, although this enzyme has a very large overall conformational stability (~40 kcal/mol), it takes only a small amount of energy (~4 kcal/mol) to unfold this enzyme into its inactive form. So that this enzyme might be engineered as a more effective tool for nerve agent countermeasures and bioremediation purposes, its operational stability (the energy required to unfold the enzyme from its active, dimeric state to its inactive, dimeric state) must be increased. For this purpose, it is necessary to understand how the enzyme unfolds into its inactive, intermediate state.

As tryptophan residues are sensitive probes of the microenvironment surrounding the residue, enzyme variants consisting of one tryptophan per subunit were constructed. Unfortunately, these variant enzymes did not fold into active conformations, and so could not be used to develop an accurate unfolding profile for the wild type enzyme.

Limited proteolysis of OPH by thermolysin revealed detailed information on the unfolding process of OPH in chemical and thermal denaturing conditions. Mild denaturing conditions induced an initial enhancement of activity with a subsequent loss of catalytic activity upon more aggressive treatment. Under thermal conditions from 35 – 55 ˚C, the enzyme developed a well populated and active intermediate that displayed maximal activity. Similarly, the enzyme displayed maximal activity when incubated at 1.0 M urea. The regions of the enzyme, which became accessible to proteolysis at 45 ˚C and 1 M urea, were identical. This suggested that increased flexibility of these regions was coupled with the increase in the enzyme's catalytic activity.

Two regions that were determined by limited proteolysis to be the first to unfold were bridged with a novel disulfide bond. The result was an enzyme with an increased operational stability and resistance to proteolysis. This enzyme retained approximately 70% of its original activity in 8 M urea while no activity remained for the wild type enzyme when incubated in 6.5 M urea.

DEDICATION

To my family

ACKNOWLEDGEMENTS

I would like to thank Dr. Wild, a mentor and friend, for his guidance, help and encouragement throughout the course of my graduate career here at Texas A&M. I would also like to thank Dr. Melinda Wales and Dr. Janet Grimsley for their suggestions, the long talks about science, and their friendship.

I would like to thank my committee members for their suggestions and continued patience throughout the course of this study.

I've made many friends and learned a great deal about science from the people with whom I've worked. Thanks go to Shane Gold, Mauricio Rodriguez, Scott Pinkerton, Rory Kern, Tony Reeves, Boris Novikov, and Leamon Viveros.

Most of all, I would like to thank my family. I could not have completed this dissertation without their love, support and encouragement. My love and thanks go to my wife, son, my soon-to-be-born baby girl, mom, dad, grandpa, Wendell and Zelma.

TABLE OF CONTENTS

LIST OF FIGURES

FIGURE Page

FIGURE Page

LIST OF TABLES

CHAPTER I

INTRODUCTION

BACKGROUND

Characteristics of Organophosphorus Hydrolase. Organophosphorus hydrolase (OPH, E.C. 3.1.8.1) is an $(\alpha\beta)_8$ homodimer of the TIM Barrel fold family of hydrolases and a member of the amidohydrolase superfamily of enzymes (*1*). Its architecture is that of a distorted α/β barrel with eight parallel β-sheets and fourteen α-helices. Like all TIM barrel enzymes, OPH's active sites are located at the C-terminal portion of each monomer. Additionally, there are two antiparallel β-strands at the N-terminal end of each monomer (*2-4*).

OPH is a metalloenzyme requiring divalent cations for activity, with maximum activity resulting from the presence of two divalent cations per active-site (four per molecule). The enzyme is capable of binding several different metals (including Zn^{2+}, Co^{2+}, Ni^{2+}, Cd^{2+}, Mn^{2+}, Cu^{2+} and Fe^{2+}), with the catalytic activity dependent upon the identity of the metal in the active site. The cobalt substituted variant is the most catalytically active (*5, 6*). The activity of the Co^{2+} form of the enzyme is consistently five to twenty fold higher than that of the Zn^{2+} form (*7*).

Organophosphates (OPs) comprise a diverse chemical family that includes many neurotoxic agents which are used as pesticides and chemical warfare agents. They all share a common structural attribute: a central phosphorus atom with three groups bound

---

This dissertation follows the style of *Biochemistry*.

by single bonds and an oxygen or a sulfur atom bound to the phosphorus center by a double bond. Many OPs are phosphotriesters in which the phosphorus center is bound to four oxygen atoms. In other types of OPs, one of the esters bound to the phosphoryl center is replaced with a sulfur (phosphorothiolate), fluorine (phosphorofluoridate), or carbon (phosphoroamidocyanate) group. Their toxicity is determined by the reactivity of the phosphoryl center which binds to and inactivates the acetylcholinesterases (AChE) of target organisms (*7*). OPH is capable of hydrolyzing many of these OPs including the P-F bond of Sarin and Soman and is the only OP-degrading enzyme capable of detoxifying the nerve agent VX (P-S bond) (*8*). A comparison of the catalytic abilities of several OP hydrolyzing enzymes is shown in Table 1.1.

Table 1.1: Comparison of the catalytic abilities of organophosphate degrading enzymes.

Enzyme[a]	**P - O**	**P - F**	**P - S**	**P - CN**
OPH[b]	+	+	+	+
OPAA[c]	+	+	-	+
Human Paraoxonase	+	+	-	+
Squid DFPase	-	+	-	-

a Data for the table was found in (*7*).
[b] Organophosphorus Hydrolase.
[c] Organophosphorus Acid Anhydrolase.

OPH has a broad substrate specificity and it has been shown that mutagenesis of active-site residues can enhance the substrate specificity of OPH towards some substrates while decreasing the substrate specificity against others. Additionally, the stereo-selectivity of the enzyme can be enhanced or reversed through active-site mutagenesis (*7-12*). For example, both His 254 and His 257 appear to have some influence on the structure and function of the enzyme's active-site pocket. His 257 forms part of the hydrophobic substrate pocket while His 254 forms stacking interactions with active site residues His 257 and His 230. It has been suggested that these residues are involved in a stabilization of the van der Waals stacking interactions. Additionally, His 254 forms hydrogen bonds with the side chains of Asp 232, Asp 233 and the metal ligand Asp 301. Mutagenesis of these residues (H254R / H257L) has retained much of the wild-type activity for the hydrolysis of paraoxon and gained a 17-fold increase in enzymatic activity against demeton-S, an analog for the chemical warfare agent VX. H254R / H257L also gained an 18-fold increase in specificity against NPPMP, an analog for the chemical warfare agent Soman (*7*).

The enzyme mediated hydrolysis of organophosphates has been shown to occur through a S_N-2 like mechanism where an activated water molecule attacks the phosphorous center of the substrate. This results in the cleavage of the scissile bond (*13*). The enzymatic hydrolysis of OPH's preferred substrate, paraoxon, occurs at diffusion-controlled rates (10^8 M^{-1} sec^{-1}) while the hydrolysis of the P-S and P-F bonds occurs at much slower rates.

OPH::Zn^{2+} has a molecular weight of 72 kDa and has a global conformational stability of > 40 kcal/mol (*14*). This stability, at least in part, comes from the protein's organization at the tertiary and quaternary level. Under chemical denaturing conditions, the enzyme has been shown to unfold via a three-state pathway from an active (*) dimer (N_2*) to an inactive, dimeric intermediate (I_2), to inactive monomers (U) as shown in Scheme 1.1.

Scheme 1.1

$$N_2^* \leftrightarrow I_2 \leftrightarrow 2U$$

The stability of the first transition ($N_2^* \leftrightarrow I_2$) has been found to be 4.3 kcal/mol and the second ($I_2 \leftrightarrow 2U$) is 36.1 kcal/mol. Although the overall conformational stability of the enzyme is large, its operational stability (the energy required to unfold the enzyme from its dimeric functional state (N_2*) to that of its inactive dimeric intermediate (I_2)) is much lower (*14*). An understanding of the dynamics of active site unfolding may provide insight into how to increase the stability of the active site.

OPH has been used in many different applications including an additive for coatings for use in military, industrial and health care functions (*15*), enzyme-based biosensing systems for the detection of neurotoxic war agents (*16-18*), and liposome encapsulated OPH has been shown to provide prophylactic and therapeutic protection against OPs when used alone or when used in combination with atropine and 2-PAM (*19*).

The Importance of Oligomerization for TIM Barrel Enzymes. The oligomerization of TIM barrels appears to be important for maintaining maximum catalytic activity and stability. Attempts to increase the activities of engineered monomeric TIM barrels have been only marginally successful. More active monomeric variants of MonoTIM from *Trypanosoma brucei* were constructed using a combination of directed evolution and random mutagenesis. While two variants of MonoTIM displayed an 11 fold increase in the k_{cat} and 4 fold decrease in the K_m when compared against MonoTIM, they displayed a 106 fold decrease in k_{cat} and a 4.5 fold increase in K_m when compared to the wild-type *Tb*TIM (*20*). The changes introduced into the monomeric variant of the enzyme did not stabilize the interface region of the enzyme and, thus, reduced the increased conformational entropy resulting from interface disruption.

Comparisons of crystal studies of TbTIM and MonoTIM have revealed that the overall structure of the monomeric subunits were very similar to those of the wild-type with the exception of the interface loop regions. In wild-type TbTIM these regions are very rigid with low *B*-values. In contrast, these same regions appear to be disordered in the crystal structure and have higher *B*-values in MonoTIM, indicating more flexibility (*21*).

In the monomeric variant of this enzyme, the active site still assumes a functional conformation although the catalytic activity of MonoTIM is greatly reduced with a k_{cat} 1000 times lower and a K_m 10 times larger than those of the wild-type enzyme. This increased flexibility appears to have two consequences with respect to catalysis. First,

the increased flexibility allows for a less ordered active site. Second, the active sites of the monomeric variants are less protected from the solvent which may lead to an increasing influence of the dielectric properties of the solvent on the catalytic abilities of the enzyme. It was also suggested that the flexibility of these interface regions plays a role in the folding of the dimeric enzyme with the monomeric variants recognizing each other through the primary association of these flexible regions. This would lead to a dimeric enzyme stabilized through tighter interactions across the dimeric interface.

The cysteine residue at position 14 of the homodimeric triose phosphate isomerase from *Trypanosoma brucei* (TbTIM) is located in the interface region of the dimer and known to be important in both the function and stability of the enzyme. When this residue was changed to a phenylalanine (C14F), the enzyme became a stable and active monomeric variant. The K_m of this enzyme was 10 fold greater than that of the wild-type while the k_{cat} was 1000 fold less. Other amino acid substitutions to C14 did not result in such a dramatic change in the catalytic activity nor did they form stable and active monomeric variants (*22*). This suggested that it was the dimerization that was necessary for the enzyme's maximum catalytic ability.

It is important to note that these α/β folds of monomeric TIM barrels were able to fold into a catalytically active conformation without the dimeric interactions. However, the low levels of activity and the lower stabilities of these enzymes suggested that dimerization was required to form the correct geometry of the active site of these enzymes to enable maximal activity (*20-22*).

Oligomerization can also occur with the binding of different proteins to form higher quaternary structures. The homodimeric triosephosphate isomerase from *Thermotoga maritima* forms a covalently linked tetrameric complex with phosphoglycerate kinase (PGK) to form a bifunctional enzyme. Stability and catalytic studies of the isolated TIM enzyme and the PGK-TIM hybrid showed that oligomerization of the two enzymes increased the stability and the catalytic efficiency of the TIM enzyme (*23*).

A comparison of TIM barrel enzymes has revealed a relationship between the Gibbs free energy changes for folding and oligomeric association changes. In these enzymes, $\Delta G_{association}$ was larger than $\Delta G_{folding}$ signifying that oligomerization contributes more to the conformational stability of the enzyme than subunit folding (*24*).

The Stability, Functional, and Regulatory Hypotheses. The stability hypothesis states that TIM barrels form dimers and tetramers in order to increase the overall conformational stability of the enzyme while the functional hypothesis states that these enzymes form oligomeric associations in order to increase their catalytic activity against their selected substrates. As discussed, oligomerization increased both the stability and the activity of TIM barrel enzymes. The truth can be found between these two hypotheses as there seems to be interplay between stability and functionality.

Furthermore, oligomerization may play a role in the regulation of catalytic activities of TIM barrels during the different stages of the life cycles of some organisms. For example, the triosephosphate isomerase from *Giardia lamblia* (G1TIM) functions as both a dimer and a tetramer. The enzyme does not display significant differences in

thermostability between its dimeric and tetrameric forms. While both forms display the same K_m value for glyceraldehyde 3-phosphate, the tetramer's k_{cat} value against this substrate is about half that of the dimer's. Forming the tetramer might involve some allosteric effect which inactivates two of the active site regions. Since *Giardia lamblia* transforms from cysts into trophozoites during its lifecycle, the authors theorized that the tetramer might be a 'storage conformation' for the lower metabolic requirements of the cystic state (*25*).

Preliminary Studies of Native OPH. DNA restriction mapping has shown that the *opd* gene containing regions of *Flavobacterium* sp. ATC 27551 and *Pseudomonas diminuta* were very similar if not identical with a possible one base-pair difference. Southern hybridization using a *Pst1* 1.3 kb *opd* fragment from *Pseudomonas diminuta* was used as a probe and found to hybridize to the total cellular DNA from two hydrolase positive strains of *Flavobacterium sp.* ATC 27551 and not to hydrolase negative strains of the same organism. Fragments of the *opd* gene produced by digestion of the purified *Flavobacterium* plasmid DNA with restriction endonucleases, showed strong hybridization with the *Pseudomonas diminuta* probe. The strong homology of these fragments with the probe suggested that these two genes shared sequence homology. A fragment of 2.1 kb from both *Pseudomonas diminuta* and *Flavobacterium sp*. was shown to contain identical restriction maps. This homology extended for at least 0.4 kb on both sides of the *opd* gene. The DNA 5' to the homologous region did not share the same restriction pattern in the *Pseudomonas* and *Flavobacterium*. No mention was made of the DNA 3' to *opd*, and it is assumed that a restriction map of this region was not

generated. It was concluded that these two plasmids, although not completely homologous, did share a region of strong sequence homology (*26*).

Upon cell disruption of the *opd* containing *Pseudomonas diminuta*, 80 – 90% of the paraoxonase activity was found to be associated with the cellular debris. Treatment with 0.1% Triton X-100 released the activity from the cell debris. Based on sizing chromatography the enzyme was estimated to have a molecular mass of between 60 and 65 kDa (*27*). This data suggested that the native OPH existed as a membrane bound dimer in *Pseudomonas diminuta*, although it was still unclear whether the enzyme existed as a dimer in its native form or if it dimerized upon release from the membrane.

It was determined that the *opd* gene from *Flavobacterium* and *Pseudomonas diminuta* were identical with the possible exception of a G-to-C conversion in the *Flavobacterium* gene at base 295 (*28*). These genes were later shown to be identical (*29*). The native plasmids containing these genes were confirmed to be very different. The authors speculated that there may be more homology of these OP-degradative plasmids than just the *opd* gene.

Orf243, a Possible Aromatic Esterase Involved in the Hydrolysis of Para-Nitrophenol. It was shown that the homologous region encoding the OPH from *Pseudomonas diminuta* and *Flavobacterium* sp. also contained a conserved region of 7.6 kb encoding a possible aromatic esterase was located 750 bp downstream of *opd (30)*. This gene would code for an enzyme 243 amino acids long and has been named *orf243*. BLAST searches did not report any enzymes with a strong homology to the gene product of *orf243*, but a structural fold-prediction algorithm identified a strong homology to

chloroperoxidase F from *Pseudomonas fluorescens* which is also a member of the α/β hydrolase family. Further BLAST searches showed similarity of this enzyme to the aromatic degrading pathways of *Pseudomonas putida* DmpD, TodF, and XylF, *Pseudomonas azelaica* HbpD, *Rhodococcus* sp. EtbD and BphD and *Pseudomonas fluorescens* CumD (*30*).

Several *Flavobacterium* species have been shown to utilize *p*-nitrophenol as a nitrogen source for growth (*31*). Therefore, it was speculated that *orf243* might play a role in the hydrolysis of aromatic compounds such as *p*-nitrophenol (*30*). This was verified by adding *p*-nitrophenol to cultures of *E. coli* DH5-α containing *orf243* and sans *orf243*. After 8 hours, cultures that contained *orf243* showed significant degradation of *p*-nitrophenol from 20 μM to 3.1 μM while cultures without *orf243* showed no degradation of *p*-nitrophenol. Therefore, the gene product of *orf243* appeared to play a role in the degradation of aromatic compounds and may work in conjunction with OPH as degradation pathway for aromatic organophosphorus compounds.

Attempts to clone the *Flavobacterium opd* into *E. coli* resulted in no expression unless fused to an inducible *lac* promoter (*32*) in which case the enzyme was found to be associated with the cell. Further attempts to obtain high levels of soluble protein lead to the expression of the *opd* gene in *Streptomyces pilosus*. Unfortunately, only low levels of OPH were produced and found in the cell and in the extracellular medium. DNA recovered from *Streptomyces pilosus* weakly hybridized with the 1.3 kb pst1 fragment from *Flavobacterium (33)*.

In hopes that OPH could still be excreted as a soluble protein in high amounts, the *opd* gene from *Flavobacterium* was cloned into the gram-positive *Streptomyces lividans* strain 66 (*32*). *Streptomyces lividans* is known to secrete proteins with and without signal sequences. OPH was expressed as a soluble protein that was found in the extracellular medium at low levels. When the native *Flavobacterium opd* promoter was used a higher level of expression of OPH resulted.

Approximately 80 – 90 % of OPH was found in soluble form contradicting earlier studies in *Flavobacterium* and *Pseudomonas* where the majority of the enzyme was found associated with the membrane. Additionally, the enzyme appeared to be more stable as it was not inactivated with repeated freezing and thawing as it had been in earlier studies with *Flavobacterium* (*34*). Interestingly, HPLC size exclusion chromatography revealed one peak of enzymatic activity with a mass of 34 kD, suggesting that the *Streptomyces lividans* OPH may have existed as an active monomer. It is possible that the dimeric structure of these enzymes had disassociated into monomeric subunits under the low concentrations used in the study. Cell-free extracts were found to have additional peaks of activity greater than 100 kD suggesting that the enzyme had formed oligomeric complexes with itself or other proteins. The mass comparison of intracellular and extracellular OPH from *Streptomyces lividans* was not performed it is not known whether a cleavable leader sequence was involved in the export of the enzyme was made as N-terminal sequencing of the enzyme was not performed. The observations that the enzyme was found in the cytoplasm and the extracellular medium, but not associated with the membrane, coupled with the fact that

the enzyme was more stable than in earlier studies, suggests that it may have formed a dimeric association. Table 1.2 lists the molecular weight determinations of OPH as expressed in various systems with and without the leader sequence. It is interesting to note that studies that suggested that OPH was a monomer used denaturing conditions to arrive at that conclusion.

Post-Translational Processing of the Native Leader Sequence. It was found that expression of the *opd* gene from *Pseudomonas diminuta* in *E. coli* was approximately 10 fold less than its native source, as followed by activity (*35*). Examination of the *opd* gene product from *Pseudomonas diminuta* showed that the nascent enzyme is translated as a 365 amino acid peptide from which the first 29 amino acids were post-translationally removed (*36*). This was the first suggestion that the enzyme had a signal sequence of 29 amino acids that was cleaved in the mature protein. Examination of this leader sequence showed that it had the characteristics of a typical signal peptide (*37*): (i) The presence of an N-terminal basic residue, (ii) a stretch of hydrophobic or weakly polar amino acids in the middle of the primary structure of the signal peptide, and (iii) a C-terminal peptidase region characterized by the -3/-1 "von Heijne" rule that contains a cleavage site. It is interesting to note that these authors made specific mention of the twin arginine repeat at the N-terminal portion of the signal peptide, as this signal sequence may be a TAT signal sequence (discussed below).

Table 1.2: Preliminary studies on the leader sequence and oligomeric state of OPH.

Source [a]	Organism [a]	Oligomeric State	Molecular Weight	*opd* coded L.S.	N-Terminal Residue	Association [k]	Purity [m]	Reference
*F.*sp.	*F.* sp.	Monomer	50 kDa	Yes	N/D	Cp	PaP	(*34*)
P. diminuta	Sf9	Monomer	39 kDa	Yes	N/D	Cp	Hm	(*5*)
F. sp.	*F.* sp.	Monomer	35 kDa	Yes	N/D	Mb	Hm	(*29*)
P. diminuta	*E. coli; P. diminuta*	Dimer [b]	60 - 65 kDa	Yes	N/D [o]	Mb	PaP	(*27*)
P. diminuta	*E. coli*	Dimer	72 kDa	No	S 30	Mb	Hm	(*2*)
P. diminuta	*E. coli* FM5	N / D	N / D	Yes [f]	S 30	Cp	CFX; Pap	(*36*)
F. sp.	*F.* sp.; *E. coli*	Monomer [c]	35 kDa [c]	Yes	S 30	Mb [i, j]	Hm	(*38*)
P. diminuta	Sf9; E. coli	Monomer [c, d]	35 - 38 kDa [c, d]	Yes	G 29; S 30 [n]	Cp	CFX; Hm	(*41*)
F. sp.	*S. lividans*	Monomer	34, >100 kDa	Yes	N/D	Cp; Ex	Hm	(*32*)
F. sp.	*S. lividans*	No Metion	34,37-38 kDa [d]	Yes	N/D	Cp; Ex	CFX	(*42*)
F. sp.	*S. lividans*	No Metion	41 kDa [g]	Yes [e]	N/D [l]	Cp; Ex [g]	PaP	(*40*)
F. sp.	*S. lividans*	Monomer [c, d]	35 kDa [d]	Yes	S 30	Ex	Hm	(*39*)

[a] *F.* sp. = *Flavobacterium* sp. (ATCC 27551), *P. diminuta* = *Pseudomonas diminuta* MG, Sf9 = *Spodopter frugiperda* (fall army worm), *S. lividans* = *Streptomyces lividans*

[b] The enzyme was found to be a dimer after it had been removed from the membrane with 1M NaCl and 0.1% Triton X 100.

[c] The enzyme is assumed to be monomeric based upon previous papers

[d] The enzyme is assumed to be monomeric based upon migration on an SDS-PAGE gel.

[e] The native OPH leader sequence and the leader sequence from S. lividans β-galactosidase

[f] N-terminal sequencing shows that the enzyme's leader sequence has been removed via post-translational processing

[g] The mature protein is associated with the soluble fractions while the precursor protein is found in the insoluble frations.

[h] The precursor and the mature proteins are found to be cell-associated while only the mature product is found in extracellular samples

[i] The enzyme is assumed to be membrane bound based upon previous studies

[j] The enzyme expressed in E. coli is found predominatly in the cytoplasm

[k] Cp = cytoplasm, Mb = membrane, Ex = Extracellular medium

[l] Not determined with the native opd promotor, leader sequence and gene

[m] Partial Purification = PaP, Homogeneous = Hm, Cell-Free Extract = CFX

[n] Gly 29 was found to be the N-terminus of the OPH purified from Sf9 insect cells, Ser 30 was the N-terminus of the OPH expressed in E. coli

[o] The N-terminal sequence was determined for an OPH / b-galactosidase peptide hybrid. The sequencing reported an N-terminus at Thr 171 of OPH

Mulbry and Karns examined the *opd* gene product from *Flavobacterium sp*. ATCC 27551 and found that the enzyme was considerably smaller (~35 kDa) than what was predicted from the *opd* gene (39 kDa, (*29*). They concluded, in agreement with the previous studies, that the nascent protein was subjected to post-translational cleavage of a signal sequence to form a smaller, mature protein. Additionally, they found that the N-terminal region of this mature enzyme was the same as that found in the mature *Pseudomonas diminuta* OPH, with the first 29 amino acids of the nascent enzyme removed to form the mature enzyme, although they didn't state any comparisons between the two gene products. The sizing of the 35 kDa fragment was based on the migration of the protein on an SDS-PAGE gel (*29, 38*) and on the use of a RP-HPLC sizing column with a trifluoroacetic acid and acetonitrile gradient (*36*). These are both denaturing methods, and it can be reasonably assumed that OPH had dissociated into monomeric subunits which led to the conclusion that OPH existed as a monomer. Table 1.2 lists several of the primary studies of OPH, its leader sequence, and the study's oligomeric determination of the enzyme.

Even when inducible promoters were used, attempts to express the *Flavobacterium* OPH in *E. coli* met with limited success. It was suggested that the larger precursor enzyme was improperly processed in *E. coli* and that proper processing was necessary for the best possible enzyme activity. To this end, the coding region for the first 33 amino acids of the full length OPH was replaced with the coding region of first 5 residues of *lacZ* to form a *lacZ-opd* fusion. The result was an increase in activity. Cells containing the fusion protein showed a two fold increase in activity when

compared to those containing the original. Additionally, the mass of the mature *Flavobacterium* enzyme and the lacZ-OPH enzyme were identical, suggesting that the *Flavobacterium* enzyme was not processed further once the leader sequence was removed. They also suggested that, despite earlier discrepancies in the sequencing of the *Pseudomonas diminuta* and the *Flavobacterium opds*, they were almost certainly identical (*29*).

It was later found that only the mature form of OPH, when expressed in *Streptomyces lividans*, was found in extracellular medium. Both the full-length and the mature form of OPH were found to be cell associated, and N-terminal portion of the mature form of the enzyme was found to be the same as the mature enzyme in *Flavobacterium (39)*. This suggested that the *opd* product from both organisms was post-translationally processed in the same manner and was probably dimeric. In earlier studies, nearly one third of OPH activity was found to be associated with cellular fractions. When the native OPH signal sequence was replaced with a native *S. lividans* signal sequence from *β*-galactosidase, more OPH was found in the extracellular medium (*39*). With both signal sequences, only mature OPH was found in the extracellular medium while full length and mature forms were found in the cell-associated fractions. Unfortunately, no mention was made in this study about the oligomeric state or the molecular weight of the enzyme in the extracellular milieu. However, it can be assumed that since the N-terminal portion of the enzyme is post-translationally processed, it must exist as a dimer (*2, 27*).

Later studies used immunoprecipitation with (OPH) phosphotriesterase antibody cells to determine the cellular localization of OPH. The secretion and cell-association of the recombinant OPH was compared to that of the native *Streptomyces limosus* α-amylase enzyme. The soluble and active mature form of OPH was found in the extracellular medium, while the precursor protein was predominantly found in the cell-associated fractions. This suggested that the leader sequence was used in the insertion or the secretion of the enzyme into or across the membrane and then processed. Fractionation experiments with the cell-associated OPH suggested that the full-length enzyme was transcribed and then associated with the membrane where it was processed and excreted or returned to the cytoplasm (*40*). It may be possible that a monomeric full-length variant of OPH associated with the membrane, and once processed, it dissociated from the membrane and oligomerized to form its active, dimeric state.

Expression of OPH in insect tissue-culture cells (Sf9 of *Spodoptera frugiperda*) resulted in a post-translationally processed enzyme similar to that of *E. coli*'s OPH except that the N-terminus of the enzyme was found to be at G29 instead of S30 (*41*). Upon sonication of insect cells, over 97% of enzymatic activity was released into the supernatant suggesting that the enzyme was not membrane bound but free in the cytosol. Only the processed form of the enzyme could be detected by western blot and while the oligomeric nature of the enzyme was not determined, the size of the processed enzyme was estimated to be 35 kDa based on the mobility of the enzyme with SDS-PAGE.

The mechanism of secretion of the *Flavobacterium* OPH in *Streptomyces lividans* was investigated using [^{35}S]methionine pulse chase experiments (*42*). Each

monomer has 5 methionine residues and the leader sequence has one additional methionine, making a [^{35}S]methionine pulse chase and excellent way examine the secretion of this enzyme. The recombinant *Streptomyces lividans* was grown in media conditions that disfavored the secretion of protein into the extracellular medium. The cells were grown and pulsed with [^{35}S]methionine and followed by a chase of unlabeled methionine. Protein was then recovered by immunoprecipitation and visualization by fluorography. Only five minutes after the pulse, full-length precursor protein was visualized having a mass of approximately 37-38 kDa. In fact, no processing of the leader sequence was observed until 40 minutes after the pulse. It was later found that the leader sequence wasn't processed until the cells had reached stationary phase of growth (*43*). The delay in processing may be representative of a later expression of protease or perhaps membrane association by the leader sequence of OPH until its removal from the membrane at stationary phase. Protein production was stopped by the addition of chloramphenicol, and the enzymatic activity of the supernatant was monitored. No change was observed between the samples with and without chloramphenicol suggesting that processing of the leader sequence was not dependent on the secretion of the protein.

An additional co-precipitated species was observed with a mass of 24 kDa. The gene product of *orf243* has an expected mass of about 27 kDa, and is thought to associate with OPH. It is possible that this additional species is the aromatic hydrolase coded by *orf243*, (*30*). These authors make the assumption that the OPH enzyme is a monomer. The only evidence they have for this is the visualization of a protein in the 37-38 kDa range based on the migration of the protein on a denaturing SDS-PAGE gel.

Translocation of Native OPH in E. coli. In preliminary studies of OPH localization, sucrose density gradients have demonstrated that OPH activity in the native *Flavobacterium sp*. ATCC 27551 was associated with inner membrane fractions (*29*). OPH activity in the native *Pseudomonas diminuta* was also found to be associated with the inner membrane fractions (*5*). In *E. coli*, separation of membranes from soluble proteins after lysis revealed that greater than 90 % of the observable activity was found within the soluble portion of *E. coli (43)*.

OPH-alkaline phosphatase fusions were used to determine if the signal sequence of OPH was competent for translocation across the membrane. Alkaline phosphatase requires the formation of two disulfide bonds for the correct structure and activity of the enzyme. These disulfide bonds do not form in the reducing environment of the cytoplasm of *E. coli* and PhoA would only function if transported across the membrane into the oxidizing periplasm (*44*). Fifteen *opd*Φ*phoA* fusions were produced, selected and screened for PhoA activity. They were located at unique positions throughout the *opd* sequence and all had a significant PhoA activity above that of L17R and Δ2-29 suggesting that the native leader sequence of OPH was competent for translocation across the membrane.

The deletion of the leader sequence, Δ2-29, and the insertion of a positive charge in the hydrophobic core of the leader sequence, L17R, produced alkaline phosphatase activities in the cell lysates that were 60-fold and 20-fold lower, respectively, to that of the native OPH leader sequence. Attempts to make the leader sequence more efficient by increasing its hydrophobicity (G15L / T16L) produced a leader sequence that was

much more efficient in transporting the fusion peptide across the membrane than was the native leader sequence. Therefore, changes in the leader sequence did influence the transport of the OPH-PhoA fusions in *E. coli (43)*.

Additionally, the L17R leader sequence was not processed and only full length protein was found in cultures. In cell free extract, this protein had an activity twice that of the wild-type enzyme. Further, the K_m for both of these enzymes, as well as the processed OPH and Δ2-29, against paraoxon and DFP were found to be very similar if not identical. This suggested that the enzymatically active conformation was retained in each of these variants and the presence of the leader sequence did not seem to inhibit the proper folding required for activity. The full length form was shown to be enzymatically active. There did not appear to be any correlation of the relative enzymatic activity and the presence or absence of processing demonstrating that the leader sequence was attached to the folded enzyme (*43*).

Twin-Arginine Translocation Signal. The leader sequence of OPH was originally thought to be associated with the secA translocation pathway (*43*). A secA signal sequence contains three primary characteristics: i) an N-terminal region that contains one or more basic residues within the first 5 – 8 residues, ii) a hydrophobic core usually between 10 – 15 uncharged residues, and iii) a polar region distal to the hydrophobic core containing a signal peptide cleavage site and following the -3,-1 rule (von Heijne) where the residues in the -3 and -1 positions relative to the processed N-terminus of the enzyme are small, neutral residues (*45*). This hypothesis was tested by transforming *opd* into a *secA* temperature-sensitive mutant. The presence or absence of a functional secA

leader sequence did not affect the stability or processing of OPH which suggested that the native leader sequence of OPH may not necessarily be a secA leader sequence.

A TAT signal sequence is characterized by the following factors: i) it has an N-terminus with the motif: (S/T)-R-R-x-x-L-K, ii) it is usually longer than secA signal sequences (26 - 58 residues for TAT sequences versus 18 – 26 for secA sequences), iii) the signal sequence has a higher net charge with an average of +2.8 for TAT sequences versus +1.7 for the secA sequences, and iv) it is secA independent (*46-48*). Close examination of the native OPH signal sequence revealed that it contained each of these elements (Figure 1.1).

An interesting difference between the TAT and the secA excretion pathways is that the TAT pathways excretes proteins with substantially native-like conformations while the secA pathway only excretes unfolded proteins (*48*). Comparisons of several different TAT signal sequences fused to alkaline phosphatase showed that only when the disulfide bonds of alkaline phosphatase were oxidized (i.e. when the enzyme had folded) was the enzyme transported across the cytoplasmic membrane into the periplasm. Additionally, this study identified two distinct types of TAT signal sequences. Class I signal sequences only transport proteins into the periplasm via the TAT pathway. Class II signal sequences were able to transport a small quantity of unfolded proteins across the cytoplasmic membrane. With this class of signal sequences either unfolded or misfolded enzymes were transported via the TAT pathway, or the class II signal sequences could be utilized to transport the proteins via the TAT or secA sequences. It is thought that, in these cases, folded proteins with Class II signal sequences are shuttled

through the TAT pathway while those that have not yet folded could be deferred to the secA excretion system (*48*). Presently, the characteristics distinguishing between these two classes of signal sequences are unknown.

Another difference between the TAT and secA pathways are that the secA secretion pathway is ATP driven while TAT sequences are thought to be dependent on the proton motive force (PMF) for translocation across the membrane (*49-51*).

The proton motive force (PMF) and its effect on the translocation of the enzyme across the membrane of *Streptomyces lividans* was examined (*42*), and 2,4-dinitrophenol and carbonyl cyanide chlorophenylhydraxone (CCCP) was used to dissipated the PMF. The excretion of OPH into the extracellular environment did not appear to be dependent upon the PMF.

The leader sequence of OPH appears to be that of a TAT signal, but it does posses characteristics that are similar to that of a secA signal, namely it is shorter than most TAT sequences (only 29 amino acids) and it posses a smaller, more Sec-like charge (+2) than

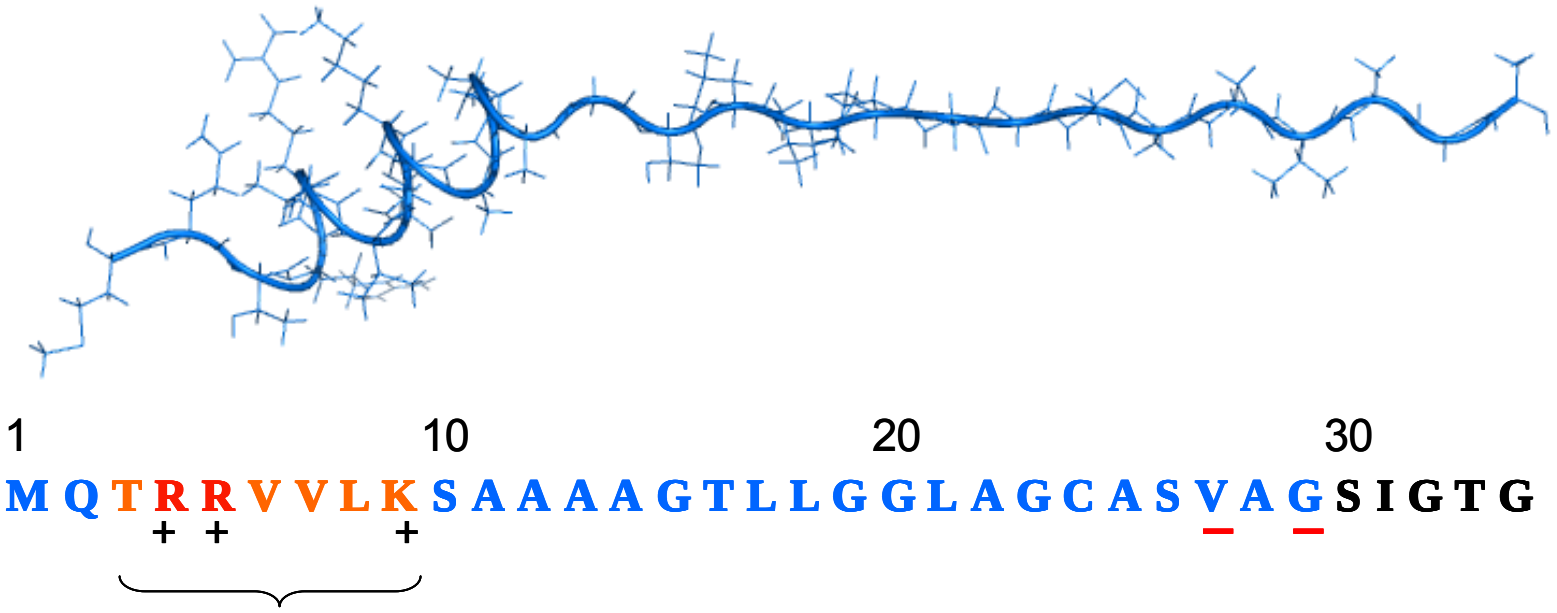

Figure 1.1: Native signal sequence of OPH. The secondary structural characteristics of the leader sequence were calculated using the Chou Fasman method (*43*). The von Heijne residues, G27 and V30, are indicated. The TAT motiff, T3-K9, is also indicated.

the average charge of Tat signals (*46, 47*). From the available information it would appear that the native leader sequence of OPH would be competent for translocation via the Tat pathway and the Sec pathway (class II TAT signal sequence). More research is needed to test this hypothesis.

Transposable Elements. Each of the *opd* genes from *Flavobacterium* and *Pseudomonas* were located on plasmids and appear to have transposable elements associated with them (*30, 52, 53*). As shown by sequence analysis, the *opd* gene is flanked by an insertion sequence encoding an IstAB operon with significant homology to IS21 family of transposons and tnpA and tnpR genes which are characteristic of the Tn3 family of transposons. Although no transposition events were detected in the screening of 10^{10} cells, the linkage to the *opd* gene of IS elements and transposase genes suggested that there could be widespread distribution of the *opd* gene due to a combination of both transposition and plasmid transfer (*30*).

OpdA, a 35 kDa OPHase from Agrobacterium P230, has a high sequence homology (94.2 % similar and 90.0 % identical) to the OPH from Pseudomonas diminuta MG (*52*). The residues of the small and leaving group pockets are strictly conserved between OPH and OpdA. Residues H254, H257 and L271 in the large pocket of the OPH active site are R, Y, and F, respectively, in OpdA. It was hypothesized that these changes have the effect of shrinking the size of the leaving group pocket in OpdA enhancing the activity of the enzyme against dimethyl substrates as compared to the activity of OPH. These results are consistent with the results from changing the H254 residue to an R in OPH (*54*). OpdA also has a leader sequence that is post-

translationally processed to yield a mature enzyme. The leader sequence has one less amino acid than that of the leader sequence of OPH. Additionally, there is a frame-shift mutation near the 3' end of the *opdA* gene that results in an additional 16 amino acids on the C-terminal portion of the enzyme.

While it is not mentioned how these authors arrived at the 35 kDa determination above, it was most likely made based on the size of the gene and analysis of the leaderless gene product migration distance on an SDS-PAGE gel. Due to the high homology between these two enzymes, it is likely that OpdA also exists as a homodimer and not a monomer. In fact, crystallization of OpdA has shown that the enzyme is indeed a homodimer (*55*), pdb file 2d2g).

Further studies have shown that the *opdA* is located downstream of a transposase gene, *tnp A*, and inverted repeats, suggesting insertion sequences, flanking the two genes (*53*). *TnpA* has 100% sequence identity to TN610, the transposase from *Mycobacterium fortuitum*. It was determined that this transposable element could indeed insert *opdA* as well as antibiotic resistance genes into the chromosome of *E. coli*. The presence of this transposable element may help to explain how OPHases have moved across geographically diverse locations and different taxonomical organisms.

Concluding Remarks. Oligomerization is necessary for the optimal stability and catalytic activities of TIM barrel enzymes, and OPH does not appear to be an exception. The native OPH was thought to be a monomeric enzyme, and the criteria for this based largely on estimation from genetic structure and denaturing methods. This assumption persisted though many studies. Crystallization of OPH (without the leader sequence)

provided convincing proof that the enzyme existed as a dimer (*2*). The fact that the enzyme is post-translationally processed in its native organisms suggested that this enzyme exists as a dimer in these organisms as well. Although the presence of the leader sequence may prevent dimerization, OPH's kinetic parameters appear unchanged with and without a leader sequence (*43*). In light of the fact that the catalytic abilities of monomeric TIM barrel enzymes are diminished when compared to their oligomeric counterparts, it appears that the leader sequence of OPH does not hinder the dimerization process.

The native OPH has a leader sequence that appears to share elements of both secA and TAT signal sequences. Although the signal sequence does not translocate OPH out of the cytoplasm of *E. coli*, it has been found to be competent for translocation in other organisms.

OPH is a remarkable enzyme that has the potential to be developed for a wide variety of applications. Although the enzyme has a very large global stability, the energy required to unfold the enzyme into its inactive state is very small. The structural alterations that stabilize this enzyme must be better understood. Once this unfolding profile has been determined, rational design can be employed to prevent these undesired changes, and increase the enzyme's operational stability in harsher environmental conditions.

CHAPTER II

TRYPTOPHAN-TO-PHENYLALANINE SUBSTITUTIONS

Tryptophan residues are sensitive probes for following the unfolding of a protein as it is exposed to increasing concentrations of a denaturant. Unfortunately, more than one fluorophore in a protein will give an average of the unfolding properties (regions) of the enzyme and will provide limited information about the structural and dynamic properties of unfolding. A solution to this problem is to replace one or more of the fluorophore side chains, in this case tryptophan, with a less fluorescent side chain, such as phenylalanine, using site-directed mutagenesis and then examine the remaining fluorophores during chemical-denaturation (*56, 57*). A limitation to this method is that the enzyme should not contain tryptophan residues important for folding or function (*58*).

Protein models engineered to contain a single tryptophan have revealed detailed information on the structure of folding intermediates, kinetic parameters of unfolding, conformational changes upon ligand binding, and resolution of the protein's unfolding profiles (*56, 58-61*). Alternatively, if a variant enzyme lacking tryptophan residues can be engineered that doesn't differ significantly from the activity or the structure of the wild type enzyme, a larger unfolding profile of OPH can be developed. This would enable a tryptophan reporter to be inserted in any region of the protein allowing the unfolding characteristics of that region to be determined.

Intrinsic tryptophan fluorescence is a sensitive probe of the solvent state of tryptophan residues and can be used to determine how the protein unfolds under chemical denaturing conditions. The wavelength of maximum emission (λ_{MAX}) is sensitive to the polarity of the local microenvironment of the tryptophan residue and ranges from 308 nM to 355 nM in proteins. As the microenvironment surrounding the tryptophan becomes increasingly polar, the λ_{MAX} will shift to longer wavelengths (red shift). As the microenvironment becomes more non-polar, the λ_{MAX} will shift to shorter wavelengths (blue shift) (*56, 62-64*). The common interpretation is that the λ_{MAX} will red shift as the fluorophore is exposed to the more polar conditions of the solvent as the protein unfolds in denaturing conditions. In this way, the fluorescence emission can provide valuable information regarding localized unfolding. If there are two or more tryptophan residues present in the protein, the fluorophores will all contribute to the emission profile and any changes in the λ_{MAX} will be representative of the regional unfolding of the enzyme.

In order to develop an accurate picture of unfolding, tryptophan-to-phenylalanine variants may be used to study unfolding of individual regions of OPH. Those enzymes should resemble the native enzyme in form, catalytic function, and stability. Since partitioning the localized unfolding profile of wild type OPH is what was ultimately desired, it was important that these tryptophan-to-phenylalanine variants retain the function and structure of the wild type enzyme. If they differed in their activities or structures, any data that they provided regarding unfolding would not accurately represent the unfolding profile of wild type enzyme.

There were two goals of this project. The first was to use variants containing only one tryptophan per subunit to monitor the localized unfolding of OPH (in the regions containing the fluorophores) in denaturing conditions. Secondly, a tryptophan-less enzyme could be constructed and used to probe different regions of localized unfolding through the evaluation of tryptophan substitutions elsewhere in the enzyme.

Thus, enzyme variants were constructed whereby each tryptophan residue was independently changed to a phenylalanine residue leaving only three remaining tryptophan residues per subunit. Four variants were constructed that contained only one tryptophan residue per subunit (three substitutions per subunit; OPH^{69}, OPH^{131}, OPH^{277} and OPH^{302} where the superscript number indicates the designation of the remaining tryptophan residue) and one variant was constructed that contained no tryptophan residues (tryptophan-less, W^{Φ}) anywhere in the enzyme. The resulting fluorescent patterns were then compared to the wild type enzyme (WT).

The location of each tryptophan residue in the OPH homodimer is represented in Figure 2.1. The tryptophan residues are widely distributed across the molecule and

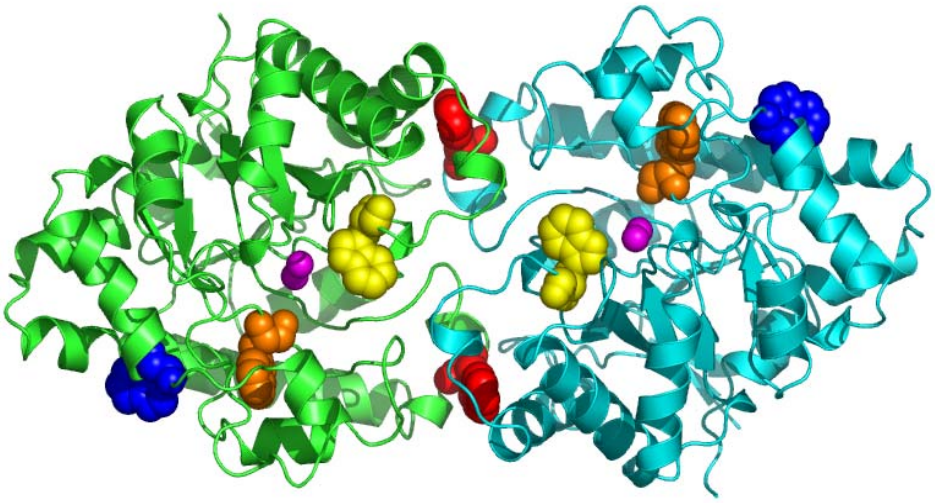

Figure 2.1: Location of tryptophan residues in OPH. The tryptophan residues are displayed in space filled representation. W69 is colored red, W131 is yellow, W302 is orange, and W277 is blue. The monomeric subunits are colored green and cyan. The active site metals are represented as magenta spheres. The coordinates for the diagram were acquired from the pdb file 1dpm (*4*).

would seem to serve as useful probes for monitoring how different regions of the enzyme unfold in chemical denaturing conditions. W69 is located in the interface of OPH. It is involved in stacking interactions with F72 of its own subunit and F149 of the opposite subunit. F72 forms edge on stacking interactions with F69 and F73 of its own subunit. Additionally, F65 participates in stacking interactions with M138 and F104, both of the opposite subunit (*2*). W131 forms part of the hydrophobic leaving group pocket of the active site of OPH. It forms an aromatic stacking interaction with F132 (*4, 65*). W131 has been suggested to play a part in orienting the substrate through π-stacking interactions (*9*). W277 forms edge on stacking interactions with F327 and F335. While it is positioned near the large pocket of the active site, it is located 17.2 angstroms from the α-metal (1dpm) of the active site and so is not expected to be involved in catalysis of substrates. It is also located 33.8 angstroms away from the α-carbon of W69 (in the intersubunit interface) and is not thought to be involved in any subunit-subunit interactions. W302 forms part of the small pocket of the active site and is involved in stacking network with H230, H254, H257 and N321 (*4*). The residues that are involved in this stacking interaction are important in the structure and function of this enzyme (*4, 7, 66, 67*) as well as metal coordination. The tryptophan interactions are represented in Figure 2.2.

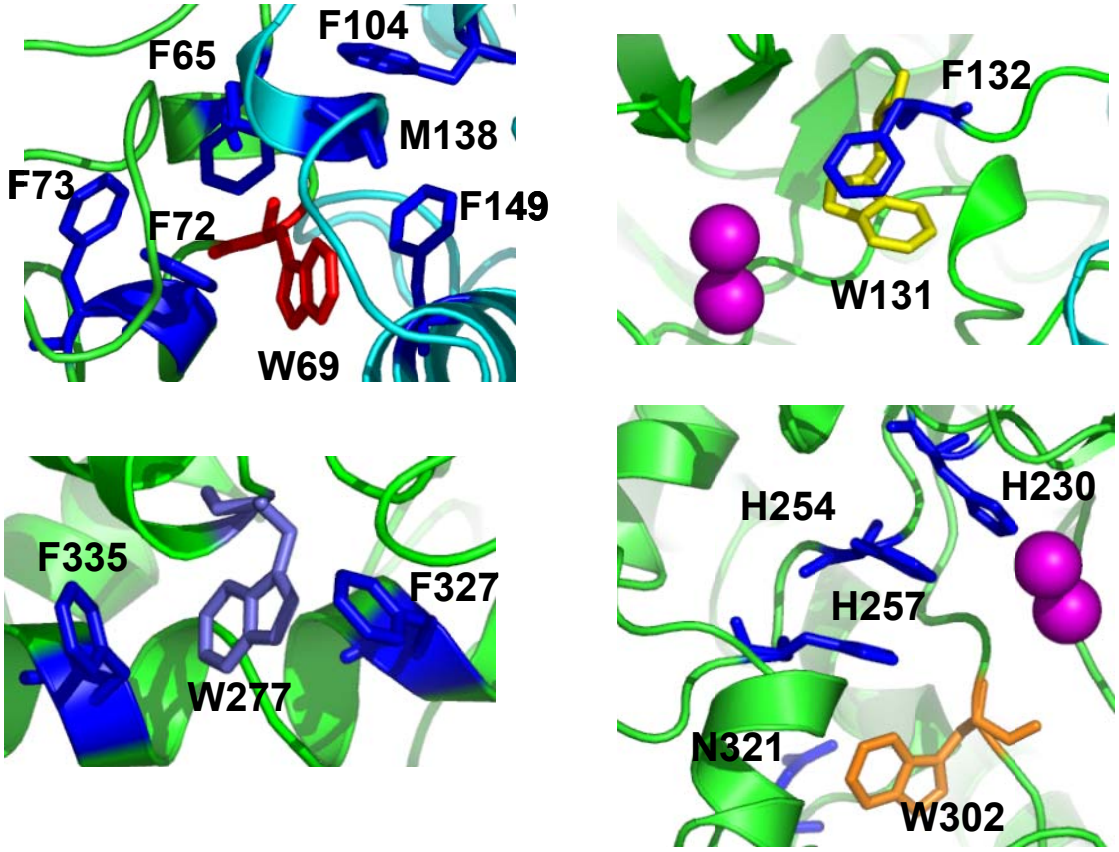

Figure 2.2: Stacking interactions of the tryptophan residues in OPH. The tryptophan residues are colored according to the legend in Figure 2.1. Residues contributing to the stacking interactions are colored dark blue, the divalent cations in the active site are represented as magenta spheres, and the OPH molecule is represented as a green ribbon. Residues are numbered as marked. The coordinates for this diagram were taken from the pdb file 1dpm.

MATERIALS AND METHODS

Materials. Paraoxon was obtained from ChemService (Westchester, PA) and prepared as previously described (*7, 68*). All buffer and assay reagents (CHES, potassium phosphate, $CoCl_2$, and ANS) were obtained from Sigma (St. Louise, MO). Site-directed mutagenesis kit and reagents were purchased from Stratagene® (Cedar Creek, TX). Oligonucleotides were purchased from Integrated DNA Technologies, Inc.® (Coralville, IA). Media components for cell growth (Bacto-Tryptone, Yeast Extract, Bacto-Agar, Difco™ Terrific Broth) were obtained from Fisher Scientific (Pittsburgh, PA). *Escherichia coli* DH5α (*supE44* Δ*lacU169* [*Φ80 lacZΔM15*] *hsdR17 recA1 endA1 gryA96 thi-1 relA1*) was used to express the bacterial OPH from pUC19-*opd*.

Site-Directed Mutagenesis for Tryptophan-to-Phenylalanine Substitutions. The pUC19-*opd* gene coding for the leaderless wild-type OPH was used in all mutagenesis reactions (*69*). A Quick Change® XL Site-Directed Mutagenesis Kit from Stratagene® was used to construct all the mutations. The manufacturer's directions were followed in all cases. The oligonucleotides used in this study were synthesized in 25 nmole quantities by Integrated DNA Technologies, Inc. (Coralville, IA), desalted and freeze-dried. All oligonucleotides were resuspended in 400 μL of MilliQ H_2O prior to use. The following oligonucleotides were used to direct tryptophan-to-phenylalanine mutagenic reactions:

(W69F) 5’ TTC TTG CGT GCT TTT CCA GAG TTC TTC GGT AG 3’

3’ CTA CCG AAG AAC TCT GGA AAA GCA CGC AAG AAT C 5’

(W131F) 5’ GCT TGT TTT TCG AC CGC CAC TTT C 3’

3’ GAA AGT GGC GGG TCG AAA AAC AAG C 3’

(W277F) 5’ CGT TCG TTT CAA ACA CGG GCT CTC 3’

3’ CGT GTT TGA AAC GAA CGG ATG CCC A 3’

The underlined bases are the mismatched bases.

Sequencing reactions were performed in order to confirm the identity of each mutation. Sequencing reactions were analyzed at the Genetechnology Laboratory of Texas A&M University and the data analyzed with DNASTAR® Molecular Biology software (DNASTAR, Madison, WI). The gene pUC19-*opd* W302F was supplied by Janet Grimsley.

The double, triple and, quadruple mutants were constructed with the above primers, with the Stratagene® Quick Change® XL Site-Directed Mutagenesis Kit as shown in Figure 2.3.

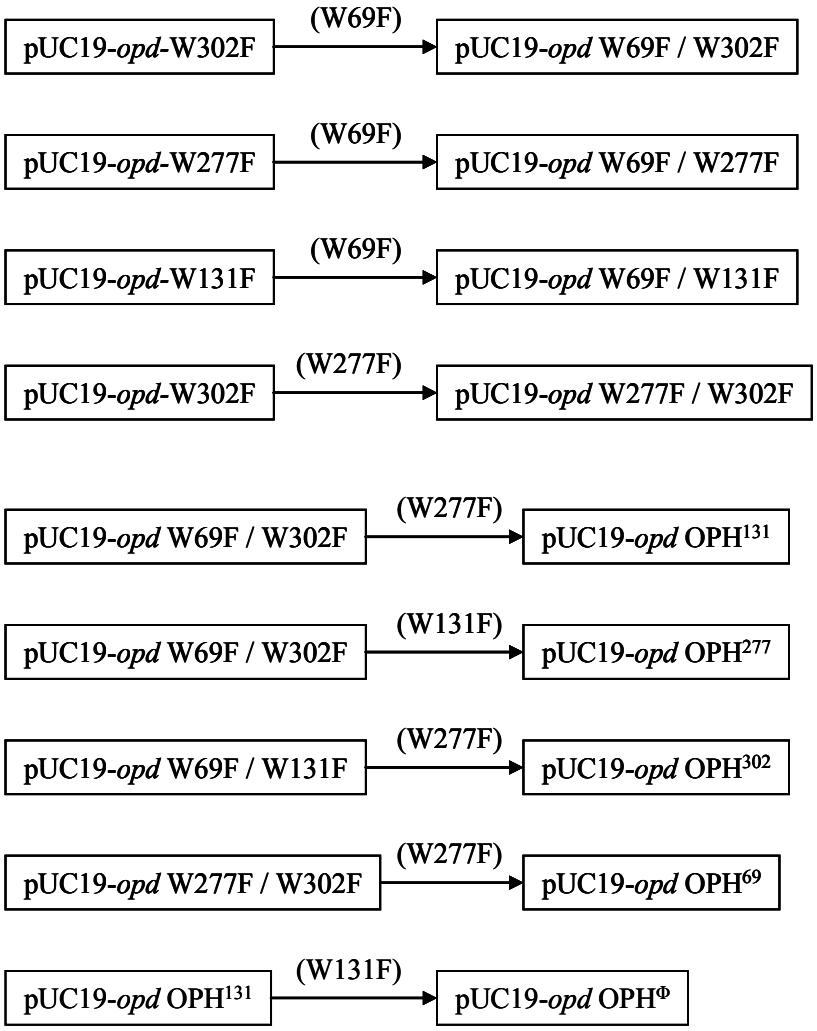

Figure 2.3: Creation of tryptophan-to-phenylalanine variants. Oligonucleotide primers used to create a particular mutation are represented in parenthesis. OPH variants containing only one remaining tryptophan per subunit are represented by the remaining tryptophan amino acid number in superscript notation. The tryptophan-less enzyme is represented by the symbol, Φ, in superscript notation.

Production and Purification of OPH. OPH was produced and purified as previously described (*14*). OPH containing fractions were pooled and concentrated to ≥ 2 mg/mL, stored at 4 ˚C, and used within 24 hours. The purity of the sample was assessed by SDS-PAGE. The extinction coefficient (ε_{280} = 58,000 M^{-1} cm^{-1}) was used to determine the concentration of OPH. Protein concentrations of the tryptophan-to-phenylalanine substitutions were calculated using the Bio-Rad Protein Assay procedure using a standard curved generated from known concentrations of wild type OPH. Concentrations determined from the Bio-Rad Protein Assay procedure were used in all experiments. The Edelhoch method (*70*) was used to predict general extinction coefficients (M^{-1} cm^{-1}) for the tryptophan-to-phenylalanine substitutions for estimation purposes. This method calculated a general extinction coefficient based upon the number of tryptophan and phenylalanine residues and number of disulfide bonds present in the protein according to equation 2.1.

$$\varepsilon(A280)(M^{-1}cm^{-1}) = (\#Trp)(5{,}500) \times (\#Tyr)(1490) \times (\#disulfides)(125) \qquad (2.1)$$

The extinction coefficients for the single tryptophan-to-phenylalanine substitutions were calculated to be 47,900 $M^{-1}cm^{-1}$, 36,900 $M^{-1}cm^{-1}$ for the double substitutions, and 25,900 $M^{-1}cm^{-1}$ for the triple substitutions. The tryptophan-less enzyme had a calculated extinction coefficient of 14,900 $M^{-1}cm^{-1}$.

Equilibrium Denaturation. Stock solutions of 10 M urea were prepared in 10 mM potassium phosphate buffer, pH 8.3, with 20 mM KCl and 50 μM $CoCl_2$. Final

concentrations of denaturant stock solution were measured by calculating the refractive index of the buffer and the denaturant stock solution as described (*71*). Stock solutions of enzyme were prepared in phosphate buffer pH 8.3 with 20 mM KCl and 50 μM $CoCl_2$ so that the addition of 250 μL of enzyme stock solution added to the samples would produce the final desired enzyme concentration. Stock solutions of denaturant, buffer, and stock enzyme were added to 12 x 75 mm Durex^{TM} borosilicate culture tubes to produce a final volume of 3 mL. Final denaturant concentrations ranged from 0 – 8 M urea. Samples were allowed to incubate overnight (≥ 18 hours) at 25 ˚C in the presence or absence of denaturant.

Intrinsic Tryptophan Fluorescence. Fluorescence measurements were acquired with an Aviv Model ATF 105 spectrofluorometer 10 mM potassium phosphate buffer pH 8.3, with 20 mM KCl and 50 μM $CoCl_2$. Kinetic measurements were performed at a protein concentration of 125 μg/mL in 3 mL quartz cuvettes with a path length of 1 cm; samples were stirred gently during measurements. An excitation wavelength of 278 nM and an emission wavelength of 320 nM were used. Measurements were averaged over 30 seconds. Raw fluorescence kinetic data were converted to fractions of enzyme folded, f_f, with the equation

$$f_f = \frac{y_{\min} - y}{y_{\min} - y_{\max}} \tag{2.2}$$

where y_{max} is the maximum kinetic measurement over the range of measurements in increasing denaturant concentrations, y_{min} is the minimum kinetic measurement of the

range of measurements, and y is the kinetic measurement at a particular denaturant concentration.

ANS Dye Binding Studies. ANS (8-anilinonaphtalene-1-sulphonate) dye binding studies were performed by combining 20 μL of a 2 mM stock concentration of ANS to 3 mL of a 125 μg/mL enzyme solution containing 0 M – 8 M urea to reach a final ANS concentration of 13 μM. This provided a final ANS:OPH ratio of 18.8:1. ANS:OPH samples were incubated at 25 ˚C in the dark for 2 hours prior to analysis. An excitation wavelength of 370 nM was used and measurements recorded from 650 nM to 450 nM. All solutions were made in 10 mM potassium phosphate buffer, pH 8.3, with 20 mM KCl and 50 μM $CoCl_2$.

Equilibrium Unfolding Curves. The linear extrapolation method (LEM) was used to measure the conformational stability of OPH according to the equation

$$\Delta G = \Delta G_{water} - m[denaturant] \tag{2.3}$$

ΔG is the conformational stability of the enzyme at a particular denaturant concentration (kcal/mol), ΔG_{water} is the conformational stability of the enzyme in the absence of denaturant (kcal/mol) and *m* is the dependence of the conformational stability on the denaturant concentration.

OPH::Zn^{2+} has been shown to unfold via the three-state unfolding pathway where N_2* represents the active (*), natively folded homodimer, I_2 represents the inactive, dimeric intermediate, 2U represents the inactive unfolded monomers and K_1 and K_2 represent the equilibrium constants of the unfolding transitions (*14*).

Scheme 2.1

$$N_2 * \xleftrightarrow{K_1} I_2 \xleftrightarrow{K_2} 2U$$

The same unfolding pathway has been assumed for OPH::Co^{2+} and the OPH variants discussed in this study.

The total protein concentration, P_T, can be represented by the equation

$$[P_T] = [N_2] + [I_2] + [U] \tag{2.4}$$

and the mole fraction of the natively folded enzyme, f_N, the dimeric intermediate, f_I and the unfolded monomeric subunits, f_U, can be expressed by the following equations (*14*).

$$f_N = \frac{[N_2]}{[P_T]} \tag{2.5}$$

$$f_I = \frac{[I_2]}{[P_T]} \tag{2.6}$$

$$f_U = \frac{[U]}{[P_T]} \tag{2.7}$$

The total mole fractions of the various species of folded states at equilibrium can be represented by the expression

$$f_N + f_I + f_U = 1 \tag{2.8}$$

The equilibrium constants of the two unfolding transitions, K_1 and K_2 can now be related to the mole fraction of each species by the equations

$$K_1 = \frac{f_I}{f_N} \tag{2.9}$$

$$K_2 = \frac{f_u^{\,2}[P_T]}{f_I} \tag{2.10}$$

Using a three-state model of unfolding, the equilibrium constants can be used to calculate the total conformational stability of the enzyme (ΔG_{TOTAL}) with the relationship

$$\Delta G_{TOTAL} = (-RT \ln K_1) + (-RT \ln K_2) \tag{2.11}$$

Origin® 7 SRI v7.03 (OriginLab Corporation, North Hampton, MA) was used for nonlinear least-squares fitting of the above equations to the spectroscopic data determined from fluorescence measurements.

Circular Diochroism. CD spectra were acquired with an Aviv Model 202 SF spectrometer with 10 mM potassium phosphate buffer pH 8.3, with 20 mM KCl and 50 μM $CoCl_2$. Far UV wavelength scans were performed at an enzyme concentration of 63 μg/mL in 3 mL quartz cuvettes. Measurements were taken in 1 nM steps from 250 nM to 200 nM and averaged for 5 seconds at every step increment. Cuvettes had a path length of 1.0 cm. Raw CD signal (milli degrees) were converted to molar ellipticity (deg cm^2 $dmol^{-1}$) with the equation

$$[\theta] = \frac{\theta_{obs} \times MW}{10 \times l \times c \times n} \tag{2.12}$$

where *[θ]* is the molar ellipticity (deg cm^2 $dmol^{-1}$), θ_{obs} is the raw CD signal in millidegrees, *MW* is the molecular weight of the enzyme, *l* is the path length in cm, *c* is the concentration in g/mL of enzyme, and *n* is the number of amino acids in the enzyme.

RESULTS

Far-UV CD Spectrometry. Wild type OPH has the structure of a distorted $(\alpha\beta)_8$ barrel with 8 parallel β-sheets surrounded by 14 α-helices. The far-UV CD spectrum of the wild type and the tryptophan-to-phenylalanine substitutions all displayed two minimum at 208 nM and 222 nM, characteristic of a protein with a high α-helical content. Since the spectra of the individual tryptophan-to-phenylalanine structures did not significantly differ from that of the wild type spectra, it can be concluded that they shared a similar overall structure to that of the wild type enzyme. The spectra are displayed in Figure 2.4.

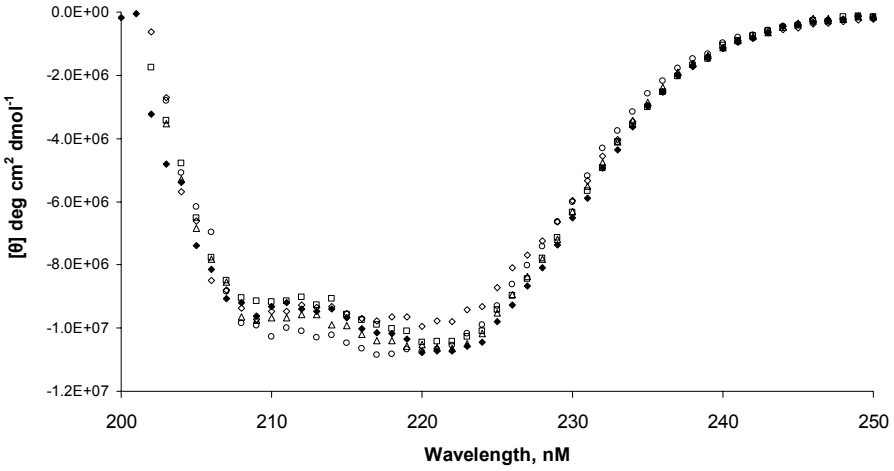

Figure 2.4: Far-UV CD wave scans of tryptophan-to-phenylalanine substitutions. Wild type OPH::Co^{2+} (♦), W69F (□), W131F (Δ), W277F (◊) and W302F (○) concentrations were 63 μg/mL.

Equilibrium Denaturation. The equilibrium unfolding profiles of wild type enzyme and the tryptophan-to-phenylalanine substitutions were followed by intrinsic tryptophan fluorescence. The equilibrium unfolding curves are shown in Figure 2.5. Enzyme concentrations of 125 μg/mL were used in all cases so that the unfolding intermediate could be seen.

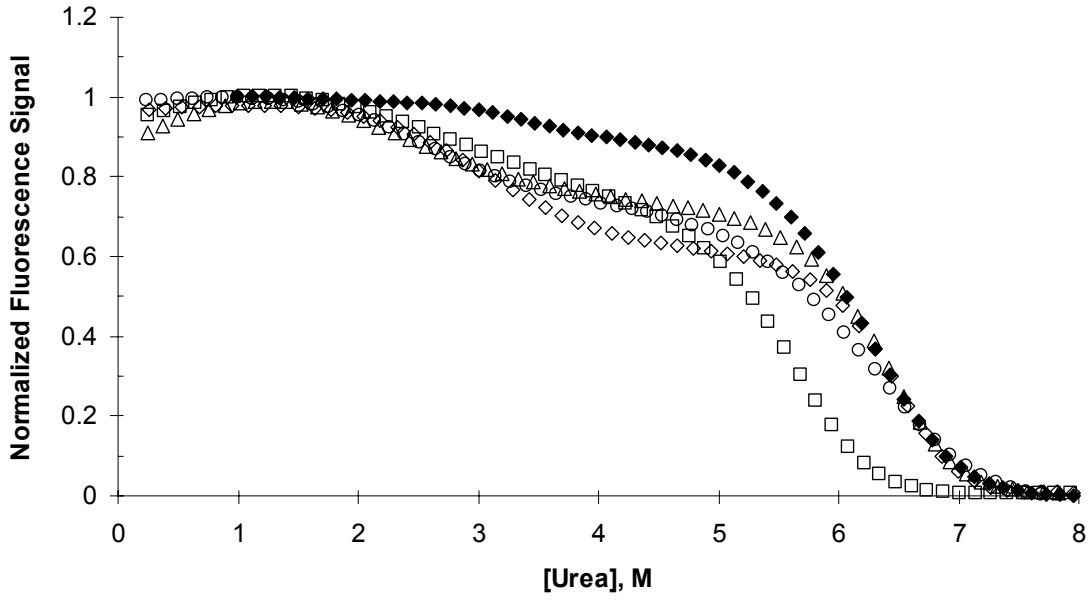

Figure 2.5: Equilibrium denaturation unfolding of wild type and single tryptophan-to-phenylalanine substituted enzymes. The unfolding data for each variant was fit to a three-state unfolding curve (*14*). Wild type OPH::Co^{2+} (♦), W69F (□), W131F (Δ), W277F (◊) and W302F (○) concentrations were 125 μg/mL.

Equilibrium denaturation unfolding profiles were determined for each of the single tryptophan-to-phenylalanine variants (three tryptophan residues remaining per subunit). In all cases, the wild type and tryptophan-to-phenylalanine variants reflected the presence of a stable folding intermediate which was observed at 3 – 5 M urea. The W69F variant showed a final unfolded state at 6.5 M urea, while wild type and the other tryptophan-to-phenylalanine substitutions showed an unfolded state at 7.0 M urea. The transition midpoints for the unfolding of the dimeric intermediate into the monomeric subunits were the most striking aspects of the unfolding curves. For all of the enzymes except W69F, the midpoints are found at 6.3 – 6.4 M urea. The midpoint for the second unfolding transition is found at 5.5 M urea. The unfolding data for each enzyme was fit to a three-state equation and the resultant conformational stabilities of each variant and wild type enzyme are determined and listed in Table 2.1.

Table 2.1: Conformational stabilities of wild type OPH and the W-to-F variants.

Enzyme[a]	ΔG_1[b]	ΔG_2[b]	ΔG_{Total} ($\Delta G_1 + \Delta G_2$)[b]	m_1[b]	m_2[b]
WT	4.1 ± 1.0	22.5 ± 3.0	26.6 ± 4.0	-0.9 ± 0.3	-2.2 ± 0.5
W69F	1.3 ± 1.0	22.3 ± 2.0	23.6 ± 3.0	-0.7 ± 0.3	-2.4 ± 0.3
W131F	3.2 ± 1.0	19.3 ± 2.0	22.5 ± 3.0	-1.3 ± 0.5	-1.7 ± 0.2
W277F	3.3 ± 1.0	28.3 ± 3.0	31.6 ± 4.0	-1.1 ± 0.2	-3.1 ± 0.4
W302F	1.5 ± 1.0	25.2 ± 2.0	26.7 ± 3.0	-0.1 ± 0.2	-2.6 ± 0.3

[a] All enzymes are the Co^{2+} / Co^{2+} - substituted form of OPH.

[b] All values are reported in units of kcal/mol.

ANS Dye Binding. The ANS fluorescence emission profiles for the wild type and single tryptophan substituted enzymes are overlaid in Figure 2.6. The emission profiles for all enzymes incubated with ANS have a similar λ_{max} values except for that of the W302F-ANS complex. The λ_{max} is significantly blue shifted in comparison to the emission spectra of the other enzyme-ANS complexes suggesting W302F enzyme provides a more non-polar environment for the ANS probe than do the other enzymes.

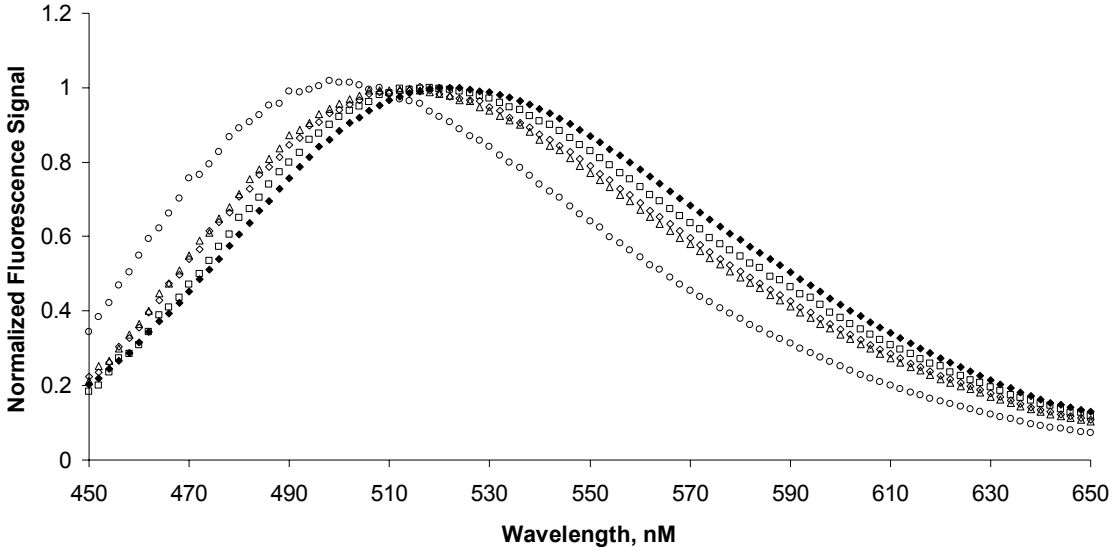

Figure 2.6: ANS dye binding studies. Fluorescence emission spectra are shown for wild type OPH::Co^{2+} (♦), W69F (□), W131F (Δ), W277F (◊) and W302F (○). The enzyme ANS ratio was 18.8:1 with an enzyme concentration of 125 μg/mL.

Enzymatic Activity Measurements. A stock solution of 8.0 mM demeton-S was made in tripart buffer (50 mM MES, 25 mM N-ethylmorpholine, and 25 mM diethanolamine) with 1% (v/v) methanol at pH 8.0. Hydrolysis of demeton-S produces a free thiol on the leaving group which reacts with 2,2-dithiodipydidine (2,2 TP) to produce 2-thiopydidone (2-TP). Hydrolysis reactions were initiated by the addition of substrate to a final volume of 1 mL and measured in a spectrophotometer. The production of 2-TP (ε_{343} = 7,060 M^{-1} cm^{-1}) was followed for 1 minute at 25 ˚C in a spectrophotometer using a 1 mL disposable cuvette with a path length of 1 cm. Activity is reported as μmoles of 2-TP produced per second. Activity versus substrate concentration was fit with the standard Michaelis-Menten equation

$$v_o = \frac{V_{MAX} \times [A]}{K_M + [A]} \tag{2.13}$$

A stock solution of 10 mM paraoxon was made in water as previously described (*14*). Reactions were carried out in 20 mM CHES buffer, pH 9.0. Hydrolysis of paraoxon produces *p*-nitrophenol (ε_{400} = 17,000 M^{-1} cm^{-1}) which was followed for 1 minute at 25 ˚C with a spectrophotometer. Activity is reported as μmoles of *p*-nitrophenol produced per second. Activity versus substrate concentration was fit with equation 2.13 and the catalytic parameters listed in Table 2.2.

Table 2.2: Catalytic parameters for the wild type and tryptophan-to-phenylalanine substituted enzymes.

	Paraoxon			Demeton-S		
	K_M (mM)	k_{cat} (sec^{-1})	k_{cat}/K_M (M^{-1} sec^{-1})	K_M (mM)	k_{cat} (sec^{-1})	k_{cat}/K_M (M^{-1} sec^{-1})
WT	0.1 ± 0.02	1.2×10^4	1.1×10^8	4.8 ± 0.2	4.2	8.7×10^2
W69F	0.1 ± 0.05	1.0×10^1	1.2×10^5	3.5 ± 0.2	0.5	1.5×10^2
W131F	0.1 ± 0.01	1.1×10^4	1.1×10^8	3.1 ± 0.2	1.6	1.1×10^3
W277F	0.1 ± 0.03	1.3×10^4	1.8×10^7	2.1 ± 0.2	0.8	3.8×10^2
W302F	0.1 ± 0.04	2.0×10^2	3.0×10^6	1.9 ± 0.2	0.3	1.6×10^2

DISCUSSION

Tryptophan Residues Play a Large Role in the Stability and Activity of OPH. Examination of the far-UV circular dicroism of the wild type and single tryptophan substitution variants indicated similar secondary structure between all enzymes (Figure 2.4). All displayed a characteristic α-helical signal in keeping with the structure of the wild type enzyme.

The equilibrium unfolding of all the enzymes as monitored by intrinsic tryptophan fluorescence indicated that they all unfolded via a three-state unfolding pathway (Figure 2.5). All enzymes displayed a mid-transition between 3 and 5 M urea indicative of the presence of a stable folding intermediate. The fluorescence contribution of each variant was similar with some slight differences. The pre-transition midpoint for each enzyme was similar and ranged from 2.8 M urea (W131F) to 3.2 M urea (wild type). The most striking difference was that displayed by W69F at the midpoint of the second unfolding transition which was found to occur at 5.5 M urea; the

midpoints of the other enzymes were found to be approximately 6.3 and 6.4 M urea. W69 is located in the interface region of the enzyme amid several aromatic staking interactions. The removal of the tryptophan might result in a less stable interface region that caused the intermediate to dissociate into monomeric subunits at lower urea concentrations. It is also possible that the W69 residue acted as the primary reporter for the dissociation of the dimeric intermediate into monomeric subunits. Removal of this fluorophore might result in a reduction of fluorescence signal for the enzyme as the dimeric intermediate disassociated. Another striking difference was observed in the profile of the wild type enzyme in relation to the other enzymes. It appeared to have a greater percentage (15 – 20% at 5.0 M urea) of folded enzyme in elevated denaturant concentrations. It is difficult to know if these unfolding profiles reflected the actual three-dimensional states of the variant enzymes relative to the wild type or if they were just relative of the general fluorescent properties of the individual enzymes with removed fluorophores.

Examination of Table 2.1 indicated that the apparent conformational stability (ΔG_{TOTAL}) is similar between enzymes. The stabilities for the first unfolding transitions of the enzymes (ΔG_1) had the most striking differences. W69F and W302F, both of which are involved in extensive stacking interactions appeared to reflect the lowest stabilities and the wild type enzyme had the largest stability of the first unfolding transition ($N_2^* \leftrightarrow I_2$).

The *m*-values calculated from the three-state unfolding of the enzymes are also listed in Table 2.1 Denaturant *m*-values represent the dependence of the free energy of

unfolding on the denaturant concentration and are correlated with the amount of protein surface (ASA) exposed to the solvent upon unfolding (*72*). The *m*-values generated for the unfolding of the first transition are identical within standard deviation of one another. The *m*-values for the second unfolding transition are similar for all enzymes with the greatest differences shown for W131F and W277F. These values represent the amount of surface area exposed upon the unfolding based on the positions of the remaining fluorophores in the molecule and do not provide much information on how these localized regions are unfolding. It is difficult to know if these apparent stabilities and *m*-values are representative of the actual properties of the variant enzymes or if the alteration in the fluorescence signal caused by the absence of a particular fluorophores resulted in reduction of the calculated stabilities and associated parameters.

ANS was used to probe the topology of the active sites of the wild type and variant enzymes. ANS is known to bind in the hydrophobic pocket of the active site and has been shown to be displaced by the addition of the competitive inhibitor, coumarin (*67*). The fluorescence emission scans of ANS are shown in Figure 2.6. The λ_{MAX} for the ANS binding was similar in all of the enzymes except that of W302F. W302 participates in an aromatic stacking network that forms part of the large pocket of the active site. Replacement of this residue shifted the ANS fluorescence signal towards shorter wavelengths, suggesting that the topology of the active site may not be as conserved with this enzyme as it is with the other tryptophan-to-phenylalanine substitutions.

The catalytic activity of each of the enzymes was measured against paraoxon (P-O hydrolysis) and demeton-S (P-S hydrolysis). Each of the enzymes was able to hydrolyze both substrates which implied that the removal of the tryptophan residues had not compromised the ability of the enzyme to reach a folded, active conformation. Not all of the enzymes hydrolyzed the substrates as efficiently as did the wild type, which suggested that the tryptophan-to-phenylalanine substitutions resulted in some unfavorable perturbations to the enzyme's structure. The catalytic parameters for the single tryptophan replacements are listed in Table 2.2.

While the catalytic activities of the wild type, W131F, and W277F enzymes against paraoxon are similar, the activities of W69F and W302F are 0.5 % and 1.5 %, respectively, of the activity of the wild type enzyme. They are less efficient in the hydrolysis of paraoxon and suggested that, while the enzyme did retain activity, the structure of the enzyme and active site had been affected. Since W302F is involved in an active site stacking network with residues important in the metal coordination and activity of the enzyme, it was not surprising that replacement of this residue resulted in an alteration of the kinetic profile. W69 is located in an interface stacking network near (in tertiary structure) the small pocket of the active site. It is possible that replacement of this residue resulted in perturbations to the active site structure. Additionally, replacement of this residue may have introduced considerable strain into the interface region. Since the dimerization of TIM barrels has been shown to be necessary to maintain optimum topology of the active site for catalysis (*73*), any strain or disruption

introduced in the interface could have negative consequences for the activity of the enzyme.

The hydrolysis of demeton-S by OPH is much slower (approximately 10^5 times) than it is for paraoxon (*74*) and these changes are reflected in the catalytic parameters represented in Table 2.2. The differences between variants are not as striking as they are with paraoxon. However, the activities (M^{-1} sec^{-1}) for the W69F and W302F variants are the lowest of the enzymes tested, thus reflecting their strained abilities.

In a similar study, the replacement of tryptophan with a phenylalanine residues in α-lactalbumin suggested that the substitution could have significant changes (≥ 2.4 kcal/mol) in the conformational stabilities of proteins (*75*). If the energy required to unfold the active native state of OPH into an inactive dimeric intermediate is only 4 kcal/mol, it is reasonable to propose that these changes could have an adverse effect upon the activity of the enzyme.

The differences in the catalytic activities between enzymes are most likely not due to variations in protein concentrations but are representative of the perturbations in operational stability caused by the tryptophan-to-phenylalanine substitutions. These enzymes do not resemble the wild type enzyme based on activity and it is reasonable to assume that their overall structure and/or active site topologies have been compromised due to these changes.

Removal of All of the Tryptophan Residues Resulted in an Unstable Enzyme.

None of the triple or the quadruple tryptophan-to-phenylalanine changes possessed any catalytic activity against paraoxon or demeton-S. Western-blots indicated

that the W^{η} and W^{Φ} enzymes had been expressed. It was concluded that these enzymes did not fold into active conformations and any unfolding profile that might be generated from these enzymes would not accurately reflect the unfolding profile of the wild type enzyme. Additionally, it is reasonable to assume that the insertion of any single tryptophan residue into the inactive W^{Φ} enzyme would most likely not restore the stability and activity possessed by the wild type enzyme.

Conclusions. From these results it can be concluded that the tryptophan residues in OPH are important in the stability and activity of the enzyme, and their removal had negative consequences for the function of the enzyme. It must therefore be concluded that the triple tryptophan substitutions may not share the same unfolding profile of the wild type enzyme since they do fold into an active conformation. Additionally, the use of a tryptophan-less enzyme for the insertion of tryptophan probes would not be a feasible model to study the localized unfolding of individual regions of the OPH enzyme. While tryptophan-to-phenylalanine substitution studies have successfully helped to produce detailed localized unfolding information for various other enzymes (*58, 59, 76-78*), this technique has not been successful for OPH. Thus, attention must be turned to alternate methods to elucidate the unfolding profile of OPH.

CHAPTER III

THE SIMILARITIES AND DIFFERENCES IN THE UNFOLDING PROFILES OF THERMAL AND CHEMICAL DENATURED OPH

Limited proteolysis is an eloquent way to follow the unfolding of an enzyme as the technique can be used to detect subtle, localized conformational changes in protein structure, often before they can be detected spectroscopically (*79-82*). Modeling studies have shown that a proteolytic event requires a conformational change (local unfolding) of at least 10 - 12 residues (*83, 84*). The targets for proteolytic enzymes are flexible loop regions where the local packing does not inhibit the localized unfolding of the substrate protein. These loops are usually solvent exposed and thus readily come in contact with the proteolytic enzyme (*84, 85*). The solvent exposed surface of a substrate peptide may have many potential sites for cleavage by a proteolytic enzyme. They are cleaved only if they have the necessary flexibility and accessibility to the proteolytic enzyme. It is possible to develop a map of unfolding for the peptide substrate by determining the identity of these cleaved protein fragments.

The chemical equilibrium unfolding profile of OPH::Zn^{2+} has been well characterized by spectroscopic methods and reported to proceed through an inactive, well-populated homodimeric intermediate (*14*). The thermal denatured unfolding profile of OPH::Co^{2+} has been examined by capillary electrophoresis and was reported to have a well populated and active unfolding intermediate at approximately 45 ˚C with an irreversible inactivation step at approximately 58˚ C (*86*). Unfortunately, detailed

spectroscopic studies have not been performed on OPH::Co^{2+}. Since the Co^{2+} form of the enzyme is the most active metal form of the enzyme (*6, 66*), it is an important target for study of the unfolding process to aid application technologies. Intrinsic tryptophan fluorescence, far UV circular dichroism, and proteolysis by thermolysin were used to investigate the unfolding and the formation of the dimeric intermediate of OPH under thermal and chemical-denaturing solvent conditions. Since the chemical denatured dimeric intermediate is inactive, it would be advantageous to understand how this enzyme proceeds from its native state to that of the intermediate state. To this end, this study investigates this enzyme's unfolding pathway and correlates it with the loss of activity upon denaturation. The following issues are considered: (i) OPH::Co^{2+} unfolds under thermal and chemical denaturing conditions to form an active and an inactive dimeric intermediate, respectively. (ii) Two intersubunit salt bridges are implicated in contributing to the differences between the thermal and chemical denatured intermediates and their relative activities. (iii) Structural rearrangements around the active-site take place that provide an increase in the catalytic activity of OPH::Co^{2+} at elevated temperatures and low denaturant concentrations.

MATERIALS AND METHODS

Materials. Paraoxon and demeton-S were obtained from ChemService (Westchester, PA) and prepared as previously described (*54, 68*). All buffer and assay reagents (DTNB, CHES, TRIZMA, MES, N-ethylmorpholine, diethanolamine, potassium phosphate, EDTA, $CoCl_2$, $ZnCl_2$, $CaCl_2$) were obtained from Sigma (St. Louise, MO). Thermolysin from *Bacillus thermoproteolyticus rokko* was also purchased

from Sigma (St. Louise, MO) and used without any further purification. Media components for cell growth (Bacto-Tryptone, Yeast Extract, Bacto-Agar, Difco™ Terrific Broth) were obtained from Fisher Scientific (Pittsburgh, PA). *Escherichia coli* DH5α (*supE44* Δ*lacU169* [*Φ80 lacZΔM15*] *hsdR17 recA1 endA1 gryA96 thi-1 relA1*) was used to express the bacterial OPH from pUC19-*opd*.

Growth and Purification of OPH. OPH was produced and purified as previously described (*14*), with the following modifications. Immediately following concentration to ≥ 2 mg/ml, the enzyme was dialyzed against 10 mM TRIZMA buffer, pH 8.0, containing 50 μM $CoCl_2$ and 200 mM KCl. The sample was then loaded onto a Superdex 200 gel filtration column as a final purification step. OPH containing fractions were pooled and concentrated to ≥ 2 mg/mL. The KCl was removed from the concentrated protein by dialysis against a solution of 10 mM TRIZMA buffer, pH 8.0, containing 50 μM $CoCl_2$. The purity of the sample was assessed by SDS-PAGE. The extinction coefficient (ε_{280} = 58,000 M^{-1} cm^{-1}) was used to determine the concentration of OPH.

Limited Proteolysis of OPH. One mL of a 1 mg/mL solution of OPH, containing 7 mM $CaCl_2$ in 10 mM TRIZMA buffer, pH 8.0, was thermal-equilibrated for 10 minutes prior to addition of thermolysin. Temperatures ranged from 25 ˚C to 75 ˚C in 10 ˚C increments. Thermolysin was used to digest OPH, since this protease retains function throughout this range of temperatures (*87*). Thermolysin was added to the mixture to achieve an enzyme:substrate ratio of 1:100, mixed gently, and returned to the water bath for the duration of the experiment. Samples were taken from 0 to 90 minutes

in 10 minute intervals, removing 15 μL of reaction and adding 5 μL of 50 mM EDTA, pH 7.0 to stop the reaction. For urea denatured samples, OPH (1 mg/mL) in TRIZMA buffer, pH 8.0, 7 μM CaCl2, 50 μM $CoCl_2$ was incubated in varying concentrations of urea for 18 hours at 25 ˚C prior to the addition of the protease. Thermolysin was added to the mixture to achieve a 1:50 enzyme : substrate ratio. At selected time points, 15 μL samples were removed and the proteolysis reaction stopped with the addition of 5 μL 50 mM EDTA, pH 7.0

Activity Profile of Thermal Denatured OPH. OPH was prepared, thermally denatured, and proteolyzed as described above. The proteolysis of OPH was monitored by the rate of hydrolysis of demeton-S at each sampled temperature. Demeton-S was chosen as a substrate for this experiment as it allowed for the proteolyzed enzyme to be transferred directly from the denaturation reactions to the enzyme activity assays without any further dilution. At 10 minute intervals, 10 μL of sample was removed and mixed with 990 μL of prepared demeton-S to a final concentration of 4 mM demeton-S in tripart buffer (50 mM MES, 25 mM N-ethylmorpholine, and 25 mM diethanolamine) with 1% (v/v) methanol at pH 8.0. Hydrolysis of demeton-S produces a free thiol on the leaving group which reacts with 2,2-dithiodipydidine (2,2 TP) which produces 2-thiopydidone (2-TP). The production of 2-TP (ε_{343} = 7,060 M^{-1} cm^{-1}) was followed for 1 minute in a spectrophotometer using a 1 mL disposable cuvette with a path length of 1 cm. Activity is reported as μmoles of 2-TP produced per second. Samples of thermolysin digested OPH were also subjected to analysis by SDS-PAGE (15% separating gel, 4% stacking gel), stained with Coomassie Blue R-250 stain, destained,

washed with distilled water, backlit and imaged. The Total Lab analysis package for 1D gels (Nonlinear Dynamics) was used for densitometric analysis of the gel bands.

Equilibrium Denaturation. Stock solutions of 10 M urea or 5 M GdnHCl were prepared in 10 mM potassium phosphate buffer, pH 8.3, with 20 mM KCl and 50 μM $CoCl_2$. Final concentrations of denaturant stock solution were measured by calculating the refractive index of the buffer and the denaturant stock solution as previously described (*71*). Stock solutions of enzyme were prepared in phosphate buffer pH 8.3 with 20 mM KCl and 50 μM $CoCl_2$ so that the addition of 250 μL of enzyme stock solution added to the samples would produce the final desired enzyme concentration. Stock solutions of denaturant, buffer, and stock enzyme were added to 12 x 75 mm Durex^{TM} borosilicate culture tubes to produce a final volume of 3 mL. Final denaturant concentrations ranged from 0 – 9 M urea or 0 – 4.25 M GdnHCl. Samples were allowed to incubate overnight (≥ 18 hours) at 25 ˚C in the presence or absence of denaturant.

Intrinsic Tryptophan Fluorescence. Fluorescence measurements were acquired with an Aviv Model ATF 105 spectrofluorometer. Samples were maintained in 10 mM potassium phosphate buffer pH 8.3, with 20 mM KCl and 50 μM $CoCl_2$. Emission scans were performed with protein concentrations of 50 μg/mL in 3 mL quartz cuvettes with a path length of 1 cm. Samples were stirred gently during measurements. As a control, wild type OPH was incubated for 18 hours at 25 ˚C in 0, 4, or 8 M urea or 0, 2, or 4 M GdnHCl. Emission wave scans of OPH::Co^{2+} were performed with enzyme concentrations of 50 μg/mL; an excitation wavelength of 278 nM was used and the emission of the sample recorded from 310 nM to 400 nM. Wavelength scans of buffer

without enzyme were subtracted from wave scans of enzyme to remove any contribution of buffer to the fluorescent signal.

ANS Dye Binding Studies. ANS (8-anilinonaphtalene-1-sulphonate) dye binding studies were performed by combining 20 μL of a 2 mM stock concentration of ANS and 3 mL of a 50 μg/mL enzyme solution ranging from 0 M – 8 M urea or 0 M – 5 M guanidine HCl to reach a final ANS concentration of 13 μM. This provided a final ANS:OPH ratio of 18.8 : 1.0. ANS:OPH samples were incubated at 25 ˚C in the dark for 2 hours prior to analysis. An excitation wavelength of 370 nM was used and the fluorescent response was recorded from 650 nM to 400 nM. All solutions were adjusted to 10 mM potassium phosphate buffer, pH 8.3, with 20 mM KCl and 50 μM $CoCl_2$.

Circular Diochroism. CD spectra were acquired with an Aviv Model 202 SF spectrometer. Samples were diluted into 10 mM potassium phosphate buffer pH 8.3, with 20 mM KCl and 50 μM $CoCl_2$. Apparent thermal stability was estimated from the change in the CD signal at 230 nM with temperature. An averaging time of 60 seconds and a temperature equilibration time of 5 minutes were monitored at every step. Measurements were recorded every 1˚C from 25 ˚C to 95 ˚C. Raw thermal CD signal was converted to fraction of enzyme unfolded, f_u, with the equation

$$f_u = \frac{y_{\max} - y}{y_{\max} - y_{\min}} \tag{3.1}$$

where y_{max} is the maximum signal over the range of temperatures, y_{min} is the minimum signal and y is the signal at a given temperature.

Determination of k_p. The digestion of thermal and chemical denatured OPH by thermolysin was followed by SDS-PAGE analysis. Densitometric evaluations of the gels were performed, and the decrease in peak areas of the intact enzyme followed pseudo-first order reactions and the rate constants of proteolysis, k_p, was determined using the following equation:

$$2.3 \log \frac{S_o}{S} = k_p \times t \tag{3.2}$$

where S_0 is the peak area at a reference time point and S is the peak area at another time point and t is the time interval between those two points. Ten sample points of peak area versus time were plotted for each temperature between 25 and 65 °C in 5 °C increments and repeated twice.

N-Terminal Sequencing. Samples of the digestion of OPH by thermolysin were prepared as described above. From each reaction, 15 µL of sample was combined with 4 µL of SDS sample buffer and run on a 4% stacking, 15% separating SDS-PAGE at 100 volts for 1 hour. The separated protein was then electroblotted onto a Millipore Immobilon –P^{SQ} PVDF Transfer Membrane (0.2 µm pore) at 100 mA overnight at 4 ˚C using a Bio-Rad Mini Trans-Blot Cell in CAPS buffer, pH 11.0 with 10% (v/v) methanol. The PVDF membranes were stained with Amido Black for 1 minute, destained with repeated washes of a 1% acetic acid solution until the protein bands were clearly visible and the background was reduced. Membranes were then washed in MilliQ water and air dried. Prominent bands were cut from the membrane and placed in a clean, 1.5 mL microcentrifuge tube and submitted to the Protein Chemistry Laboratory

(Texas A&M University) for N-terminal sequencing. The first 5 or 6 residues from each fragment were sequenced on a Hewlett Packard G1000A Automated Protein Sequencer.

Mass Spectrometry. The digestion of OPH by thermolysin was stopped by the addition of 5 μL of 50 mM EDTA, pH 7.0, and submitted to the Laboratory of Biological Mass Spectrometry (Texas A&M University) for analysis on an ABI Voyage-DE STR MALDI-TOF Mass Spectrometer. Samples were mixed with alpha-cyano-4-hydroxy-cinnaminic acid, spot dried and analyzed.

RESULTS

The native OPH enzyme has a 29 amino acid leader sequence that appears to be post-translationally processed resulting in an N-terminus of OPH beginning at S30 (*29, 35, 41*). The *opd* used in this investigation does not code for the native leader sequence; the OPH gene product begins at amino acid 30 and ends at 365. The flexible regions, D253 – S276 (termed the "271 loop" for the remainder of this study; Table 3.1) and F306 – V320 (termed the "309 loop" for the remainder of this study; Table 3.1) are both characterized by little secondary structure and high crystallographic *B* values (*2*). The terms used in this study are summarized in Table 3.1. The enzymes used in this study are the OPH::Co^{2+} populated species.

Table 3.1: Nomenclature and identification of regions referred to in this study.

Designation[a]	Fragments	Structure[b,c]
WT OPH	S30 - S365	α/β_8 TIM Barrel
271 Loop	D253 - S276	A266 - L272 α-helix
309 Loop	F306 - V320	I313 - V320 α-helix

[a] Loops are named according to the identity of the proteolytic cut site.
[b] According to the crystal structure 1dpm (4).
[c] Unless otherwise specified, the structure is a random coil.

Activity, Fluorescence, and CD Unfolding Profiles of OPH::Co^{2+}. The unfolding of OPH::Co^{2+} as followed by fluorescence shows the dimeric intermediate forming in the presence of 3 – 4 M urea (Figure 3.1). At 3.5 M urea, the population of enzyme retained approximately 68 % of its maximal activity. The enzyme began to dissociate into its monomeric subunits at 5 M urea at which point only 8 % of the original activity remained. No activity could be detected in 5.5 M urea.

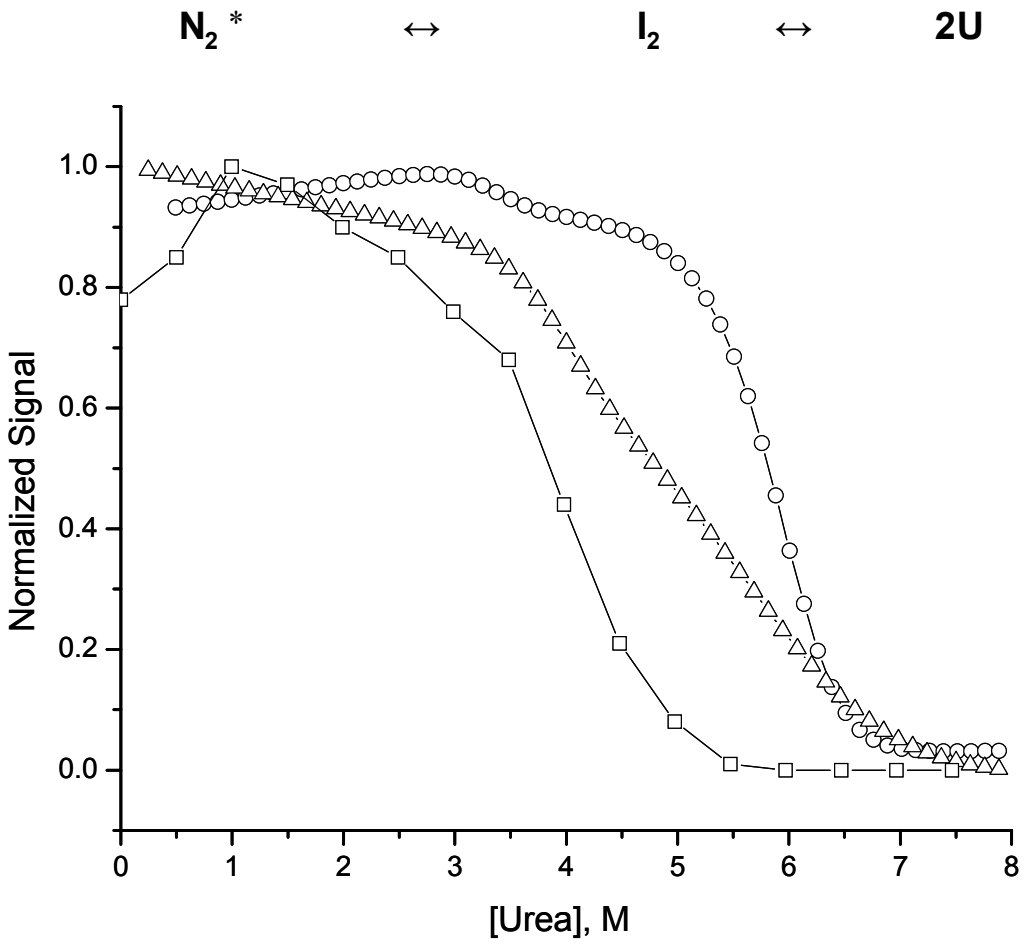

Figure 3.1: Unfolding profile of OPH::Co^{2+} in chemical denaturing conditions. Unfolding progress is shown as followed by activity (□), intrinsic tryptophan fluorescence (○), and circular dichroism (Δ). The enzyme concentrations were 50 μg/mL. Each graphical trace was normalized to its maximum signal. The unfolding scheme (N_2* ↔ I_2 ↔ 2U) was assumed (*14*).

The stabilities for the unfolding transitions for OPH::Zn^{2+} were found to be ΔG_1 = 4.3 ± 0.26 kcal/mol, ΔG_2 = 36.1 ± 1.9 kcal/mol (*14*). In the current study, the unfolding transitions for OPH::Co^{2+} were found to be ΔG_1 = 4.1 ± 0.99 kcal/mol and ΔG_2 = 22.5 ± 3.4 kcal/mol. The first transition ($N_2^* \leftrightarrow I_2$) is similar between the two metal forms, and each possessed a ΔG_1 of approximately 4 kcal/mol, but the second transitions ($I_2 \leftrightarrow 2U$) were very different. This suggested that the unfolding pathway of the first transition of the two metal forms of OPH were similar and that the metal ions in the active site are significant contributors to the stability of the dimeric intermediates.

The extent of unfolded secondary structure increased sharply at 3.5 M urea, as shown by circular dichroism. This coincides with the formation of the intermediate at 3.5 M urea as seen by fluorescence monitoring. Both the fluorescence and CD signals showed an unfolded enzyme at 7 M urea. The non-superimposable fluorescence and CD unfolding transitions suggested that the OPH::Co^{2+} enzyme had a stable unfolding intermediate much like the unfolding process of the OPH::Zn^{2+} enzyme (*14*).

Fluorescence emission scans were used to monitor the effect that nicking had on the tertiary structure of OPH (Figure 3.2). OPH that was incubated at 25 ˚C in the presence of a 1:100 enzyme:substrate ratio for 78 hours showed that nicking by the protease had little effect on the tertiary structure of OPH when compared to OPH that had not been incubated with the protease. Both samples possessed the same fluorescence intensity suggesting a lack of quenching of the fluorophores by the solvent. The digested OPH showed a maximum wavelength slightly red-shifted compared to that

of the undigested enzyme (334 nM versus 332 nM) suggesting a slight relaxation of enzyme structure.

Fluorescence emission scans were also used to monitor the effect of denaturation by urea and GdnHCl on the tertiary structure of OPH. A comparison of WT OPH incubated in 8 M urea for 18 hours and WT OPH not incubated in urea shows a striking difference in fluorescence emission wave scans (Figure 3.2). The sample digested in 8 M urea was red-shifted compared to the sample not incubated in urea (356 nM versus 332 nM). This suggested that the fluorophores of this denatured enzyme were exposed to the solvent. Additionally, there was a slight decrease in the fluorescence intensity signifying that the fluorescence intensity was quenched by the solvent. A comparison of emission scans of WT OPH incubated in the presence of 4 M urea for 18 hours and enzyme not incubated in urea revealed that the 4 M sample had greater fluorescence intensity. This increase in intensity was probably due to a lack of quenching of the fluorophores by the solvent signifying protection of the fluorophores from the solvent.

Similar effects were seen in the comparison of WT OPH incubated in the presence of 2 M and 4 M guanidine for 18 hours versus WT OPH not incubated with guanidine. Both the 2 M and 4 M guanidine samples were red-shifted with respect to the non-chemical denatured WT OPH (342 nM, 356 nM and 332 nM, respectively). Further, the fluorescence intensity of the 4 M guanidine sample was reduced compared to that of the sample incubated without guanidine suggesting that the fluorescent emission intensity of this sample was quenched by the solvent.

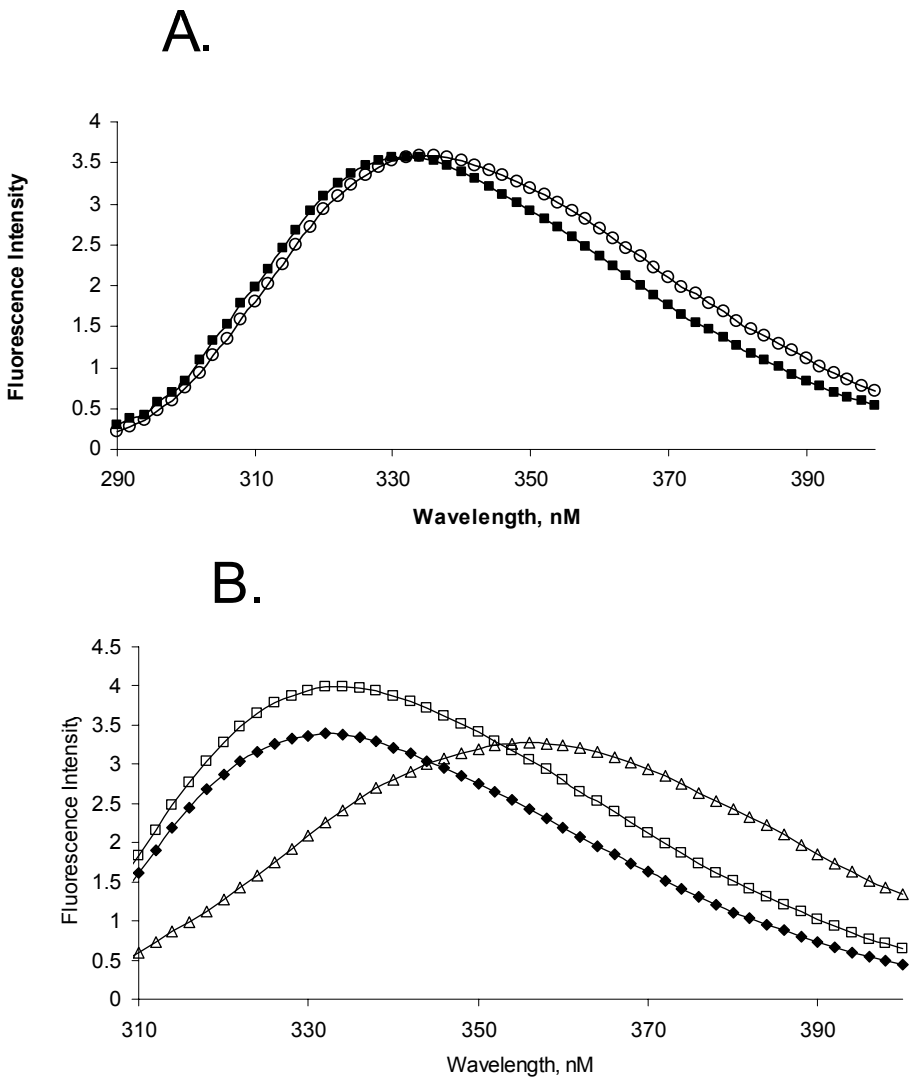

Figure 3.2: Fluorescence emission scans of nicked and denatured OPH::Co^{2+}. A) Wild type OPH::Co^{2+} was incubated for 78 hours at 25 ˚C in the presence (○) and absence (■) of thermolysin (1:100 enzyme:substrate ratio) prior to analysis. B) Wild type OPH::Co^{2+} incubated at 25 ˚C overnight in the presence of 0.0 M urea (♦), 4.0 M urea (□), and 8.0 M urea (Δ) prior to analysis.

C.

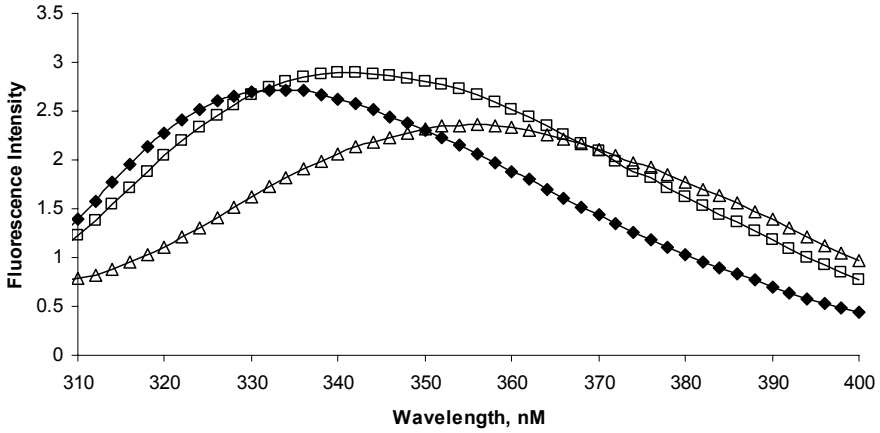

Figure 3.2 Continued: C) Wild type OPH::Co^{2+} incubated at 25 ˚C overnight in the presence of 0.0 M GdnHCl (♦), 2.0 M GdnHCl (□), and 4.0 M GdnHCl (Δ) prior to analysis.

PEST Regions. Since the folded OPH was readily degraded by thermolysin at 25°C, it was theorized that there might be one or more PEST sequences in OPH. PEST sequences are regions that are rich in proline (P), glutamic acid (E), serine (S), and threonine (T) residues and are often targeted by proteolytic enzymes (*88, 89*). PEST sequences are usually associated with eukaryotic organisms, but due to the wide divergence of OPH homologs in eukaryotic systems, it might be possible to find remnants of these regions in OPH. (*53, 90*). Theoretically, if a PEST region was found in OPH, it might be possible to remove or alter the region and, thus, improve proteolytic resistance and protein stability in denaturing conditions as done in other systems. The primary structure of OPH was submitted to the PESTfind database, http://www.at.embnet.org/embnet/tools/bio/ PESTfind/, (*89*) to identify any possible PEST sequences in OPH. No PEST sequences were identified in OPH.

Limited Proteolysis of Thermal Denatured OPH. SDS-PAGE was used to follow the progress of the thermolysin digestion of OPH in increasing temperatures (Figure 3.3A). Each lane represents the 90 minute time point at the designated temperature. Even at 25 ˚C and an enzyme:substrate ratio as low as 1:200, fragments T1 and T3 (S30 – Y309 and L271 – S365, respectively; Table 3.2) were apparent after 30 seconds (data not shown).

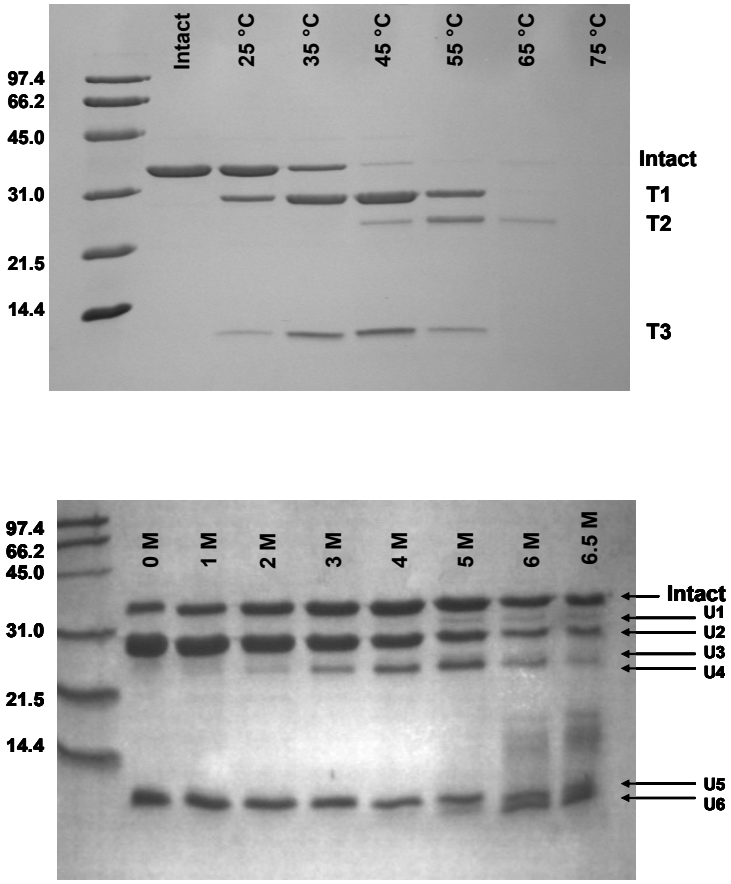

Figure 3.3: Limited proteolysis of OPH::Co^{2+} as followed by SDS-PAGE. A) SDS-PAGE of thermal denatured OPH. Each lane represents the 90 minute time point of the proteolysis reaction at the indicated temperature. Lane 1 is the Bio-Rad Low Range Molecular Weight markers. Prominent proteolytic fragments are designated T1, T2 and T3. B) SDS-PAGE of urea denatured OPH. Each lane represents the 90 minute time point of the proteolysis of OPH by thermolysin in increasing concentrations of urea. Lane 1 is Bio-Rad Low Range Molecular Weight markers. Prominent proteolytic fragments are designated U1, U2, U3, U4, U5 and U6.

Table 3.2. Fragments of OPH::Co $^{2+}$ produced by digestion by thermolysin.

Fragment	Method of Denaturation	SDS MW[a]	Calculated MW[b]	MALDI MW[c]	N-Terminal Sequence	Proposed Sequence	Conditions Observed[d]
WT OPH	None	36	36,291.5	36,370.3	S-I-G-T-G-D	30 - 365	N/A
T1	Thermal	29.0 - 30.0	20,142.3	30,120.5	S-I-G-T-G-D	30 - 309	25 °C
T2	Thermal	24.0 - 25.0	25,704.3	25,665.9	F-F-G-S-R-K	72 - 309	45 °C
T3	Thermal	10.6	10,695.6	10,718.7	L-L-G-I-R-S	271 - 365	25 °C
U1	Urea	32.0	31,853.5	N/A	F-F-G-S-R-K	72 - 365	1 M Urea
U2	Urea	30.2	30,142.3	31,143.0	S-I-G-T-G-D	30 - 309	0 M Urea
U3	Urea	27.0	26,604.4	26,870.3	L-R-A-W-P	66 - 309	3 M Urea
U4	Urea	25.7	25,704.3	25,682.9	F-F-G-S-R-K	72 - 309	1 M Urea
U5	Urea	11.2	10,695.6	10.713.1	L-L-G-I-R-S	271 - 309	0 M Urea
U6	Urea	10.5	10,676.2	10,688.0	S-I-G-T-G-D	30 - 130	3 M Urea

[a] SDS MW is measured in kDa and determined from comparison of fragment migration distance with the migration distances of Bio-Rad Low Range molecular markers.

[b] The calculated MW is the molecular weight of the proposed sequence measured in kDa.

[c] MALDI-TOF MS (m/z) values of the fragments produced by proteolysis of OPH by thermolysin.

[d] Sample conditions tht produced a particular fragment as observed on SDS-PAGE gel.

The 271 loop and the 309 loop appeared to be the primary targets of proteolytic cleavage by thermolysin. The proteolytic cut site, Y309, was located near the leaving group pocket of the active site in the 309 loop. This produced fragment T1 (S30 – Y309). In addition to T1, band T3 (L271 – S365) was produced. The cut site, L271, is located in the 271 loop near the leaving group pocket of the active site. The apparent susceptibility of the 271 loop and the 309 loop to digestion by thermolysin at 25 ˚C suggested that they are flexible and mobile in the natively folded enzyme.

As the temperature was increased to 45 ˚C another prominent fragment, T2, is observed. The N-terminal portion of this fragment, F72, is located in the interface in a region characterized by high hydrophobicity and aromatic ring stacking interactions. F72 forms part of an aromatic stacking network with F65, W69, F73, and F149 (*2*). These cut sites are shown in Figure 3.4. Since this region became accessible to thermolysin at elevated temperatures, some structural rearrangement must occur as the temperature was increased. At approximately 45 ˚C, OPH displayed its maximal catalytic activity (Figure 3.5). The apparent melting temperature of OPH::Co^{2+} was found to be 63 ˚C as followed by CD spectrometry and at 45 ˚C, approximately 85 % of the enzyme population was found in the folded form (Figure 3.6). This is consistent with previous studies that found that an active intermediate of OPH::Co^{2+} was formed at 45 °C and an unfolded, inactive state was formed at approximately 58 °C (*86*). Taken together with the activity data, this suggests that even though this region became flexible enough to be targeted by the protease, the dimer had not dissociated by 45 ˚C; therefore, under thermal denaturing conditions, an active intermediate (I_2*) is generated.

As the temperature increased, no other prominent cut sites were observed. At approximately 60 ˚C, OPH began to form denatured aggregates observable as a white precipitate. After 90 minutes at 65 ˚C, the digestion of OPH by thermolysin was almost complete, and at 75 ˚C virtually no trace of the enzyme or its fragments remained when followed by SDS-PAGE.

Rate of Proteolysis (k_p) Determination of Thermal Denatured OPH. The proteolysis of OPH by thermolysin was followed by SDS-PAGE and the disappearance of the natively folded, intact band was assessed by densitometry. The rate of proteolysis was determined as previously described. As shown in Figure 3.5, no significant change in the rate of proteolysis between 25 ˚C and 50 ˚C was observed, suggesting that both the native folded state and the intermediate are approximately equal in their proteolytic resistance. The activity data demonstrated that this intermediate had an enhanced activity compared to the folded enzyme at 25˚ C. At temperatures above 50˚ C, the rate of proteolysis of OPH by thermolysin rapidly increased as the intermediate began to unfold; the relative activity of the enzyme also began a rapid decline. OPH has a T_m of 63 ˚C as followed by circular dicroism spectroscopy (Figure 3.6). Beyond 50 ˚C, OPH began to lose activity, in agreement with the melting temperature of 63 ˚C of OPH::Co^{2+} and the formation of an inactive state of OPH at 58°C as previously reported (*86*). The comparison between the rate of proteolysis of OPH by thermolysin and activity of OPH against 4 mM demeton-S at increasing temperatures is shown in Figure 3.5.

A.

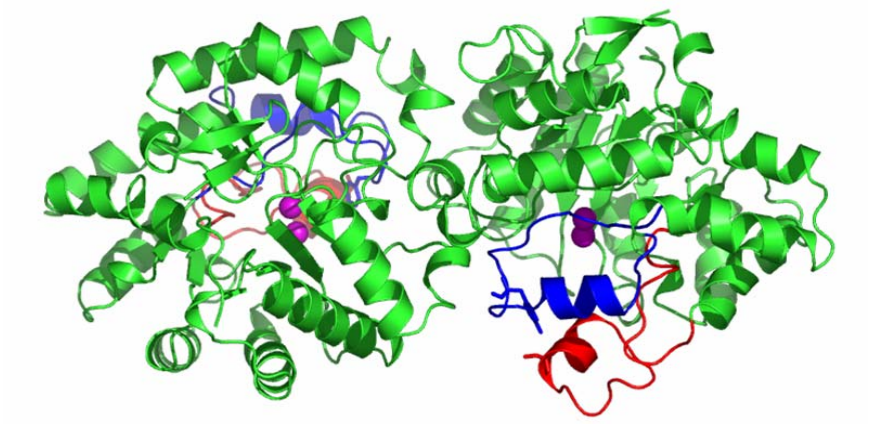

B.

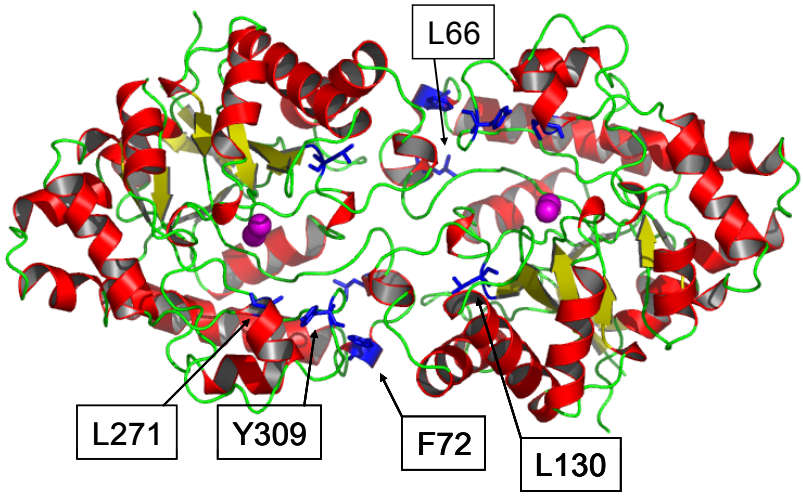

Figure 3.4: Flexible (A) and proteolytic cut sites (B) of OPH. A) The flexible loop region D253 – S276 (shown in red) and the underlying supporting region S299 – D323 (shown in blue). Y309 and S267 are shown as stick representations. Each active site is represented by the 2 metal ions shown in space-filled representation. B) The 'top view' of OPH. The cut sites are shown in blue stick designation. The coordinates were taken from the pdb structure file 1dpm and the image was produced with the PyMOL Molecular Graphics System.

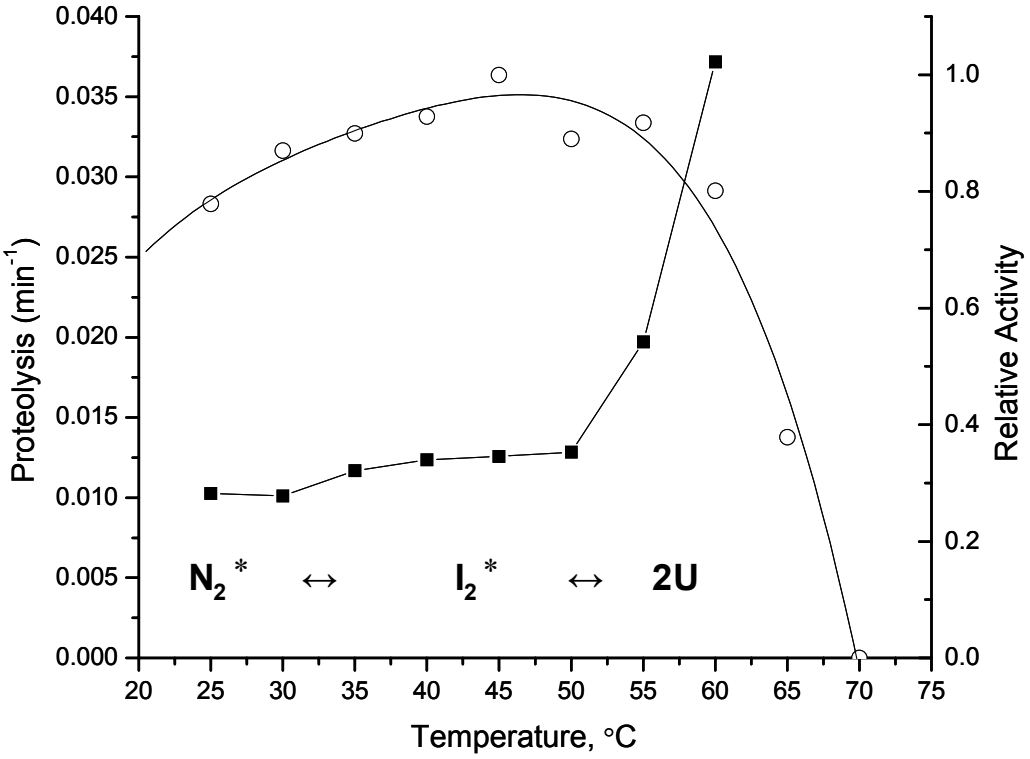

Figure 3.5: Relative activity of OPH::Co^{2+} and rate of proteolysis of OPH::Co^{2+} (k_{app}, min^{-1}) by thermolysin as a function of temperature. The rate of proteolysis (■) is shown on the left axis and the relative catalytic activity of OPH::Co^{2+} (○) against 4 mM demeton-S is shown on the right axis. The activity was measured in the absence of thermolysin. The unfolding scheme (N_2 *↔ I_2 *↔ 2U) was adopted from (*14*).

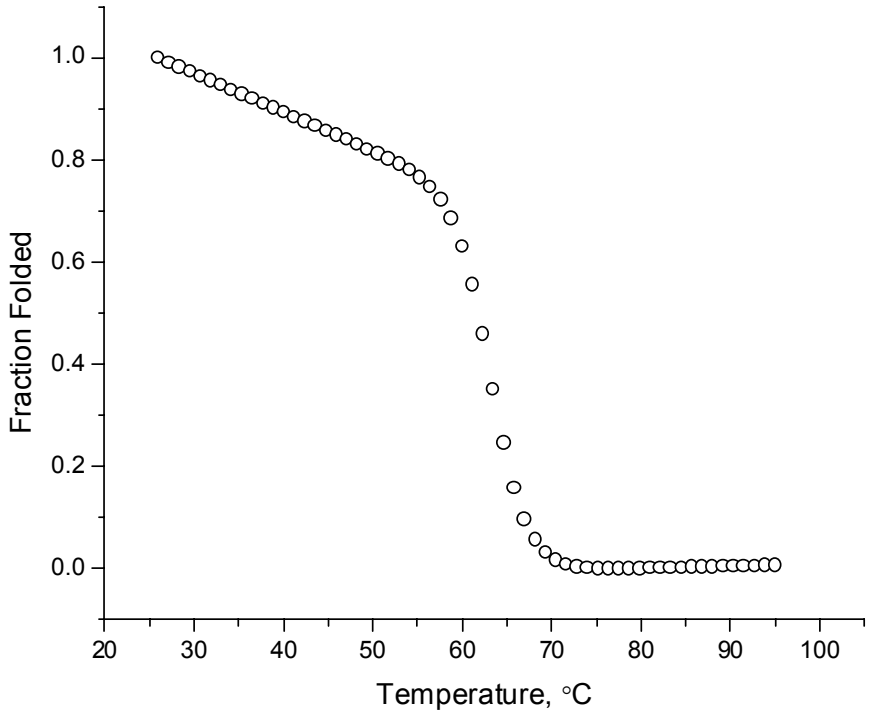

Figure 3.6: Thermal denaturation of OPH::Co^{2+} followed by circular dichroism. Enzyme concentration was 50 μg/mL.

Comparison of the rate of proteolysis of the wild type fragment and the reduction in the rate of hydrolysis by OPH against demeton-S at varying temperatures indicated that the hydrolytic activity of OPH decreased as OPH was cleaved by thermolysin. Between 35 ˚C and 45˚ C the slope of the diminishing activity and the decreasing density of the remaining wild type fragments were similar (Figure 3.7). Further comparison of the densitometry analysis versus activity data suggested that as OPH was cleaved by the protease, it became inactive (Figure 3.5). The initial cleavage of OPH by thermolysin appeared to inactivate OPH's catalytic activity, suggesting that the stabilizing weak bond interactions of its secondary and tertiary structure are not enough to maintain its catalytic activity. This observation lends support to the idea that the flexibility and mobility of these cleaved regions of the enzyme are involved in the catalytic mechanism.

Hydrogen Bonding Calculations of D253 – S276 and F306 – V320. The computational hydrogen bonding potential of OPH was examined with the WHAT IF Optimal Hydrogen Bonding Network server. This software calculates the relative importance of hydrogen bonds of proteins based on an empirical hydrogen bond force field and rates them on a scale of 0.0 to 1.0, with 1.0 being the score of a perfect hydrogen bond. This score does not relate the energetic worth of the hydrogen bond but relates its contribution to the stability of the protein relative to that of the other hydrogen bonds in the protein (*91*). While many hydrogen bonds were predicted within the flexible loop regions, Loop 271 (D253 – S276) and Loop 309 (F306 –V320), only one was predicted to bridge these two regions. The hydrogen bond between Y309 and S267

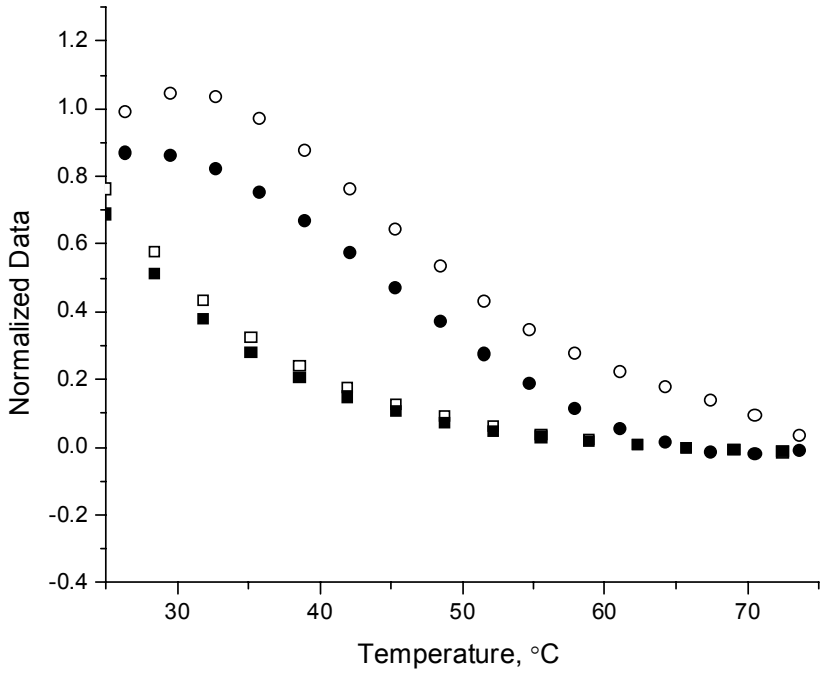

Figure 3.7: Comparison of limited proteolysis and enzymatic activity. The densitometry of intact wild-type remaining after proteolysis (1:100 enzyme:substrate ratio) at 10 minutes (○) and 90 minutes (●) in increasing temperatures. The enzymatic activity of OPH::Co^{2+} against 4 mM demeton-S in the presence of thermolysin (1:100 enzyme:substrate ratio) at 10 minutes (□) and 90 minutes (■) in increasing temperatures. Data are normalized to maximum percentage of intact wild type OPH::Co^{2+} (densitometry) and to maximum catalytic activity of OPH::Co^{2+} against demeton-S, respectively.

was accorded a high score of 0.880 suggesting that it is extremely important in the stability of this region.

Limited Proteolysis of Chemical Denatured OPH. SDS-PAGE was used to follow the progress of the digestion of OPH in increasing concentrations of urea by thermolysin, as shown in Figure 3.3B. The 1:100 enzyme:substrate ratio used for the thermal-induced denaturation studies was found to be ineffective, as no prominent bands were produced. Increasing the protease concentration in the samples (1:50 enzyme:substrate) produced several prominent cut sites.

The maximum in fluorescence intensity seen at 3 M urea was indicative of a rearrangement of protein structure which caused the intrinsic fluorophores to be more protected from the solvent and might confer some measure of proteolytic resistance to the enzyme (Figure 3.1). Additionally, digests were visualized by SDS-PAGE and analyzed by densitometry. At 10 minute increments, the percentage of intact wild type OPH as determined by densitometry were plotted against increasing urea concentrations ranging from 0 M to 6 M urea. A peak of proteolytic resistance was observed at 3 M urea, indicative of a reduction in the rate of proteolysis after 10 minutes (Figure 3.8). After 30 minutes of digestion of OPH by thermolysin, the peak began to shift at 4 M urea resulting from the increasing contribution of fragment U4 (Figure 3.3). At each time point, the maximum proteolytic resistance of OPH was observed between 3 and 4 M urea suggesting that the enzyme is at its most stable form under these conditions. This corresponded to the increase in fluorescence signal at these denaturant concentrations (Figure 3.1).

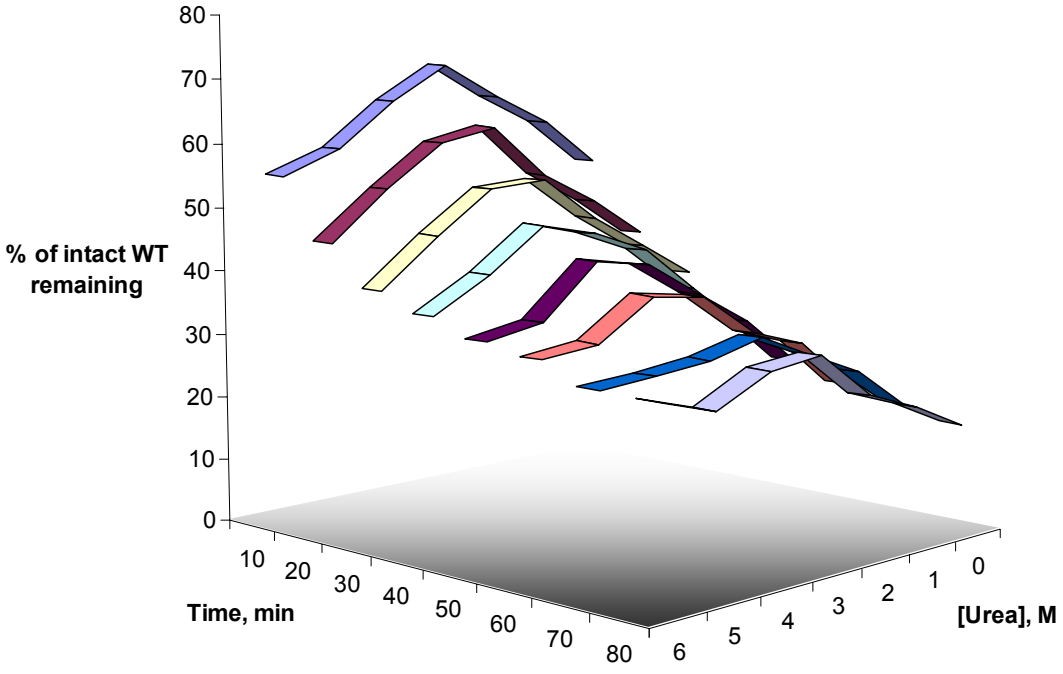

Figure 3.8: Percentage of intact OPH remaining after digestion by thermolysin in increasing urea concentrations. Digests were followed by SDS PAGE and analyzed by densitometry. At 10 minute increments, samples across increasing urea concentrations were plotted against the percentage of intact OPH remaining. Each sample has a peak between 3 – 4 M urea, representative of a greater amount of intact protein remaining after a 10 minute digest of OPH::Co^{2+} by thermolysin at these urea concentrations.

The fragment pattern observed in urea-denatured experiments was very similar to that of the thermal-denatured experiments. As seen in Figure 3.3 and Table 3.2, the first proposed cut sites occurred at positions L271 and Y309. In the presence of 1M urea, the interface region became more accessible, position F72 was the next cut site. F72 is located in the interface in an α-helix characterized by a high degree of hydrophobicity and is involved in an aromatic ring stacking network involving residues from both subunits of the homodimer (*2*). One M urea was sufficient to make the F72 region mobile and flexible enough to be accessible to the active site of thermolysin. The enzyme reached its maximum activity when incubated at 1 M urea and began to loose activity at urea concentrations greater than 1 M (Figure 3.1). In the thermal-denaturation experiments, proteolysis at this site was observed to occur at 45 ˚C. Thus, the increased flexibility of this region apparently did not have any adverse effects on the catalytic ability of the enzyme.

Additional fragments were not observed until OPH had been incubated in the presence of 3 M urea. At this concentration of denaturant, two new cut sites were observed: L66 and L130. These are located in the interface region, suggesting that the region lost the protection offered by the other subunit and was more exposed to the solvent. Additional prominent bands were not observed at higher concentrations of urea; thus, the integrity of the bands gave way to band smearing as the enzyme became increasingly unfolded and more completely degraded by the protease.

DISCUSSION

OPH::Zn^{2+} has been reported to form an inactive dimeric intermediate in chemical denaturing systems (*14*). In these early studies, the unfolding process was followed with fluorescence and circular dicroism spectroscopic methods which did not report specific information regarding localized unfolding. In the present study, in addition to fluorescence and circular dichroism spectroscopic techniques, limited proteolysis was used to monitor the Co^{2+} variant enzyme as it unfolded from its native, folded form to its inactive dimeric intermediate state. This has been a valuable technique to determine subtle changes in conformational structure. For example, changes in the conformational structure of ribonuclease A were detected with limited proteolysis in the pre-transition region of its unfolding profile (*81*). The subtle rearrangements that were detected by limited proteolysis were also implicated in the inactivation of ribonuclease A. This inactivation preceded any changes in the spectroscopic determined unfolding profile (*80*).

Many proteins in their natively folded state are resistant to proteolysis. The secondary and tertiary structures of their native fold offer some protection from the protease (*85*). In the case of the holo form of sperm-whale myoglobin (myoglobin with the heme cofactor), resistance to degradation by thermolysin was observed even after 24 hours. When the heme group was removed to form apomyoglobin, helix F was destabilized and became readily susceptible to digestion by the protease (*92*). In contrast, OPH::Co^{2+} was readily susceptible to degradation by thermolysin at 25 ˚C, which suggested the presence of exposed, flexible loop regions possibly devoid of

regular secondary structure. The crystal structure (1dpm), when colored according to *B* factors, provides clues as to the regions which are likely candidates for these flexible regions. Loops 271 and 309 appear to fit these criteria, and this explanation is consistent with the loop regions being cleaved by thermolysin at 25 °C. Thermolysin is a stable metalloendopeptidase that displays broad substrate specificity, with a preference for amino acids with bulky hydrophobic side chains, and is active under a variety of harsh, solvent conditions (*93*), consistent with its use as the protease in this study.

An Active, Dimeric Intermediate of OPH::Co^{2+} was Formed Under Thermal-Denaturing Conditions. OPH::Co^{2+} is readily susceptible to proteolysis by thermolysin at 25 ˚C. Y309 and L271 are the primary targets of proteolysis and appear to be generated at the same time. Examination of Table 3.2 reveals that these fragments overlap in their primary structure. This overlap suggests that the production of these fragments is not necessarily cooperative and each proteolytic event may take place independently of one another on the different subunits of the homodimer. There appears to be significant native flexibility of the enzyme in these regions which makes OPH::Co^{2+} readily susceptible to proteolysis.

The following scheme for the thermal unfolding pathway of OPH::Co^{2+} has been devised in which there are two possible directions of unfolding, either through a dimeric intermediate (I_2) or through a monomeric intermediate (2I, scheme 3.1) (*86*).

Scheme 3.1

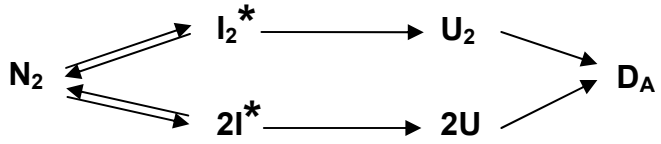

The asterisk indicates an active intermediate. In either case, at elevated temperatures (≥ 60 °C), an inactive unfolded state leading to denatured aggregates (D_A) was observed. This study found that the intermediate displayed its greatest activity and was well populated at approximately 45°C.

As seen in Figure 3.5, the proteolysis rate remained consistent from 25 °C to 50 °C which suggests that the intermediate is similar in proteolytic resistance and stability as the native folded enzyme (N_2). Comparison of the rate of proteolysis with the activity data showed that this intermediate was the most active form of OPH::Co^{2+} in the conditions tested. Beyond 50 °C, k_{app} increased rapidly and the catalytic activity of OPH::Co^{2+} began to fall as the enzyme became more denatured.

Studies of engineered monomeric TIM barrel systems have shown that dimerization is a prerequisite for the optimum activity and stability of TIM barrels (*21, 94-96*). In the case of a trypanosomal TIM from *Trypanosoma brucei*. For example, the K_m of the engineered monomer was 20-fold greater and the k_{cat} was 1000 fold less than that of the wild type dimer (*21*). Wierenga suggested that dimerization in TIM barrels was crucial for maintaining the correct geometry of the active site (*97*). In fact, examination of the crystal structure of OPH::Co^{2+} suggested that L136 and L140 of one subunit contributed to the structure of the active site's leaving group pocket of the opposite subunit.

There was no evidence in the present study to suggest that an increase in catalytic ability resulted from the disassociation of the two subunits of OPH::Co^{2+}. However, at increasing temperatures, the stabilizing forces of the interface must relax for this region

to become accessible to the protease. The activity of the enzyme during thermal-induced unfolding was maintained through the formation of the intermediate which preceded the formation of the denatured aggregates. There are two interpretations of this observation: 1) a portion of the interface from one subunit remained attached to that of the opposite subunit or 2) the unfolding profile of OPH::Co^{2+} included the formation of active, monomeric intermediates. This later hypothesis is unlikely because a large portion of the interface appeared unaffected by the protease. This would indicate that, at least initially as the interface becomes more mobile, the dimer remained intact. The location of the proteolytic cut sites within the crystal structure of OPH revealed significant portions of the interface that appeared to be protected from the protease. The model for the unfolding pathway of OPH::Co^{2+}, based on the results of this study, under thermal denaturing conditions can now be represented as shown in the following scheme where I_2^* represents an *active* dimeric intermediate (Figure 3.5). .

Scheme 3.2

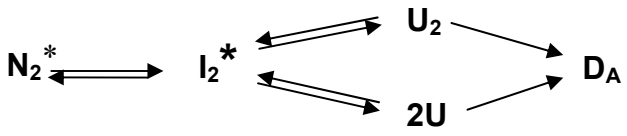

This model is similar to the one devised for OPH::Zn^{2+} unfolding in chemical denaturing conditions (Scheme 2.1), (*14*) except that in chemical denaturing conditions the intermediate is inactive (Figure 3.1). It is not known whether the enzyme unfolds from its active dimeric intermediate into a dimeric or monomeric unfolded state or if the enzyme forms denatured aggregates (D_A) directly from the intermediate state.

An Inactive, Dimeric Intermediate of OPH::Co^{2+} Was Formed Under Urea-Denaturing Conditions. In the presence of 1 M urea, OPH::Co^{2+} had a digestion pattern similar to that of the thermal denatured OPH and the activity of the enzyme began to quickly decrease with increasing urea concentrations. The increased flexibility of this region beyond 1 M, as shown by limited proteolysis, does not alone explain the decrease in activity. In fact, increased flexibility in this region was shown to have a positive effect on the activity of the enzyme. The generation of new cut sites at L66 and L130 at 3M urea demonstrated that regions protected from proteolysis in the non-denatured structure were now exposed and made accessible to the protease.

Both the thermal denatured and the chemical denatured proteolytic pathways had similar cut patterns, and the increase in the flexibility of OPH::Co^{2+} around F72 correlates with an increase in the catalytic activity of the enzyme (as seen at 45 ˚C and 1 M urea). This enjoins the question, "Why is the thermal denatured dimeric intermediate active while the chemical denatured intermediate inactive?" The presence of two additional proteolytic cut sites in the chemical denatured system that are not present in the thermal denatured system may provide the answer. These proteolytic cute sites are located at L66 and L130 and are seen at 3 M urea (Figure 3.9B).

L66 is located in a helical turn in the interface that is proposed to significantly contribute to the stability of the dimeric interface (*2*). F65, W69, F72, and F73 all participate in various intrachain hydrophobic and aromatic stacking interactions. Additionally, F65 forms interchain stacking interactions with M138 and F104 of the opposite subunit (*2*). L130 is located in a β-sheet and is situated adjacent to this aromatic stacking network in the opposite subunit. The fact that both of these areas were cleaved provided evidence that this area opens up to the solvent and becomes accessible to the protease at 3 M urea. The unfolding data followed by both fluorescence and CD revealed an unfolding transition at 3 M urea (Figure 3.1). As shown by the fluorescence data, the inactive dimeric intermediate began to form at 3 M urea. This suggested that this portion of the interface was not involved in forming the stabilizing interactions of the dimeric intermediate in chemical denaturing conditions and unfolding of these regions might account for the loss of activity in the chemical induced dimeric intermediate. No other prominent cut sites were observed elsewhere in the enzyme, which is typically indicative of a compact degree of structure that remains inaccessible to the protease even in increasing concentrations of urea.

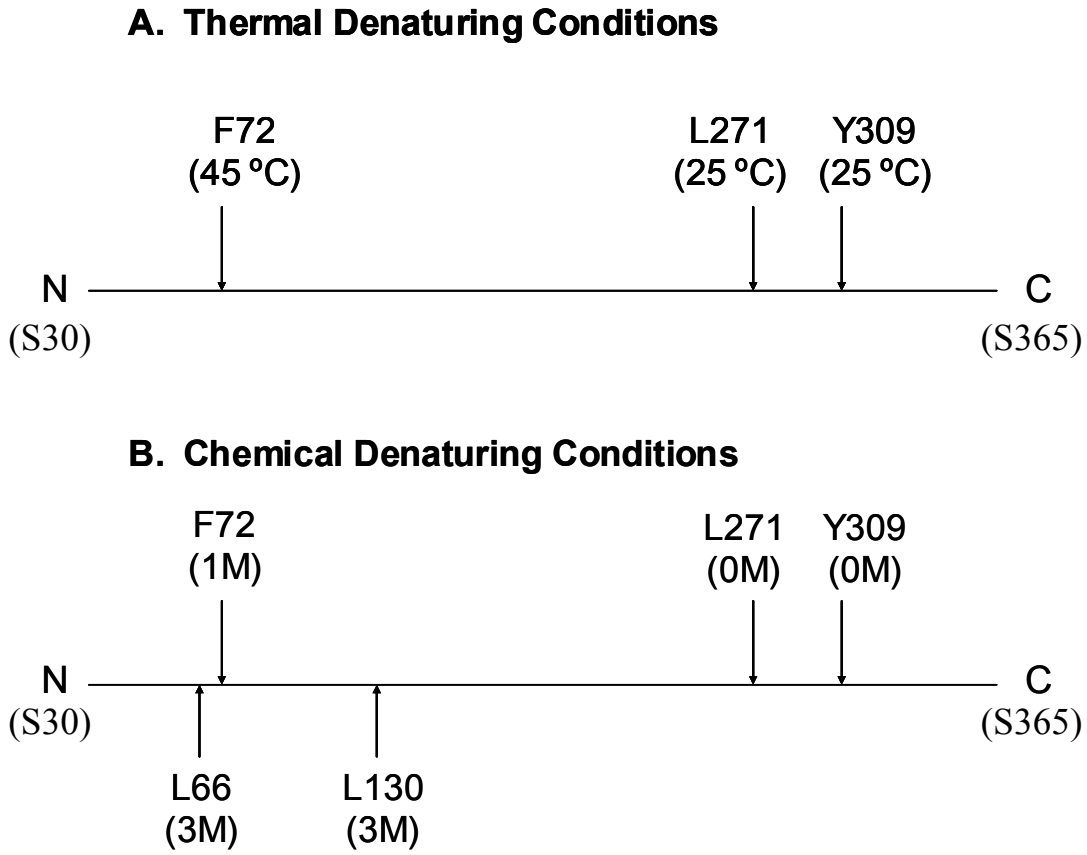

Figure 3.9: Protease digestion map of OPH::Co^{2+} by thermolysin under A) thermal-denaturing and B) chemical-denaturing conditions. The horizontal line represents the primary structure of OPH starting at S30 and ending at S365. Temperatures and concentrations of denaturant where each cut site is observed are shown in parenthesis.

The Increased Flexibility of the Active Site is Responsible for the Increased Catalytic Activity of OPH::Co^{2+} at 45 ˚C and 1 M Urea. Y309 is located in an α-helix near the interface, and it forms part of the leaving group pocket of the active site. It is hydrogen-bonded to S267 which forms part of a small α-helix (A266-L272) in the 271 loop. Y309 was proposed to be a stabilizing factor in the development of the negative charge of the *p*-nitrophenolate leaving group of paraoxon. The interaction of Y309 with the substrates could be the rate limiting step of the catalytic reaction (*98*); however, replacing the tyrosine residue with a phenylalanine, thus removing the hydrogen bond forming capability of the hydroxyl group of tyrosine, did not produce a difference between the catalytic properties of Y309F and the wild-type enzyme (*74*). The results presented in this study support a structural role for Y309 through its hydrogen bonding with S267 which, in turn, supports the flexible loop region of D253 – S276.

According to Figures 3.1 and 3.5, the maximum catalytic activity of OPH::Co^{2+} occurred at 1 M urea and 45 °C, respectively. Under both of these conditions, the emergence of the proteolytic cut site at position F72 was observed. It appears that there was a correlation between the maximum catalytic activity of OPH::Co^{2+} and the increased flexibility of this region of the enzyme. A kinetic model for the hydrolysis of organophosphates by OPH is shown in scheme 3.3. In the final step, k_5, two products (P) are released from the enzyme and the free enzyme (E) is regenerated.

Scheme 3.3

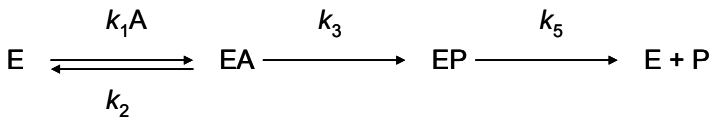

For slower substrates such as demeton S, the rate limiting step is k_3, the hydrolysis of the scissile bond. For faster substrates such as paraoxon, the rate limiting step is k_5, the release of the hydrolyzed substrate from the active site and the regeneration of the free enzyme (*99*).

The leaving group pocket is characterized by residues W131, F132, F306 and Y309 (*65*). It has been proposed that the increased mobility of the region around F72 permits increased flexibility of the leaving group region surrounding Y309 and S267. This increased mobility would have the effect of increasing the size of the leaving group pocket of OPH permitting a faster release of product and regeneration of free enzyme (k_5). This hypothesis would explain the increased activity under these conditions (1 M urea and 45°C) and is consistent with the data presented here.

According to molecular dynamics simulations, loop 271 is very mobile and changes positions to varying degrees depending on the substrate present in the active-site (*98*). Computationally, it can be proposed that the side-chain of L271 could move up to 10 angstroms, relative to the side-chain of the active site residue, F132, depending on whether or not the active site was occupied by a substrate and the degree of change was dependent on the substrate used. As shown in Table 3.2, L271 is a cut-site characteristic of fragments T3 and U5, which further demonstrates the flexibility of this region. As

these regions are cleaved by protease, OPH loses its catalytic ability, further supporting the idea that these flexible regions are necessary for the catalytic activity of OPH.

Proteins are not static structures and enzyme flexibility is often a requirement for catalysis. Enzymes have evolved under pressure for optimal structured dynamics (*100*) and enzyme motions can even be the limiting factor in the turnover rates in TIM barrel enzymes (*101, 102*). The dynamics of enzyme motion can take place in the presence or the absence of substrate (*100*) and in the case of OPH, are dependent upon the identity of substrate present in the active site (*98*). Since this intrinsic, dynamic nature of OPH is important for the enzyme's catalytic activity, it would be reasonable to expect that a decrease in the flexibility of these 'dynamic regions' surrounding the enzyme's active site would result in a decreased turn-over rate for all substrates or, alternatively, that an increase in flexibility would result in an increase in the turn-over rate. It is important to remember that enzymes are dynamic structures with motions that are essential structural aspects of the enzyme's catalytic mechanism and not just static structures.

The initial cleavage of OPH::Co^{2+} by thermolysin did not result in a significant structural rearrangement as shown by fluorescence emission scans (Figure 3.2). A comparison of WT OPH::Co^{2+} samples denatured in 8 M urea and 4 M guanidine with OPH::Co^{2+} in the absence of denaturant show that these denatured enzymes display a striking difference in both their fluorescence intensities and their maximum wavelengths when compared to the natively folded WT OPH::Co^{2+}. Since the catalytic ability of OPH diminishes as it is incubated with the protease, it can be concluded that these

flexible loop regions are important in the catalytic activity of the enzyme and they must remain intact for catalysis to occur.

Potential Intersubunit Salt Bridges May Contribute to the Differences in Catalytic Activity Observed between Thermal and Chemical Denatured OPH::Co^{2+}. There are three intersubunit salt-bridges that span the dimeric interface of OPH. For simplicity, the designations of these salt bridges, listed in Table 3.3, are used throughout the remainder of this discussion.

Table 3.3: Intersubunit salt bridge identification.

Designation[a]	Residues Involved
SB 67	R67 - D109[b], E159, D160
SB 71	E71 - R152
SB 133	D133 - R139

[a] SB stands for Salt Bridge

[b] In addition to forming a potential intersubunit salt bridge with R67, D109 also forms a theoretical intrasubunit hydrogen bond with R67.

At moderate temperature, salt bridges provide little structural stabilization, if not actually destabilizing protein structure due to a large desolvation penalty required to bring the two oppositely charged groups together. However, as the temperature increases, the desolvation penalty is reduced due to the hydration free energy of the charged groups becoming less favorable. This results in the salt bridge providing more stabilization at higher temperatures (*103*). Therefore, salt bridges are strong candidates

for the stabilization of OPH's active site at elevated temperatures which, in turn, leads to the formation of an active intermediate under thermal denaturing conditions.

A portion of the dimer interface, D133 – R152 was observed to form extensive intermolecular contacts with the opposing subunit (*2*). At 3M urea, this area remained exposed to the protease and is likely the region of the interface that is holding together to form the dimeric intermediate. In fact, no prominent fragments were produced by proteolytic cleavage of this region even when the enzyme was denatured (6.5 M urea), suggesting that this region retained its structure even upon dissociation of the dimeric intermediate into its composite monomers.

L130 is located near to L131 and L132 (residues that form part of the leaving group pocket of the active site). Significant unfolding of the active site would have to occur for L130 to be available as a proteolytic cut site. Closer examination of the region surrounding L130 revealed a nearby intersubunit salt bridge, SB 133. The homodimeric nature of OPH and the close proximity of these two residues (which form the salt bridge) in the primary structure of OPH mean that there are two salt bridges in close proximity.

Two additional salt bridges can be found in the region surrounding L66: SB 67 and SB 71. R67 forms a complex salt bridge with D109, E159, and D160 of the opposite subunit. R67 also forms a theoretical hydrogen bond with D109 of its own subunit. E71 forms a salt bridge with R152 of the opposite subunit. The homodimeric nature of the enzyme means that these are four additional salt bridges across the interface of OPH. F72 was observed as a cut site at 45 ˚C suggesting that SB 71 is not responsible for the stabilization of the thermal denatured dimeric intermediate. This

region of the enzyme is flexible at this temperature and SB 71 can not be expected to anchor this region of the enzyme in increasing temperatures. F72 was also observed as a cut site at 1 M urea further displaying its flexibility.

The remaining salt bridge, SB 67 is a strong candidate for the stabilization of the intersubunit interface in thermal denatured conditions. E159 is the only amino acid that did not adopt an allowed backbone dihedral angle according to the Ramachandran plot, with φ, ψ angles of 51.5˚ and -127.9˚, respectively. It is approximately 15 angstroms from the active site and has not been implicated in playing a role in the catalytic mechanism of OPH (*2*). E159 was also not as well conserved as the other members of this salt bridge and exists as a lysine residue in the OPH from *Flavobacterium* sp. MTCC 2495, as shown in Figure 3.10. D160 is located near the subunit-subunit interface region and is not calculated to form any theoretical hydrogen bonds with any other residue (WHAT IF Software, 1dpm). It is 90% solvent exposed and can be expected to form hydrogen bonding interactions with the solvent as well as contributing a charge for the formation of the salt bridge. D109 forms part of an intersubunit salt bridge and a theoretical intrasubunit hydrogen bond with R67 from the opposite and same subunit, respectively. While neither R67 nor D109 have been implicated in contributing to the catalytic activity, they do lie close in primary structure to active site residues. The residues G60, S61and I106 form part of the small pocket of the active site (*65*). If a localized unfolding event were to take place in the region around L66 it would not be unreasonable to assume that these residues would be affected by the conformational change. As can be seen from Figure 3.1, the relative activity of

A.

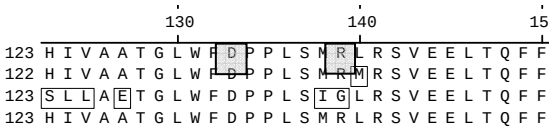

B.

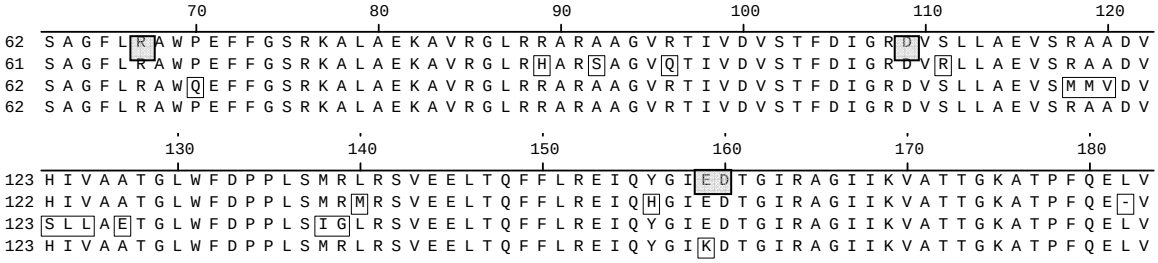

C.

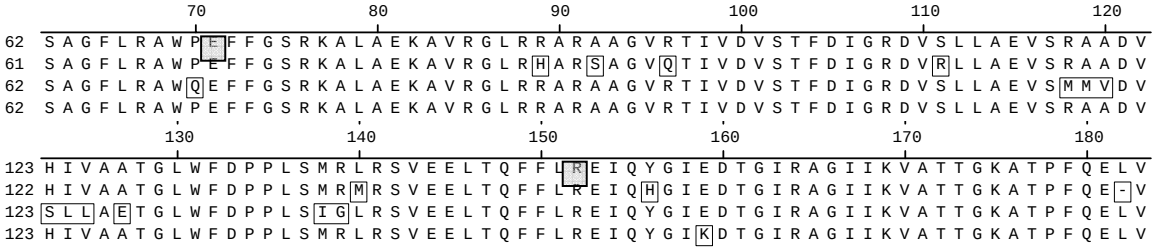

Figure 3.10: Sequence alignments for several OPHases for regions containing salt bridges. Salt bridges shown are A) D133 – R139, B) R67 – D109, E159, and D160, and C) E71 – R152. Residues different from WT OPH are boxed while residues that form salt bridges in WT OPH are shaded. The residue number of WT OPH is marked at the top of each alignment. The alignments from the top down are those of OPHases from *Pseudomonas diminut*a, *Agrobacterium radiobacter* P230, *Flavobacterium balustinum*,

and *Flavobacterium* sp. ATCC 2495. They are 86%, 96%, and 96% identical, respectively to wild type OPH.

OPH::Co^{2+} began to decline rapidly between 3 and 3.5 M urea, the same concentration of urea that the proteolytic fragment characterized by N-terminal L66 was observed.

Based on the results of this study, SB 133 and SB 67 are strong candidates for maintaining the active site in the correct conformation for catalytic activity during thermal denaturing conditions.

Conclusions. OPH::Co^{2+} is readily susceptible to proteolysis at 25 ˚C. Analysis of the digestion fragments identified two flexible loop regions (Loop 271 and Loop 309), located adjacent to active site. In mildly denaturing conditions (1 M urea and 45 ˚C) a new fragment, characterized by F72, is produced. This residue is located in the intersubunit interface amid several aromatic stacking interactions. OPH::Co^{2+} displays its maximum enzymatic activity at approximately 45 ˚C and 1 M urea and the same proteolytic fragment pattern is observed under both conditions. This pattern suggests that a region of the interface near the active site becomes more flexible which ultimately leads to an enlargement of the leaving group pocket of the active site and the increase in activity observed under mild denaturing conditions.

No further fragments are produced by proteolytic digestion of OPH in increasing temperatures. In chemical denaturing conditions (3 M urea), however, two new fragments are observed (characterized by L66 and L130). These are located in the intersubunit interface, adjacent to the active site, and their exposure helps to explain why the enzyme looses activity under these conditions.

OPH::Co^{2+} unfolded in thermal denaturing conditions to form an active intermediate. In contrast, an inactive intermediate is formed in chemical denaturing conditions. There are six intersubunit salt bridges that span the interface of OPH, four of which are strong candidates of providing the stabilization leading to the active intermediate in thermal denaturing conditions.

Comparison of the structural differences between the thermal and chemical denatured forms of OPH::Co^{2+} will provide useful information for the design of novel enzymes with enhanced operational stabilities.

CHAPTER IV

INCREASING THE OPERATIONAL STABILITY OF OPH

BACKGROUND

Native-Like Structure and Denaturant Effects. NMR studies on Δ131Δ, a truncation of staphylococcal nuclease, have shown that it retains a native-like topology in elevated urea concentrations (8.0 M urea). In fact, the global topology of Δ131Δ in 8 M urea was found to be very similar to its structure in water (*104*). It was concluded that the long-range hydrophobic interactions may continue to orient native-like protein topology since hydrophobic interactions between residues are not completely eliminated even in high urea concentrations (*105*). Additionally, through a limited number φ and ψ angles, steric interactions between residues may assist protein structure in achieving a native-like fold. In denatured systems, the side chains of peptides will achieve an ensemble of low energy conformations, some of which may resemble native-state structures (*104, 106*).

Even in GdnHCl concentrations as high as 6 M, proteins can have significant amounts of structure (*105*). GdnHCl has been found to be approximately 2.3 times as effective a denaturant as urea. Urea is an uncharged molecule that functions in protein unfolding through chaotropic effects while GdnHCl is an ionic molecule that works by both ionic and chaotropic effects. Therefore, the use of the two different denaturants can provide information as to the importance of electrostatic interactions to the stability of a given protein (*107-109*).

Models of Stabilization of Protein Structure Offered by Disulfide Modification. The Doig and Williams model of protein stabilization by disulfide bridges predicts that the disulfide crosslinks stabilize the folded protein structure enthalpically but destabilize them entropically. The stabilization results from a decrease in non-polar surface areas resulting in a decrease in the hydrophobic effect, which drives the folding process (*110*). They concluded that the enthalpic stabilization of the native state results from less optimal hydrogen bonding and van der Waals networks in the unfolded structure due to the presence of the disulfide crosslink. The entropic destabilization results from a decrease in the amount of ordered water molecules in the unfolded state of the protein relative to the unfolded, uncrosslinked protein. Therefore, the unfolded protein becomes more stable relative to the folded protein. Any stabilization of the folded state by the formation of a disulfide linkage would be greatly offset by the increased stabilization of the unfolded state. Thus, the stabilization of the folded state by a disulfide bond would have to result from the enthalpic stabilization. Based on the author's data set, a disulfide bond stabilizes the folded state of a protein by approximately 3.1 kcal mol^{-1}.

In the case of the chloride dependent α-amylase from *Pseudoalteromonas haloplanktis*, the insertion of a novel disulfide bond near the active site had the effect of stabilizing the global structure of the enzyme (in terms of conformational stability) while not affecting the thermal stability of the enzyme (*111*). Since the contribution of the enthalpy of denaturation of the disulfide mutant was greater than the entropy of denaturation, the authors concluded that the disulfide bond stabilized the enzyme

structure through primarily an enthalpic contribution, which is in agreement with the Doig and Williams model.

Alternatively, the Chain Entropy model assumes that the presence of a disulfide bond decreases the conformational entropy of the unfolded state thereby driving the equilibrium towards the folded state (*112*). The *m*-value has been observed to increase as disulfide bonds were reduced. The *m*-value represents the dependence of the conformational stability of an enzyme on denaturant concentration and correlates with the available surface area (ASA). The larger the *m*-value the more surface area is exposed upon unfolding. Since the *m*-values of proteins were found to increase upon disulfide reduction, it can be assumed that more of the enzyme surface became exposed and more denaturant was able to interact with the unfolded molecule.

The contribution of the disulfide linkage to the conformational entropy of a protein can be estimated by the equation

$$\Delta S_{conf} = -1.2 - (\frac{3}{2})R \ln n \tag{4.1}$$

where *n* is the number of residues that are joined by the crosslink.

Steric Hindrance. Attempts to increase the stability of phage T4 lysozyme by introducing disulfide bonds found that those inserted into flexible locations in the folded protein structure had the greatest chance of increasing the thermostability of the protein. This was because the flexibility of the region allowed the novel disulfide bond to obtain an optimal or a near-optimal geometry that minimized the negative effects on protein structure. On the other hand, those novel disulfide bonds inserted into more compact

regions of the enzyme caused a reduction of thermal stability due to the strain imposed on the stabilizing interactions of neighboring residues (*113*).

The introduction of a disulfide bridge in a protein can also have a negative contribution to the stability of the protein by introducing conformational strain (*114*). Additionally, the use of novel disulfide bonds does not always increase the stability of the modified enzymes. For instance, the introduction of a novel disulfide into poplar plastocyanin, an enzyme involved in the photosynthesis process in poplars, led to a decrease in the thermal stability of the enzyme when compared to that of the wild type plastocyanin (*115*). The authors concluded that any increase in the stability of the protein offered by the novel disulfide bridge was offset by strain introduced by the formation of the disulfide bridge. Stabilizing forces such as the electrostatic, van der Waals and hydrophobic interactions could be perturbed by the new disulfide bridge and be forced out of their optimal binding conformations. Therefore, the stability of the protein as a whole would be affected by the less optimal placement of these stabilizing interactions.

Studies using a combination of x-ray crystallography and differential scanning calorimetry (DSC) to examine the role of the disulfide bridge in the stability of human lysozyme have suggested that the effects of disulfide bridges on the stability of proteins is not due solely to the entropy changes in denaturation but to enthalpic factors as well (*116*).

The introduction of novel disulfides into barnase has provided evidence that the effects of stabilization by disulfide bonds do not conform simply to one model or the

other. Instead, they take on characteristics of both (*117*). None of the mutants solely displayed characteristics inherent to the Chain Entropy model and equation 4.1, nor to the characteristics explained by the Doig and Williams model. The authors concluded that the introduction of a disulfide bridge affected both the native and denatured states of the enzyme and that there exists a balance between various solvation contributions and intermolecular forces in both states that can lead to the unpredictable thermodynamic characteristics of modified enzymes.

Studies involving the insertion of novel disulfide bonds into and the removal of native disulfide bonds from *Cucurbita maxima* trypsin inhibitor-V, have revealed that cross-links can stabilize both the native and the denatured states of proteins. Depending on where the stabilization takes place (either the native state or the denatured state) the disulfide contributes to a gain or a loss in the stability of the folded protein (*118*). The hydrophobicity of a protein can change depending upon the placement of a novel disulfide bond and loss of hydrophobicity can have a negative effect upon the stability of the folded enzyme. Additionally, residual structure in the unfolded state of a protein and flexibility near the inserted disulfide bridge can also have an effect on the stability or instability of a protein. In agreement with previous studies (*117*), these authors concluded that neither model completely explained the stabilization provided by novel disulfide bonds and that both enthalpic and entropic contributions are responsible for the observed stabilization of protein structure by engineered disulfide bonds.

Indeed, it would be difficult to expect that the introduction of a disulfide bond would only have effects on the denatured state of an enzyme. The folded state should

experience some of these effects, as well. According to the Destabilizing Strain Energy model, the native state structure can be perturbed by the addition of a new covalent crosslink (*114*). This may help to explain why the introduction of novel disulfide bonds into protein structure is often not successful in stabilizing proteins.

According to the two models of stabilization by disulfide crosslinks, the Chain-Entropy model and the Doig and Williams model (*110, 112*), the disulfides increase the stability of the enzymes through denatured state effects. It is interesting that most of these studies focus on the stabilization of monomeric enzymes with two state unfolding pathways. Fewer studies have examined the effect that novel disulfide crosslinks would have on the stability of larger enzymes with more complex unfolding pathways. The same forces that govern the increase in stability offered by the disulfide bond in smaller systems should be conserved in these larger systems with the exception being that the disulfide bonds could increase stabilities of multi-state unfolding enzymes through intermediate-state effects, native state effects and/or denatured-state effects.

As stated previously, the conformational stability of OPH is large, but the energy required to unfold the enzyme into its inactive, dimeric intermediate is small. Therefore, it would be advantageous to increase the energy required for the enzyme to proceed through the first unfolding transition to its inactive state.

According to the limited proteolysis data, the first unfolding event takes place at flexible regions Loop 271 and Loop 309. The use of a novel disulfide bond inserted into these flexible regions was found to hinder the unfolding process of the OPH, increase its proteolytic resistance and increase its operational stability.

MATERIALS AND METHODS

Activity versus Denaturant Determinations. Enzymes (50 μg/mL or 125 μg/mL) were diluted in 10 mM potassium phosphate buffer pH 8.3 with 50 μM $CoCl_2$ and 20 mM KCl, and incubated in denaturant ranging from 0 M to 8 M (for urea) and 0 M to 4.25 M (for GdnHCl) for ≥ 18 hours at 25 ˚C. Fresh denaturant stocks (10 M urea and 5 M GdnHCl) were prepared prior to use with 10 mM potassium phosphate buffer pH 8.3, 50 μM $CoCl_2$ and 20 mM KCl. The pH of denaturant solutions was brought to 8.3 with KOH or HCl. The concentrations of the denaturant stock solutions were confirmed with refractometry (*71*). After incubation, samples were checked for activity against 4 mM demeton-S or 1 mM paraoxon using a Bio-Rad Ultramark Plate Reader and a 340 nM and a 405 nM filter, respectively. Sample conditions consisting of buffer and substrate with increasing concentrations of denaturant to match the denaturant concentration of the sample were used and compared to buffer and substrate without denaturant.

Activity versus Temperature Denatured Enzyme. A 1 mg/mL solution of enzyme was prepared in potassium phosphate buffer pH 8.3 with 50 μM $CoCl_2$ and 20 mM KCl and incubated at various temperatures ranging from 25 ˚C to 75 ˚C. The enzyme was allowed to incubate at each temperature for at least 5 minutes before its catalytic activity was assayed against 4 mM demeton-S. Enzyme samples were removed from the 1 mg/mL stock solution and mixed with 990 μL of prepared demeton-S to a final concentration of 4 mM demeton-S that was incubated at the same temperature as the enzyme sample. A spectrophotometer with water-heated cell holder was used to keep the cuvette and sample at the desired temperature during analysis. Demeton-S was

prepared in 0.5 x Tripart buffer and incubated at the same temperatures as the enzyme solution. Demeton-S was chosen as a substrate for this experiment as it allowed the addition of a 1 mg/mL stock solution of enzyme without further dilution. Hydrolysis of demeton-S was followed at 343 nM in a 1 mL disposable cuvette by following the production of 2-TP (ε_{343} = 7,060 M^{-1} cm^{-1}). Activity is reported as μmoles of 2-TP produced per second and normalized to maximum activity.

Activity versus Different Substrates. Neat Substrates were obtained from ChemService (Westchester, PA).

Malathion. Neat malathion (30 μL) was dissolved in 500 μL of 100% methanol. This mixture was added to 0.5X tripart buffer (50 mM MES, 25 mM N-ethylmorpholine, 25 mM diethanolamine, 1% methanol, pH 8.0). The pH of this solution was brought to pH 8.0 with KOH and to 50 mL final volume with milliQ H_2O and let stir overnight at room temperature. The final malathion concentration was 3 mM. 10 μL of stock enzyme was added to 990 μL of 3 mM malathion pH 8.0 to initiate the hydrolysis reaction. The hydrolysis of malathion by OPH produces a free thiol on the leaving group which reacts with 2,2-dithiodipydidine (2,2 TP) which produces 2-thiopydidone (2-TP). The production of 2-TP (ε_{343} = 7,060 $M^{-1}cm^{-1}$) was followed for 3 minutes in a spectrophotometer using a 1 mL disposable cuvette with a path length of 1 cm. Activity is reported as μmoles of 2-TP produced per second.

Dimethoate. Dimethoate (57.3 mg) was dissolved in 500 μL 100 % methanol. This was added to 0.5 x tripart buffer and brought to pH 8.0 and 50 mL final volume with milliQ H_2O. The solution was allowed to stir for one hour at room temperature

prior to use. The final dimethoate concentration was 5 mM. Assays were performed using the same protocol as the malathion assays above.

Parathion. Neat parathion (50 μL) was dissolved in 10 mL of 100 % methanol. The volume was brought to 50 mL with milliQ H_2O. The concentration of the stock parathion was 13.6 mM. Assays were conducted at pH 9.0 in 20 mM CHES buffer. The production of *p*-nitrophenol (ε_{400} = 17,000 $M^{-1}cm^{-1}$) was followed for 1 minute using a 1 mL disposable cuvette with a path length of 1 cm. Activity was reported as μmoles of *p*-nitrophenol produced per second.

EPN. EPN (90 mg) was dissolved in 10 mL of 100 % methanol. The volume was brought to 50 mL with milliQ H_2O. The final concentration of EPN was 5 mM. Assays were performed at pH 9.0 in 20 mM CHES buffer as described above. Activity was reported as μmoles of *p*-nitrophenol produced per second.

Paraoxon and Demeton S. Parathion and demeton S were prepared as previously described in Chapter III.

Disulfide Reduction with TCEP, β-Mercaptoethanol and DTT. TCEP (Tris[2-carboxyethyl]phosphine) was dissolved in 10 mM potassium phosphate, 20 mM KCl, 50 μM $CoCl_2$ pH 8.3 buffer to make a final stock concentration of 50 mM TCEP. Final working concentrations of TCEP were 0.5 mM and 1.0 mM. Enzyme solutions were incubated in the presence of TCEP for at least 30 minutes at room temperature prior to analysis.

β-ME (2-hydroxyethylmercaptan; β-mercaptoethanol) was dissolved in 10 mM potassium phosphate, 20 mM KCl, 50 μM $CoCl_2$ pH 8.3 buffer and used at a final working concentration of 1 mM.

DTT (1,4 dithiothreitol) was dissolved in milliQ H_2O to make a final stock concentration of 100 mM DTT. Final working concentrations of DTT were 1.0 mM. Enzyme solutions were incubated in the presence of DTT or β-ME for at least 1 hour at 37 ˚C prior to analysis.

Site-Directed Mutagenesis for Cysteine Variants. The pUC19-*opd* gene coding for the leaderless wild-type OPH was used in all mutagenesis reactions (*69*). A Quick Change® XL Site-Directed Mutagenesis Kit from Stratagene® was used to construct all the mutations. The manufactures directions were followed in all cases. The oligonucleotides used in this study were synthesized in 25 nmole quantities by Integrated DNA Technologies, Inc. (Coralville, IA), desalted and freeze-dried. All oligonucleotides were resuspended in 400 μL of MilliQ H_2O prior to use. The following oligonucleotides were used to direct all cysteine variant reactions:

(S267C) 5’ CTAGAAGATAATGCGTGTGCATCAGC 3’

3’ TGTCTATTACGCACACGTAGTCGGGA 5’

(Y309C) 5’ GTTTTCGAGCTGTGTCACCA 3’

3’ CAAAAGCTCGACACAGTGGT 5’

(D133C / L136C) 5’ CCGGCTTGTGGTTCTGCCCGCCATGTTCGATGCGAT-

TGAGG 3’

3’ GGCCGAACACCAAGACGGGCGGTACAAGCTACGCT-

AACTCC 5’

(A63C) 5’ CTGCGGCAGCTCGTGCGGATTCTTGCGTGCTTGG 3’

3’ GACGCCGTCGAGCACGCCTAAGAACGCACGAACC 5’

RESULTS

Activity of Wild Type and Disulfide Variants of OPH::Co^{2+} as a Function of Urea Concentration. In an attempt to increase the operational stability of OPH, novel disulfide bonds were inserted into regions of OPH determined by limited proteolysis to unfold in denaturing conditions. Amino acid A63 is positioned in the intersubunit interface of the enzyme, near the small pocket of the active site. A63 of one subunit is situated adjacent to the same residue of the opposite subunit. *In silico* mutagenesis using the molecular modeling software, Pymol, indicated that the mutagenesis of this residue to a cysteine would result in an acceptable placement of the sulfhydryl groups to form a disulfide. According to the activity profile of the purified enzyme as a function of urea (Figure 4.1), this enzyme did not have the same operational range as the wild type enzyme.

D133 and L136 are found in the intersubunit interface across from their respective counterparts from the opposite subunit. *In silico* modeling suggested that these changes would place the cysteine residues in the proper conformation to allow disulfide bonds to form in oxidizing conditions. As shown in Figure 4.1, however, the relative activity of this enzyme against paraoxon as a function of urea concentration was less than that of the wild type and A63C.

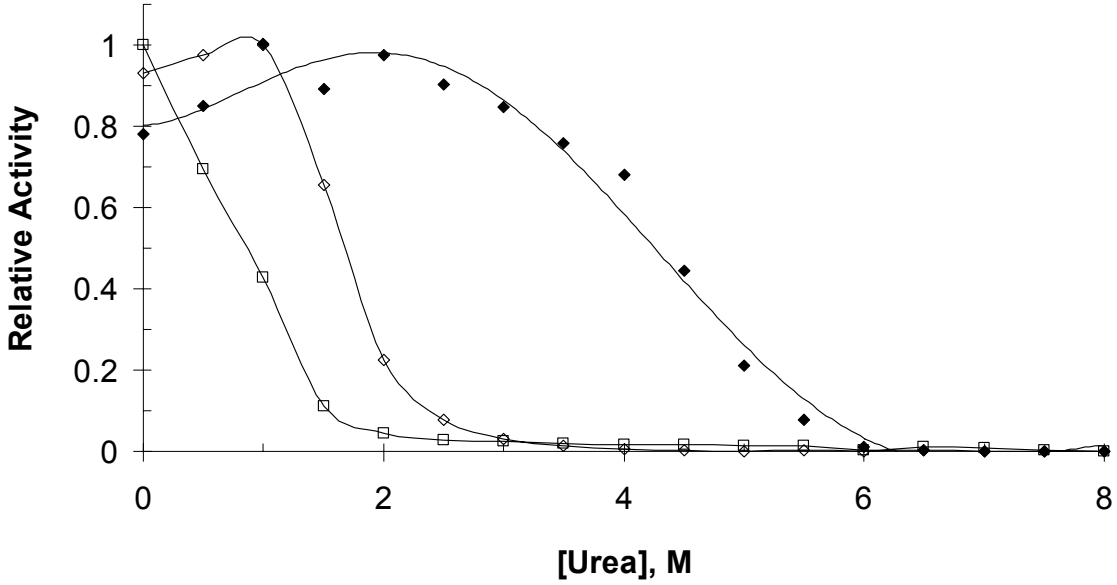

Figure 4.1: Relative activity of disulfide OPH::Co^{2+} variants as a function of urea concentration. Wild type OPH (♦), A63C (◊), and D133C / L136C (□) concentrations are 50 μg/mL.

Viscosity Effects of Denaturants. In order to determine the effects that the viscosity of denaturant solutions might have on the catalytic ability of CC and wild type OPH::Co^{2+}, the relative viscosities of the denaturant solutions (*119*) and sucrose (*99*) were compared. The addition of sucrose limited the rate of hydrolysis (μM^{-1} sec^{-1}) by as much as 2 orders of magnitude revealing that the hydrolytic abilities of OPH were inhibited by solvent viscosity (*99*). The viscosities of the different solutions are compared in Figure 4.2. A 13.3 % sucrose solution has approximately the same relative viscosity to water as a solution of 3.4 M urea or 4.0 M GdnHCl. A 15.6 % sucrose solution has an equivalent relative viscosity as 4.9 M urea or a 6 M GdnHCl solution,

while a 21.3 sucrose solution has a relative viscosity equivalent to a 6.6 M GdnHCl solution and greater than an 8 M urea solution. It is not unreasonable to assume from this data that the increased viscosity resulting from addition of denaturant to OPH will have a large, negative effect on the catalytic ability of the enzyme.

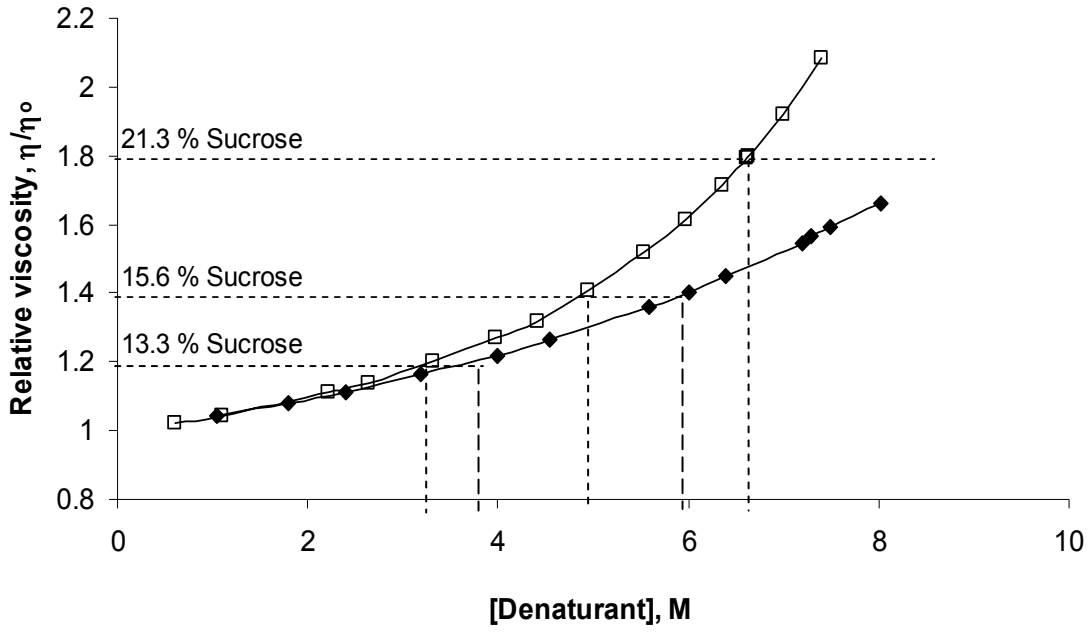

Figure 4.2: Comparison of the relative viscosities of sucrose, urea and GdnHCl. The relative viscosities of sucrose solutions at the indicated percentages were compared to the relative viscosities of the two denaturants, urea (♦) and GdnHCl (□), at increasing concentrations. The urea and GdnHCl data was taken from (*119*) and the sucrose data from (*99*).

Urea Effects on Activity of WT and CC OPH::Co^{2+}. In order to asses the effects that saturating amounts of urea had on the catalytic ability of OPH, a control (without excess urea present) was compared to a sample that was saturated with urea. In both cases, enzyme was incubated in a range of urea concentrations from 0 – 8 M urea in 1 M increments. The control utilized buffer and substrate (paraoxon) without any additional urea. The saturated sample consisted of buffer and substrates containing urea so that the final concentration of urea in the saturated samples spanned the 0 – 8 M range of urea in 1 M increments. Examination of Figure 4.3 confirmed that the samples containing saturating amounts of urea inhibited the hydrolysis of paraoxon by wild type OPH::Co^{2+}. Samples containing a final concentration of 1.0 M urea (enzyme, buffer, and substrate) showed approximately 40 % less activity than samples whose buffer and substrates did not contain urea. At 5.0 M urea, samples whose buffers and substrates contained a final urea concentration of 5.0 M urea only retained 2 % of maximal activity while those samples without urea still retained approximately 36 % activity. It is unlikely that the amount of refolding that took place in the one minute time course of this reaction contributed a difference of approximately a 40 % increase in activity. Examination of Figure 4.4 indicated that OPH has a slow refolding rate (~3 ½ hours to attain maximum activity). The slow recovery of activity (slope ~ 0.003) suggested that any refolding that took place in the one minute time course of the reaction would be negligible. As shown in previous studies, the viscosity of the solution can have a large, adverse effect on the catalytic ability of OPH (*99*). It is not unreasonable to assume that the increased

viscosity of samples containing excess urea is responsible for the decrease in activity as compared to samples that did not contain excess urea (Figure 4.3).

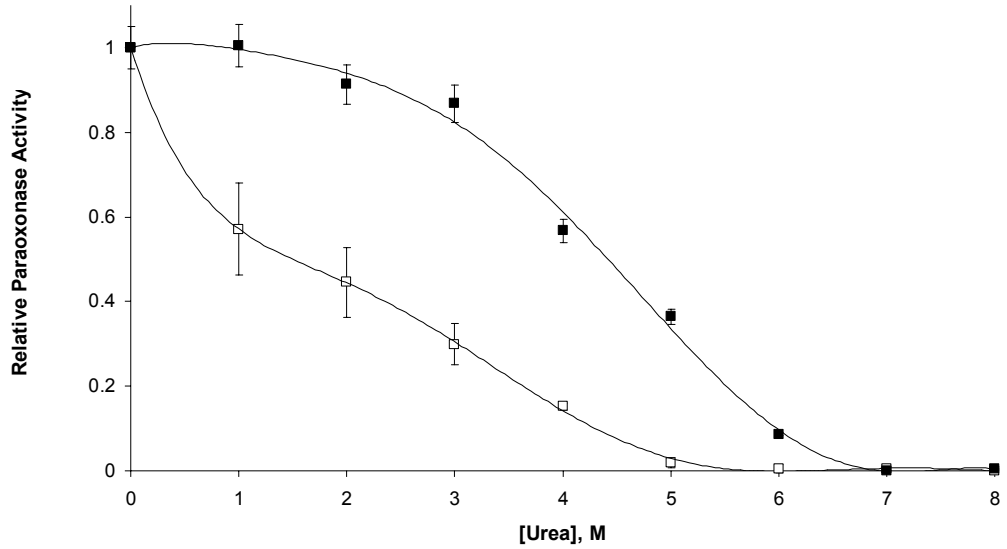

Figure 4.3: Comparison of WT OPH::Co^{2+} paraoxonase activities in different buffer conditions. Both data sets represent wild type OPH::Co^{2+} incubated in the specified concentration of urea for 18 hours prior to analysis. Samples were initiated with a final substrate concentration of 1.0 mM paraoxon in 20 mM CHES buffer, pH 9.0. Buffers and substrate without urea (control, ■) and with urea (saturated samples, □) were used to make the comparisons. Signals (A_{405}/min) were normalized to the maximum signal.

Refolding Rate of Wild Type OPH::Co^{2+}. CC and wild type OPH::Co^{2+} (125 μg/mL) were incubated in 8.0 M urea overnight at 25 ˚C. Buffer was added to the samples to bring the final concentration of OPH to 12.5 μg/mL and the final denaturant

concentration to 0.8 M urea. Since maximum activity for OPH::Co^{2+} was observed at 1.0 M urea, it was thought that this would be the enzyme would refold under these conditions. Upon dilution with buffer, the sample was allowed to incubate at 25 ˚C for the indicated amount of time (Figure 4.4) prior to analysis. Reactions were initiated with substrate (to a final concentration of 1 mM paraoxon) and the progress of the reaction followed for one minute in a spectrophotometer at 405 nM. As observed in Figure 4.4, the activity of the enzyme reaches a maximum activity after approximately 3 ½ hours. Although the increase in activity, symbolizing refolding of the enzyme, appeared to begin upon dilution of the denatured enzyme, it did not appear to be significantly changed over the course of one minute. The activity versus dilution time data (Figure 4.4) was fit with a best-fit line and its slope found to be 0.003. After the course of one minute of dilution time, we would expect an increase in the activity of OPH by approximately 0.3%. It took at least 3 ½ hours for the enzyme to attain maximum activity and it was unlikely that the enzyme would have achieved a significant extent of refolding during the one minute time course of a hydrolysis reaction.

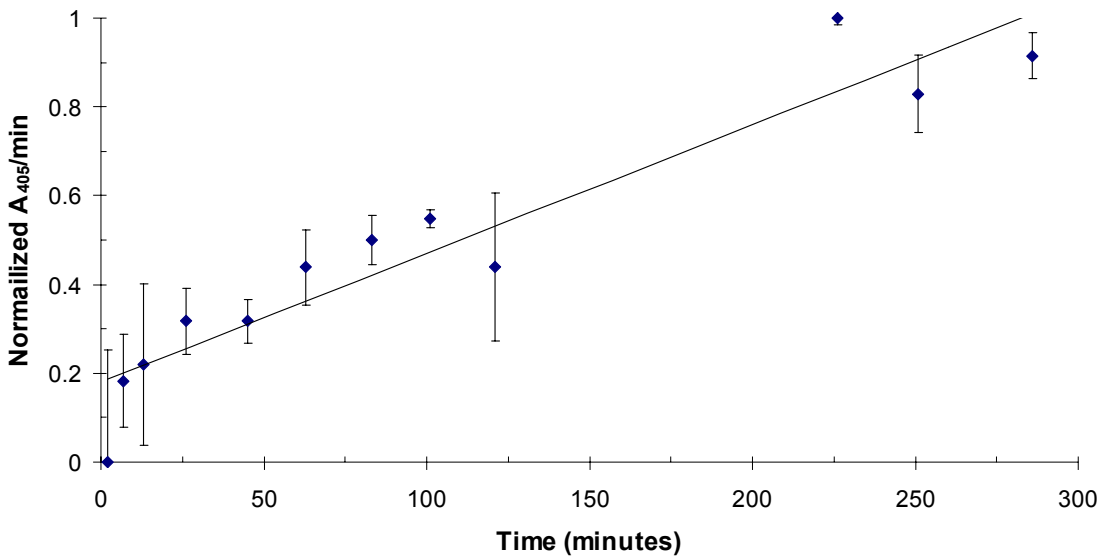

Figure 4.4: Refolding kinetics of denatured OPH (8.0 M urea) as a function of dilution time. The activity of the diluted samples was normalized to maximum activity, represented as A_{405}/min. The dilutions were done in triplicate. The best-fit line is shown.

Activity of Wild Type and CC OPH::Co^{2+} as a Function of Urea Concentration. According to the unfolding model developed from the limited proteolysis data, the 271 and 309 loop regions are flexible, mobile regions that are the first to unfold in denaturing conditions. It was hypothesized that the insertion of a novel disulfide bond bridging these two regions together would hinder the unfolding process and confer increased operational stability to the enzyme. Residues forming a hydrogen bond, S267 and Y309, were chosen as candidates to change via site-directed mutagenesis to cysteine residues. *In silico* mutagenesis of these residues to cysteines suggested that the resultant mutations would be located in acceptable positions to form a disulfide bond. As shown in Figure

4.5, the disulfide mutant S267C / Y309C (CC) does increase the operational stability of the enzyme in elevated urea conditions as compared to that of wild type OPH. Both wild type and the CC enzymes displayed an increase in initial activity in mild urea concentrations. The CC mutant retained up to 70 % of its original activity in 8.0 M urea whereas the wild type had no activity remaining by 6.25 M urea.

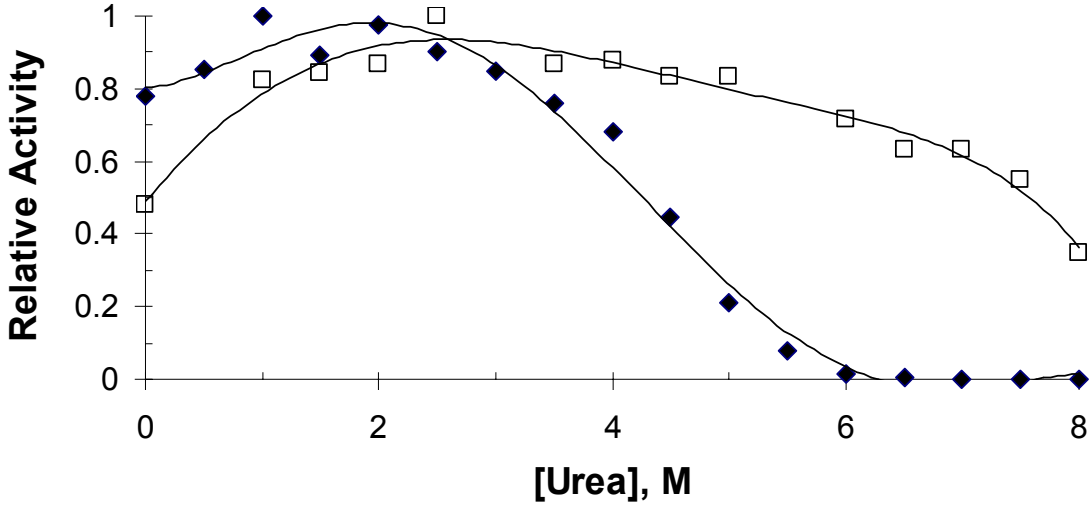

Figure 4.5: Paraoxonase activity of WT and CC OPH::Co^{2+} as a function of urea concentration. Wild type OPH::Co^{2+} (♦) and CC OPH::Co^{2+} (□) were incubated in the presence of the indicated concentration of urea for ≥ 18 hours at 25 ˚C prior to analysis against 1.0 mM paraoxon. Each curve is normalized to its maximized activity.

Activity of Cysteine Variants versus GdnHCl Concentration. The catalytic activities of the cysteine variants and wild type OPH::Co^{2+} as a function of GdnHCl concentration are shown in Figure 4.6. The catalytic activities of the single cysteine variants, S267C and Y309C, appeared to overlap with the activity profile of the wild type enzyme. The disulfide enzyme variant showed an expanded range of activity in GdnHCl as compared with the other enzymes. Although not as striking a difference between the wild type and disulfide enzymes as when denatured in urea, there is certainly an increase in the operational stability of the disulfide variant. For instance, at 1 M GdnHCl, the wild type, S267C, Y309C and disulfide enzymes had 5%, 16%, 11%, and 35% of their maximum catalytic activities against demeton-S remaining, respectively. Additionally, all of the enzymes tested appeared to have the same initial increase in activity when incubated in the presence of 0.25 M GdnHCl.

Comparison of the Activities of WT OPH::Co^{2+} and CC OPH::Co^{2+} as a Function of Temperature. Comparison of the activity profiles of the wild type and disulfide variant of OPH as a function of temperature indicated that both enzymes had the same activity versus temperature profile. Both enzymes formed an observable white precipitate at ≥ 60 °C and began to rapidly lose activity at approximately 55 °C. Comparison of activity versus temperature profiles where the buffer and substrate are held at 25 °C (Figure 4.7B) with the profiles where the buffer and substrate were incubated in increasing temperatures (Figure 4.7A) indicated that they were very similar.

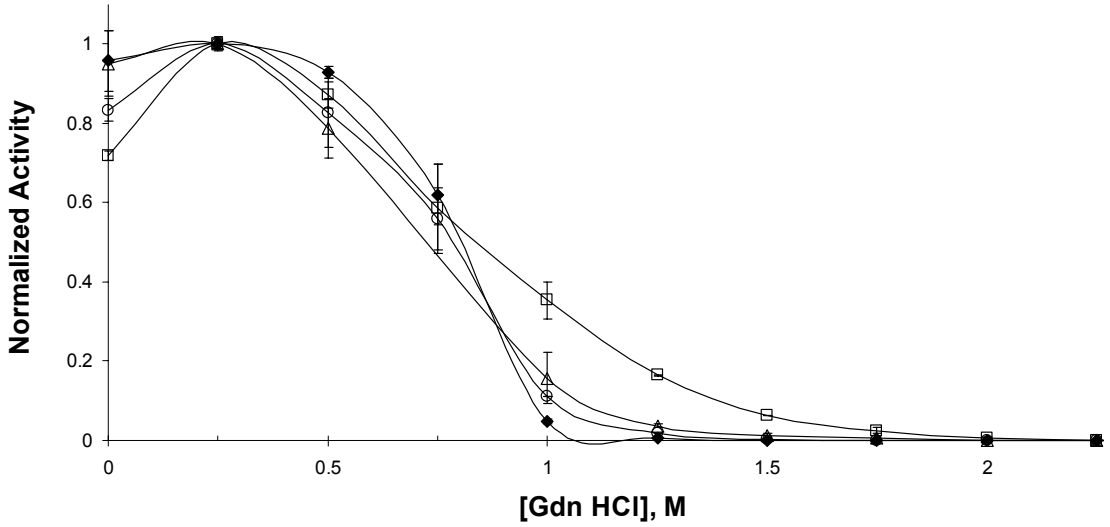

Figure 4.6: Activity of cysteine variants and wild type OPH::Co^{2+} as a function of GdnHCl concentration. Samples were incubated in the indicated concentration of GdnHCl for ≥ 18 hours at 25 ˚C prior to analysis. Activity against demeton-S is normalized against maximum activity. Wild type (♦), CC (□), S267C (Δ), S309C (○) OPH::Co^{2+} concentrations are 50 μg/mL.

Perhaps the most striking difference between the two methods was the rate of increase in activity between 25 °C and 50 °C. The slopes of wild type and CC are 0.019 (wild type) and 0.021 (CC) in Figure 4.7A and 0.0076 (wild type) and 0.0076 (CC) in Figure 4.7B. This suggested a much more rapid formation of detectable product at 343 nM in samples where all of the reagents were incubated in increasing temperatures versus samples that contained buffer and substrate held at 25 °C for the entirety of the experiment. This suggested either a more rapid hydrolysis of substrate by the enzyme or a breakdown of substrate and buffer components in increasing temperatures. In fact, for

those samples in which all of the reagents were incubated at the assay temperature the y-intercept (ΔAbs) increased as the temperature increased. The y-intercept remained the same throughout the course of the experiments where only the enzyme was incubated in increasing temperatures. In all samples, the concentration of demeton-S was held constant (4 mM), so it is unlikely that any small change in concentrations of substrate, from one experiment to another, would cause such a difference in hydrolysis. More probable was a breakdown of substrate or buffer products at elevated temperatures that give the appearance of a detectable product.

In all cases, denatured aggregates were observed as a white precipitate at temperatures ≥ 60 °C suggesting that the aggregation pathway of OPH in thermal denaturing conditions was the same in the presence and absence of the disulfide bridge at position 267 and 309. Thus, the presence of the disulfide bond does not appear to increase the operational stability of the enzyme under thermal denaturing conditions.

A.

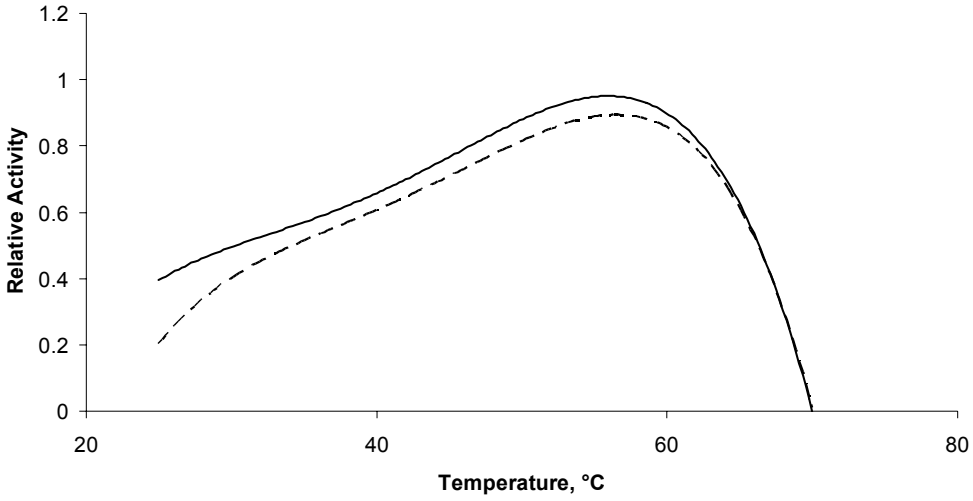

B.

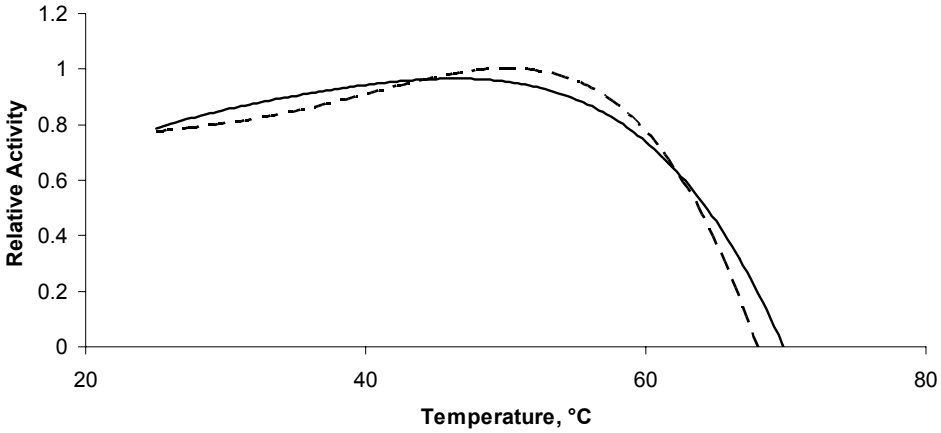

Figure 4.7: Activity profile of wild type versus CC OPH::Co^{2+} as a function of temperature. Wild type (continuous line) and CC (dashed line) were incubated at a particular temperature for 5 minutes prior to analysis. A) Wild type (continuous line), CC (dashed line), buffers and demeton-S were incubated at a particular temperature for 5 minutes prior to analysis. Samples were taken at 25 °C, 36°C, 46 °C, 51 °C, 56 °C, 62°C, and 70 °C. B) Buffers and demeton-S were held at 25 °C. Samples were taken at 5 °C increments from 25 °C to 70 °C.

ANS Studies of Cysteine Variants. In order to assess the active-site topologies, wild type and cysteine variants that had been incubated in increasing concentrations of GdnHCl overnight were incubated with ANS (final ANS:enzyme ratio of 18.8:1) and monitored by fluorescence. ANS binds in the active site of OPH and has been shown to be excluded from the active site using the inhibitor, coumarin (*67*). As seen in Figure 4.8, the emission wave scan for each enzyme was very similar and had a maximum emission at 1.25 M GdnHCl. This suggested that the modifications to the wild type structure did not significantly perturb the active site topology of OPH::Co^{2+}.

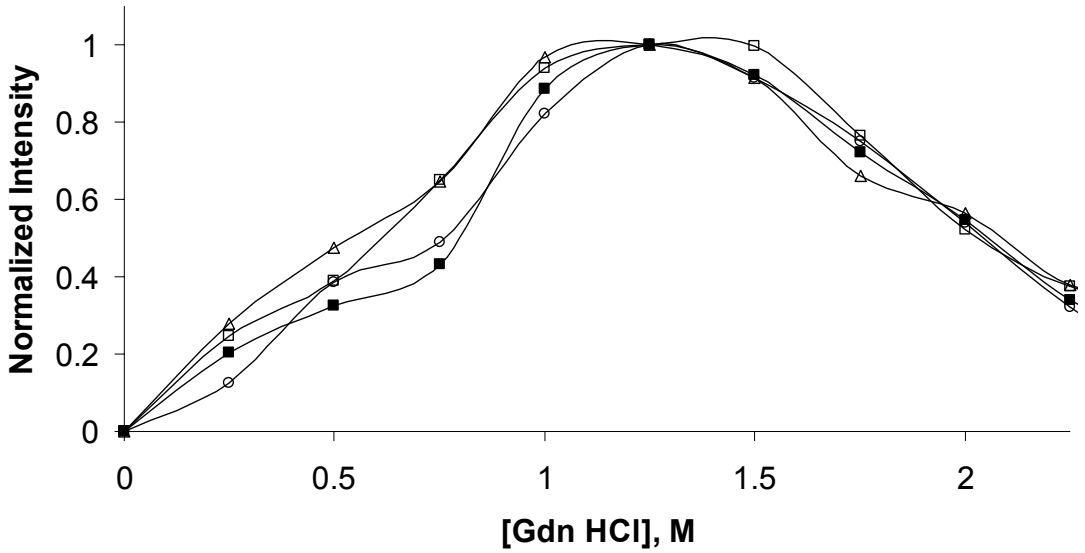

Figure 4.8: ANS dye binding emission spectra of cysteine variants. Wild type (♦), CC (□), S267C (Δ), and Y309C (○) OPH::Co^{2+} were incubated in the indicated concentration of GdnHCl for ≥ 18 hours at 25 ˚C prior to incubation with ANS. The fluorescence emission spectra of each variant were normalized to maximum signal.

Reduction of the Disulfide Bond. Tris(2-carboxyethyl)phosphine (TCEP) was used to reduce the disulfide bond, S267C / Y309C as an alternative to β-mercaptoethanol and dithiothreitol (DTT) for the purpose of determining the effects on proteolytic resistance and enzyme catalysis of OPH by the disulfide bond. DTT and β-mercaptoethanol were each tested and, when incubated with the enzyme, found to form a precipitate. DTT is also known to be oxidized by the presence of transition state metals (*120, 121*). TCEP, on the other hand, does not appear to form complexes with divalent cations and did not appear to form a precipitate when incubated with the enzyme over the course of time required for limited proteolysis and enzymatic catalysis experiments. TCEP reduces the disulfide bond via the following reaction:

$$(CH_2CH_2COOH)_3P: + RSSR + H_2O \rightarrow (CH_2CH_2COOH)_3P{=}O + 2RSH$$

(*122*). TCEP, final concentration ranges of 0.5 mM to 1.0 mM, was added to enzyme solutions, mixed and allowed to incubate at 25 ˚C for at least 30 minutes prior to analysis.

A.

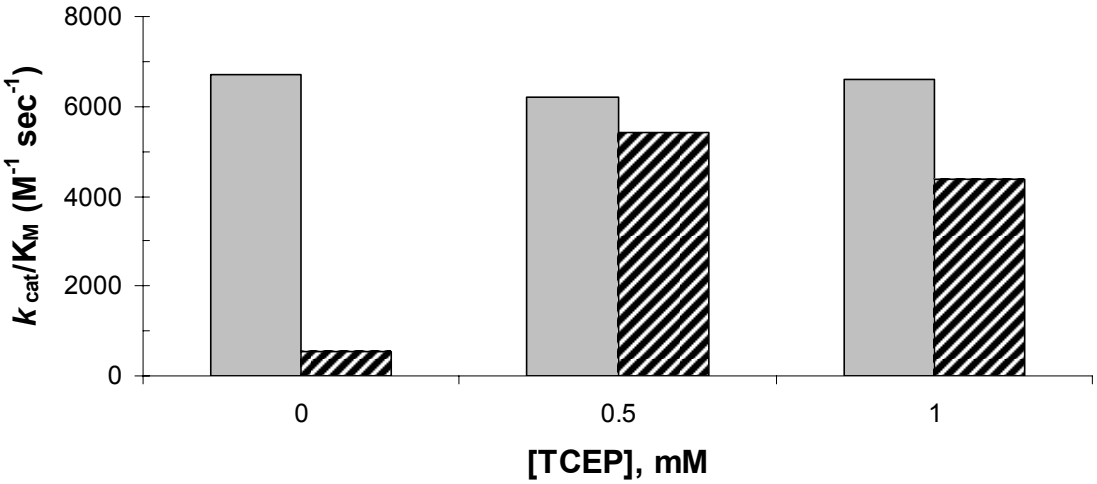

B.

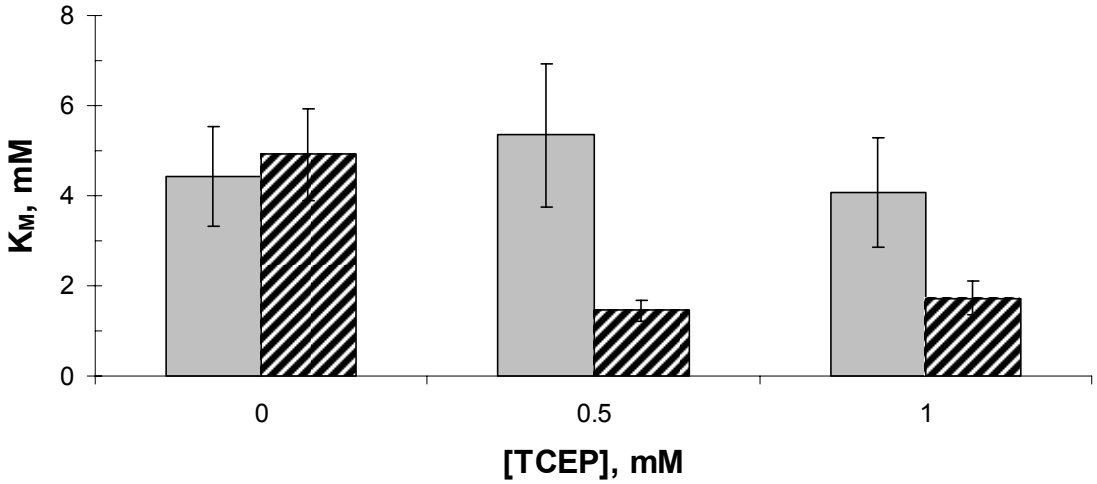

Figure 4.9: Effects of TCEP on the catalytic parameters of WT and CC OPH::Co^{2+} against paraoxon. The solid bars represent wild type OPH while the lined bars represent CC OPH. A) k_{cat}/K_M as a function of TCEP concentration. B) K_M as a function of TCEP concentration.

As seen in Figure 4.9A, the presence of the disulfide bond had an adverse effect on the activity of the enzyme against paraoxon (M^{-1} cm^{-1}). When the disulfide was incubated in the presence of TCEP, however, the disulfide bond was reduced and the activity of the CC enzyme against paraoxon was increased so that it is similar to that of wild type OPH. The presence of TCEP did not appear to alter the activity of the wild type enzyme. As shown in Figure 4.9B, the addition of TCEP to the disulfide enzyme lowered the K_M of the enzyme against paraoxon. This was likely due to the increased flexibility of Loops 271 and 309. Amino acids in these loops are involved in forming the leaving group of the active site (*65*) and their motions are thought to play a role in the catalysis of the enzyme (*98*). The incubation of TCEP with the wild type enzyme did not appear to affect the K_M of the enzyme.

Kinetics. The catalytic values for the hydrolysis of paraoxon and demeton-S are presented in Table 4.1. In all cases, the wild type enzyme displayed the most activity against both substrates. The K_M values of all enzymes for the hydrolysis of demeton-S were similar as were the K_M values for the hydrolysis of paraoxon by the enzyme variants. The k_{cat} for the hydrolysis of paraoxon by CC was slower than by the other enzymes.

Table 4.1: Comparison of kinetic parameters of wild type OPH::Co^{2+} and CC OPH::Co^{2+} against demeton-S and paraoxon.

	Paraoxon			Demeton-S		
Enzyme[a]	K_M (mM)	k_{cat} (sec^{-1})	k_{cat}/K_M (M^{-1} sec^{-1})	K_M (mM)	k_{cat} (sec^{-1})	k_{cat}/K_M (M^{-1} sec^{-1})
WT	0.2 ± 0.03	3.6×10^3	2.4×10^7	4.8 ± 1.0	4.2	8.7×10^2
CC	0.3 ± 0.1	6.9×10^2	2.8×10^6	3.2 ± 0.6	0.2	8.7×10^2
S267C	0.1 ± 0.02	1.2×10^3	1.2×10^7	2.6 ± 0.3	0.7	8.7×10^2
Y309C	0.2 ± 0.03	1.8×10^3	9.7×10^6	4.2 ± 0.5	1.8	8.7×10^2

[a] All enzymes are the Co^{2+} form of OPH.

Multiple Substrates. Endpoint assays were performed in order to determine the relative activities of the wild type enzyme as compared to the activity of the disulfide variant against several different substrates. Both enzymes were tested in the presence and absence of the reductant, TCEP, to determine what affect the disulfide bond had on the activity of OPH. TCEP did not appear to confer any advantage or disadvantage to the wild type enzyme. In the case of the disulfide variant, however, the reduction of the disulfide bond increased the activity of the enzyme against all substrates except for EPN. The results of the endpoint assays are listed in Table 4.2. The structures of the substrates used are represented in Figure 4.10.

Table 4.2: Activities (sec^{-1}) of wild type and CC OPH::Co^{2+} enzymes in the presence and absence of TCEP against multiple substrates.

Substrate	Final [Substrate]	WT (-) TCEP[a]	WT (+) TCEP[a]	CC (-) TCEP[a]	CC (+) TCEP[a]
EPN	0.5 mM	9.0×10^{1}	8.2×10^{1}	1.1×10^{2}	3.2×10^{0}
Parathion	1 mM	2.0×10^{3}	2.0×10^{3}	3.4×10^{1}	7.7×10^{1}
Paraoxon	1 mM	6.1×10^{3}	5.4×10^{3}	4.6×10^{2}	1.4×10^{3}
Demeton-S	4 mM	2.0×10^{0}	2.0×10^{0}	1.0×10^{-1}	3.0×10^{-1}
Dimethoate	5 mM	1.0×10^{-2}	1.0×10^{-2}	1.0×10^{-2}	3.0×10^{-2}
Malathion	3 mM	2.0×10^{-2}	2.0×10^{-2}	N/D[b]	2.0×10^{-2}

a All error is ≤ 10 % of the indicated value
b Not detectable

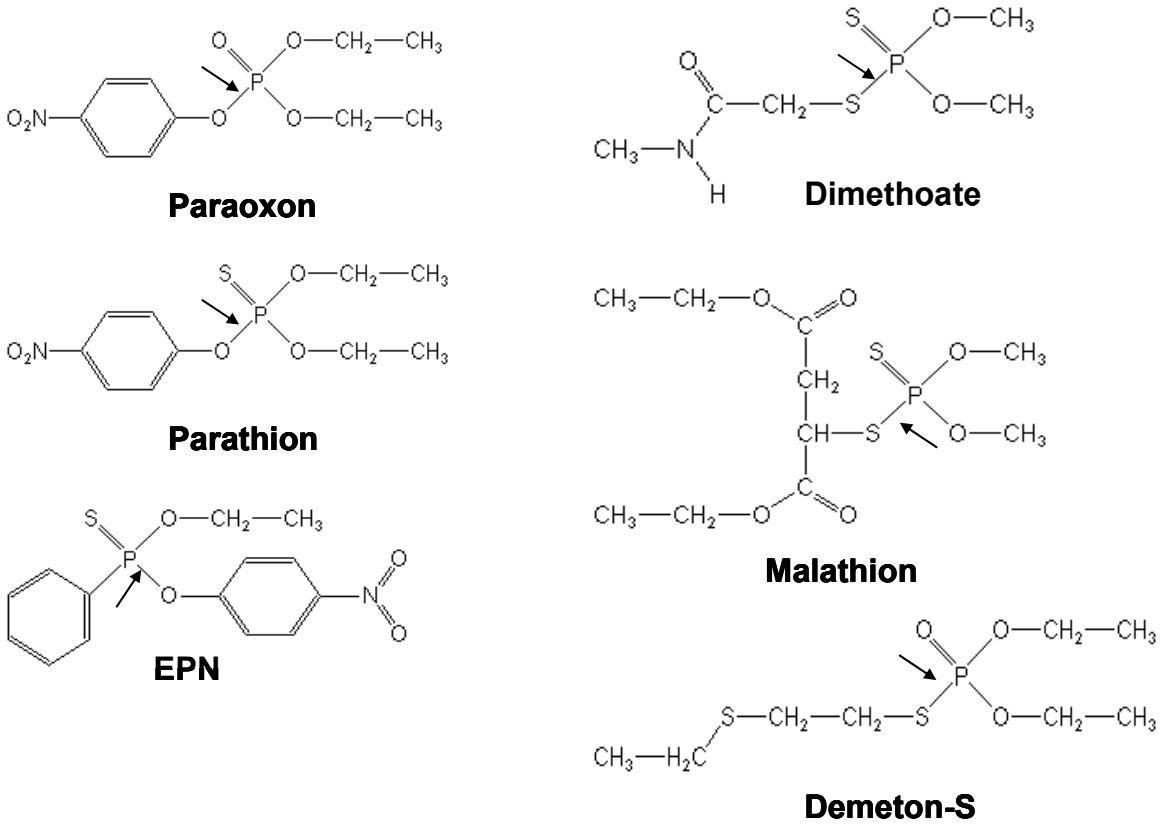

Figure 4.10: Substrates used in this study. The arrow represents the scissile bond hydrolyzed by OPH.

Effect of Enzyme Concentration on Activity. In order to determine if the presence of the disulfide bond prevented the loss of activity of OPH in low concentrations, enzyme samples were diluted to a final concentration ranging from 0.01 mg/mL (0.14 μM) to 1.0 mg/mL (14 μM) and incubated at 25 ˚C for 2 hours. Samples were tested for activity against 1.0 mM paraoxon and the k_{cat} determined. Figure 4.11 indicates that decreasing concentrations of wild type OPH and CC OPH have overlapping activity profiles. This indicated that the presence of the disulfide bond did not provide added protection against the loss of activity in low enzyme concentrations. This also suggested that the loss of activity and possible disassociation of the two monomers of OPH was occurring in the same manner regardless of the presence or absence of the disulfide bond.

Limited Proteolysis of CC OPH::Co^{2+}. Thermolysin was used to probe the resistance to proteolysis offered by the novel disulfide bond. SDS-PAGE was used to follow the progress of thermolysin digestion of CC OPH::Co^{2+} in increasing urea concentrations in the presence of TCEP (Figure 4.12A) and absence of TCEP (Figure 4.12B) at 25 ˚C. Each lane represents the 90 minute time point of the digestion at an Thermolysin:OPH ratio of 1:100. Upon incubation with TCEP, the CC OPH::Co^{2+} enzyme lost the protection offered by the disulfide bridge and the digestion pattern generated by the thermolysin digest looked very similar to that of wild type OPH::Co^{2+} in the presence of urea (Figure 3.3B). In fact, the same sized fragments were generated

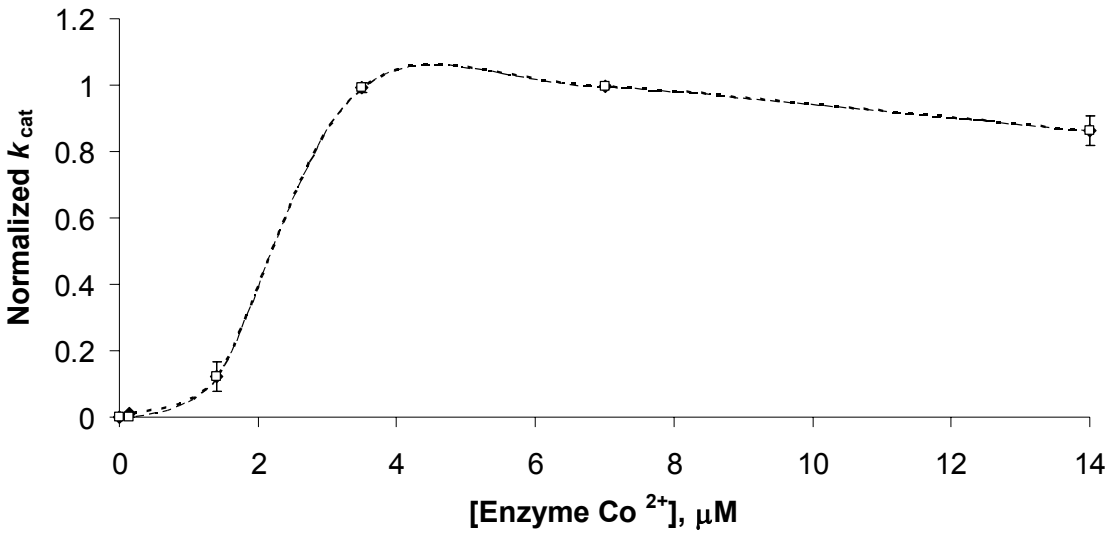

Figure 4.11: The activity (sec^{-1}) of WT and CC OPH::Co^{2+} as a function of enzyme concentration. The catalytic activities of WT (□; dashed line) and CC (♦; dotted line) were normalized to the maximum activity of each enzyme.

in both experiments. On the other hand, in the absence of TCEP there did not appear to be any fragments generated. The amount of CC OPH::Co^{2+} enzyme did not appear to change over the course of the reaction which suggested that the disulfide offered complete protection against proteolysis by thermolysin. Even when CC OPH::Co^{2+} was denatured in 6.0 M urea, new fragments generated by proteolysis were not observed. The fact that no fragments were produced even in elevated denaturant concentrations suggested that the presence of this disulfide hindered the unfolding process and none of the regions that became exposed in the WT OPH::Co^{2+} or CC

OPH::Co^{2+} (without TCEP) proteolysis reactions (Figure 3.3B and Figure 4.12A respectively) were able to unfold and present themselves to the protease.

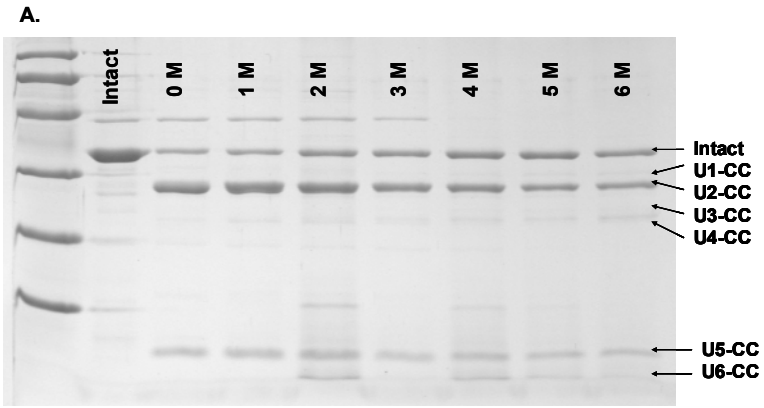

Figure 4.12: Limited proteolysis of chemical denatured CC OPH::Co^{2+} by thermolysin as followed by SDS-PAGE. A) SDS-PAGE CC OPH::Co^{2+} incubated with 1 mM TCEP. Each lane represents the 90 minute time point of the proteolysis reaction at the indicated temperature. Lane 1 represents the Bio-Rad Low Range Molecular Weight markers. The remaining lanes represent the digestion of CC OPH::Co^{2+} digested in the indicated concentration of urea. Prominent proteolytic fragments are designated U1-CC, U2-CC, U3-CC, U4-CC, U5-CC and U6-CC and correspond in size to those generated by proteolysis of wild type OPH::Co^{2+} by thermolysin (U1, U2, U3, U4, U5 and U6; Figure 3.3B).

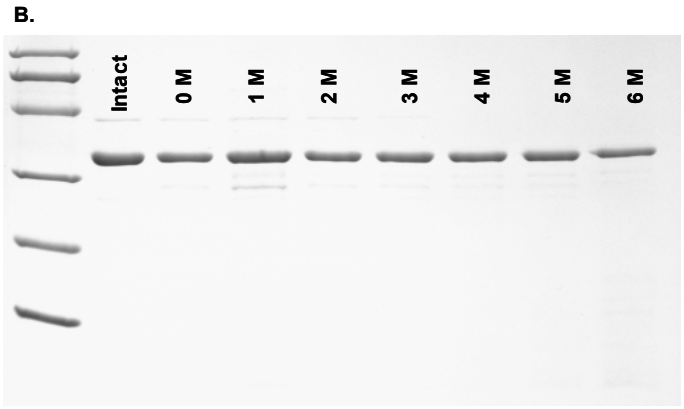

Figure 4.12 Continued: B) SDS-PAGE CC OPH::Co^{2+} in the absence of 1 mM TCEP. Each lane represents the 90 minute time point of the proteolysis of OPH by thermolysin in increasing concentrations of urea. Lane 1 represents Bio-Rad Low Range Molecular Weight markers. The remaining lanes represent the digestion of CC OPH::Co^{2+} digested in the indicated concentration of urea.

Limited Proteolysis of Thermal Denatured CC OPH::Co^{2+}. At 45 ˚C the digestion of OPH by thermolysin produces fragment T2. The N-terminus of this fragment, F72, is found in the intersubunit interface of OPH. It was hypothesized that the presence of the disulfide bond at positions 267 and 309 would inhibit the unfolding pathway of OPH and fragment T2 would not be produced upon incubation of CC OPH with thermolysin. SDS-PAGE was used to follow the progress of the thermolysin digestion of wild type and CC OPH at 45 ˚C (Figure 4.13A). Fragments T1, T2, and T3 were produced upon incubation of the wild type enzyme with thermolysin at 45 ˚C. All three fragments are noticeable after 10 minutes of digestion time (Figure 4.13B; Lane 2).

On the other hand, CC OPH was resistant to proteolysis by thermolysin at 45 ˚C during the 90 minute length of the experiment. The disulfide bond appeared to inhibit the unfolding pathway of OPH::Co^{2+} as probed by limited proteolysis.

A.

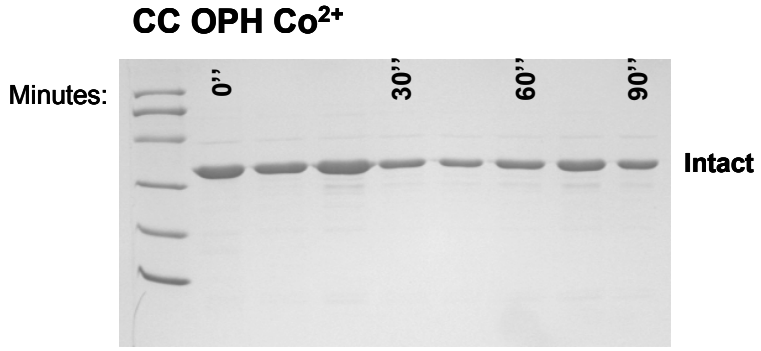

B.

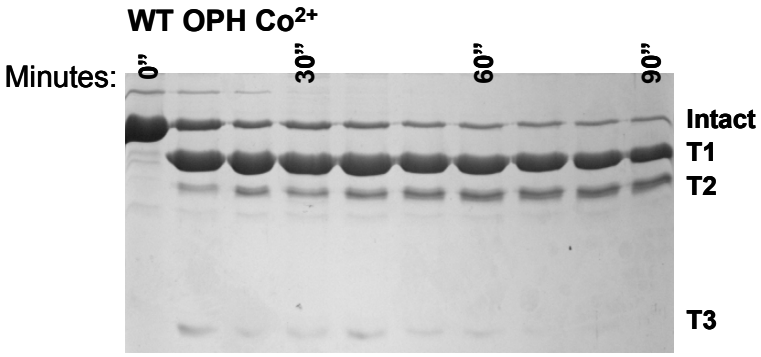

Figure 4.13: Limited proteolysis of A) S267C / Y309C OPH::Co^{2+} and B) wild type OPH::Co^{2+} by thermolysin at 45 ˚C as followed by SDS-PAGE. The time points of the stopped limited proteolysis reaction are A) lane 2, 0 minutes; 3, 1 minute, 4, 15 minutes; 5, 30 minutes; 6, 45 minutes; 7, 60 minutes; 8, 75 minutes; 9, 90 minutes. Lane 1 represents Bio-Rad Low Range Molecular Weight Markers. B) Lane 1, 0 minutes; 2, 10 minutes; 3, 20 minutes; 4, 30 minutes; 5, 40 minutes; 6, 50 minutes; 7, 60 minutes; 8, 70 minutes; 9, 80 minutes; 10, 90 minutes.

Far UV CD Spectra of Cysteine Variants. The far-UV CD spectrum of the wild type and the cysteine variants (Figure 4.14) all displayed a double minimum at 208 nM and 222 nM, characteristic of a protein with a high α-helical content. The far-UV spectra of each of the enzymes did not significantly differ and it was concluded that they shared a similar overall structure to that of the wild type enzyme.

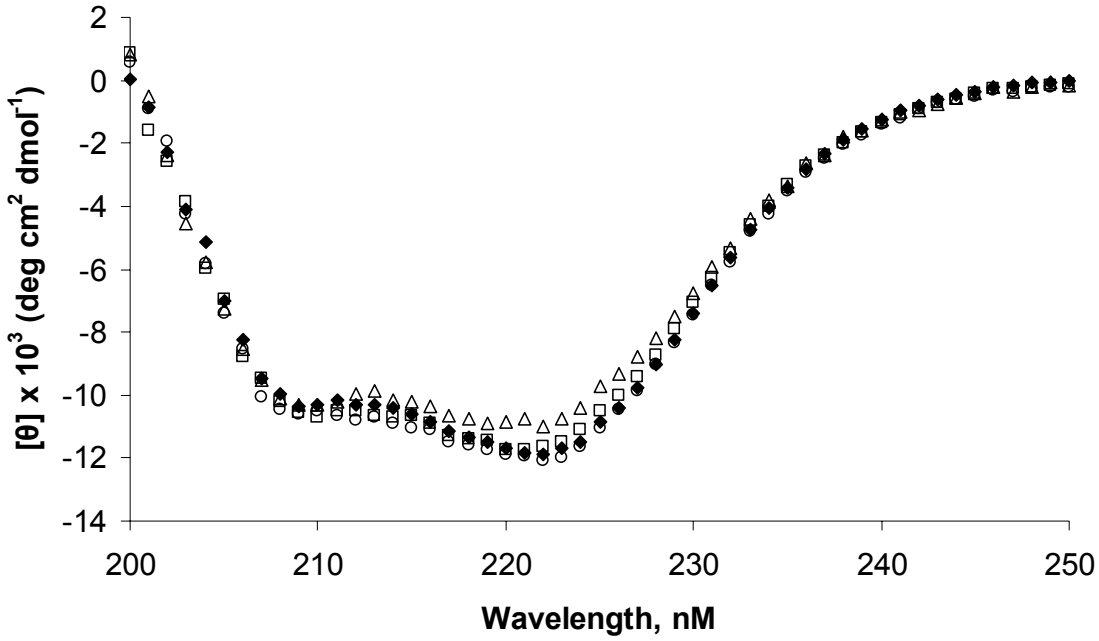

Figure 4.14: Far-UV CD wave scans of the cysteine variants and WT OPH::Co^{2+}. Wild type (♦), CC (□), S267C (Δ), S309C (○) OPH::Co^{2+} concentrations are 63 μg/mL.

Far-UV CD spectrometry of the wild type and disulfide OPH::Co^{2+} was used to assess the extent of changes in secondary structure in increasing denaturing conditions. As shown in Table 4.3, when the enzymes were incubated in the presence of urea, the disulfide variant retained a larger amount of α-helical signal than did the wild type enzyme beyond 3.0 M urea; the point where the dimeric intermediate begins to form. Additionally, there existed an increase in the percentage of secondary structure of both enzymes when incubated at 1.0 M urea, which is in agreement with the spectroscopic and densitometric data as shown in the limited proteolysis studies (Chapter III). There did not appear to be a significant difference between the extent of remaining α-helical structure between the wild type and the disulfide variant enzymes when incubated in GdnHCl.

Table 4.3: Percentage of α-helical structure as a function of denaturant concentration. The percentage of secondary structure is based on the CD signal (milli degrees) obtained at 222 nM.

[Urea], M	WT OPH	CC OPH	[GdnHCl], M	WT OPH	CC OPH
0.0	100.0	100.0	0.0	100.0	100.0
1.0	102.4	101.2	0.5	87.7	91.6
2.0	97.6	98.0	1.0	67.4	74.0
3.0	92.6	93.3	1.5	58.9	61.5
4.0	77.1	86.3	2.0	51.9	51.1
5.0	55.1	70.5	2.5	41.8	37.7
6.0	35.2	48.9	3.0	24.3	28.4
7.0	22.5	35.5	3.5	20.1	23.4
8.0	19.4	25.7	4.0	15.6	22.7

Apparent Melting Point Temperature Determination. Circular dichroism was used to measure the thermal stabilities of the disulfide variant and wild type OPH::Co^{2+} as shown in Figure 4.15. Thermal denaturation of OPH is non-reversible as the enzyme precipitates at temperatures ≥ 60 ˚C. Therefore only an approximate melting temperature can be determined and no attempt to obtain a detailed thermodynamic characterization of thermal unfolding was made. Wild type OPH had the highest $T_{Mapprox}$ at 63.3 ± 0.1 ˚C while the disulfide had a $T_{Mapprox}$ of 56.7 ± 0.1 ˚C. The single cysteine variants and the disulfides were found to be similar at 55.7 ± 0.5 ˚C for S267C and 55.1 ± 0.2 ˚C for Y309C. The disulfide mutant appears to have slightly more residual folded structure between 25 ˚C and 50 ˚C than does the wild type enzyme but begins a rapid thermal unfolding transition at a lower temperature than did the wild type enzyme.

Equilibrium Unfolding of Cysteine Variants and Wild Type OPH::Co^{2+}. Each of the cysteine variants and the wild type enzyme were subjected to equilibrium denaturation in GdnHCl and the unfolding changes were measured by intrinsic tryptophan fluorescence as shown in Figure 4.16. GdnHCl was selected as a denaturant because it was capable of inactivating the disulfide enzyme whereas the enzyme still retained activity in 8.0 M urea (Figure 4.5) and, therefore, was assumed to not be completely denatured. Based on the unfolding profile of OPH::Zn^{2+} and the data presented for OPH::Co^{2+} in Chapter III, all enzymes were assumed to unfold via a three-

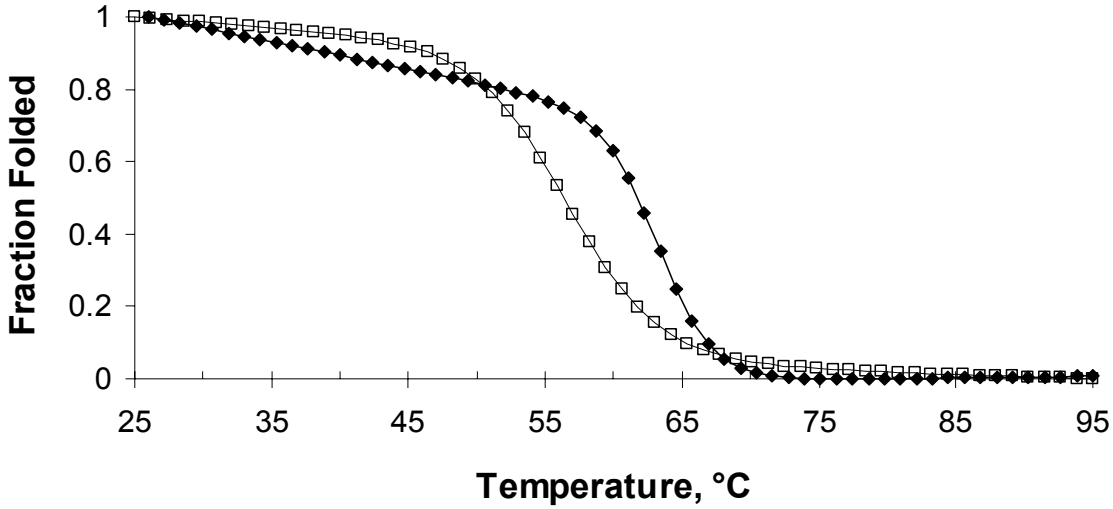

Figure 4.15: Thermal denaturation curves of wild type and CC OPH::Co^{2+}. Wild type (♦) and CC OPH::Co^{2+} enzyme concentrations were 63 μg/mL.

state process (N_2* ↔ I_2 ↔ 2U) and fitted with a three-state equation. There were no clear pre- or post-transitions in any of the unfolding curves which made fitting the data difficult and values generated by the fits, uncertain.

The GdnHCl induced unfolding curves as monitored by fluorescence are shown in Figure 4.16. The figures shared a midpoint around 2 M GdnHCl and reached a predominantly unfolded state at approximately 3 M GdnHCl. Both the wild type and the Y309C enzymes shared a more striking transition at approximately 2.0 M GdnHCl than do the disulfide and S267C variants, which exhibited a smoother transition from the folded state to the unfolded states.

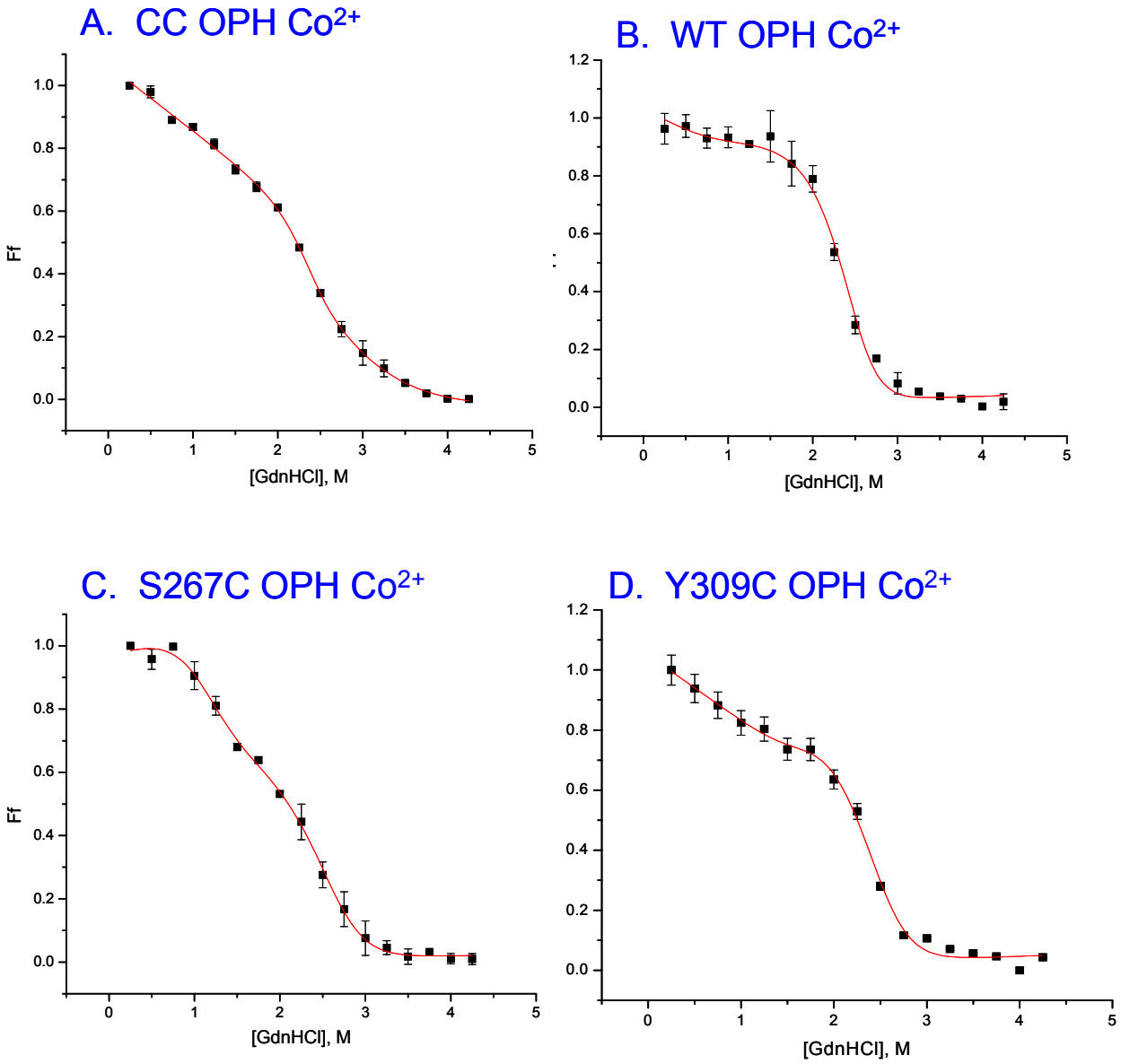

Figure 4.16: GdnHCl induced unfolding of A) CC OPH::Co^{2+}, B) wild type OPH::Co^{2+}, C) S267C OPH::Co^{2+}, and D) Y309C OPH::Co^{2+}. Enzyme concentration was 50 µg/mL. Fluorescence emission was measured at 320 nM with an excitation of 278 nM.

Effect of Enzyme Concentration on the Unfolding Transitions. Figure 4.17 demonstrates the importance of enzyme concentration upon the unfolding profiles of OPH::Co^{2+}. As the protein concentration increased for the wild type Co^{2+} unfolding profile, there was a shift in the midpoint of the second transition toward higher urea concentrations (Figure 4.17A). The results suggest that subunit dissociation occurs in the second unfolding transition of wild type OPH::Co^{2+}, as it does with the Zn^{2+} substituted enzyme (*14*). No striking concentration dependence was observed for the S267C / Y309C disulfide variant (Figure 4.17B). This suggested that the presence of the disulfide bond prevented the disassociation of the enzyme at higher urea concentrations which may explain why the enzyme retained activity in these elevated denaturant conditions.

DISCUSSION

As discussed in Chapter III, the overall conformational stability of OPH is large (~40 kcal/mol for the Zn^{2+} form and ~ 29 kcal/mol for the most catalytically active Co^{2+} form) while the energy required to inactivate the enzyme is much smaller (~4 kcal/mol for both the Zn^{2+} and Co^{2+} metal forms). It was therefore desirable to develop an understanding of how the enzyme unfolded into its inactive form so that it could be reengineered to resist unfolding. By increasing the conformational stability of the first unfolding transition, it was hoped that the operational stability of the enzyme could be enhanced in harsher environmental conditions.

A.

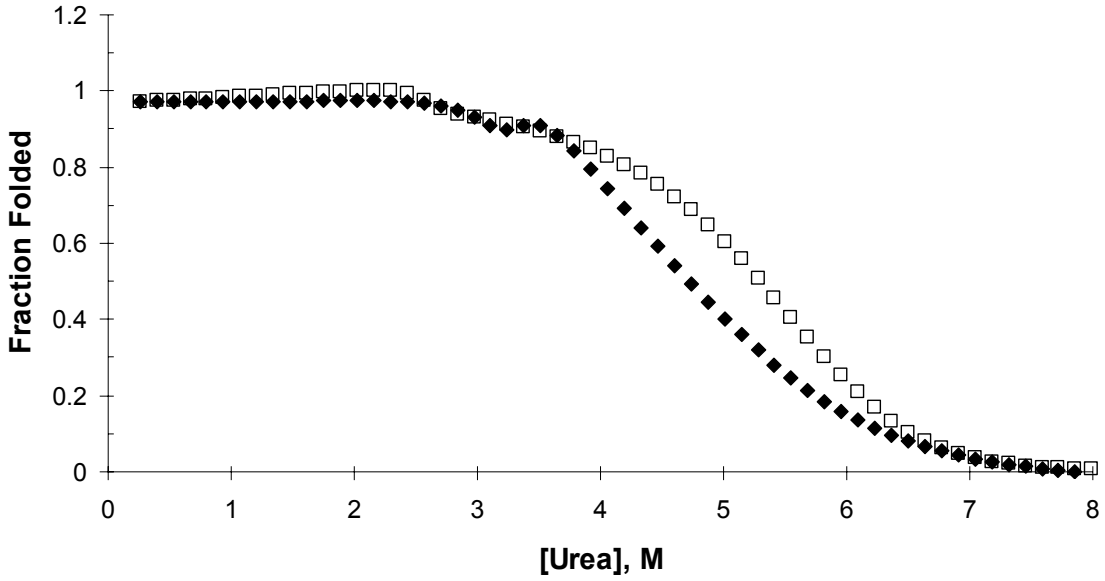

B.

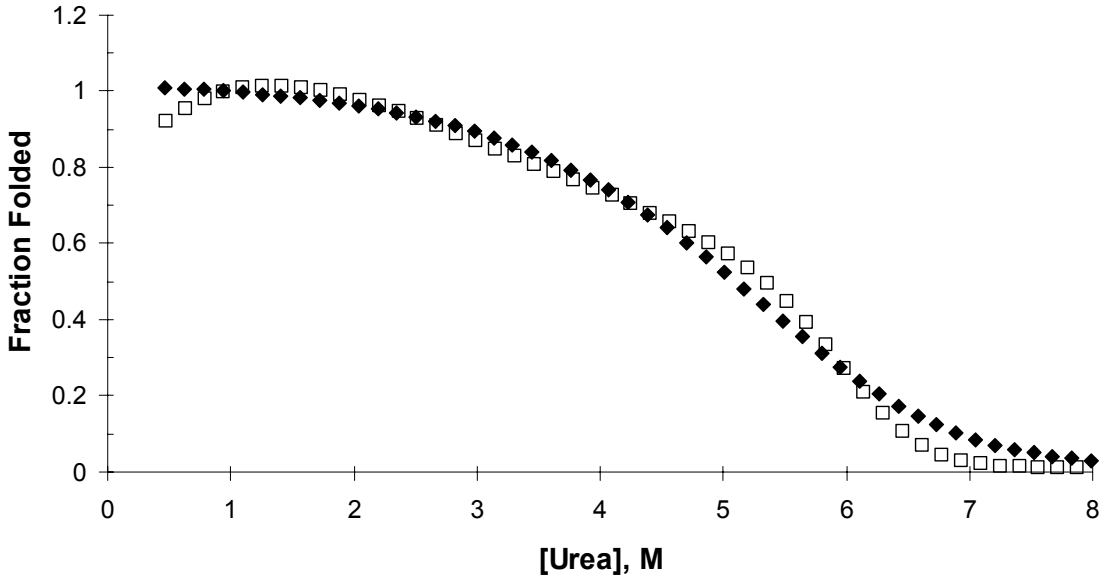

Figure 4.17: The dependence of concentration on the unfolding of OPH::Co^{2+}. A) Wild type and B) CC enzyme concentrations are 50 μg/mL (♦) and 120 μg/mL (□). The three-state fit of the data is presented.

In gram-negative cells, the cytoplasmic space is a reducing environment due to the presence of the thioredoxin / thioredoxin reductase and glutaredoxin / glutaredoxin reductase systems. The periplasm contains disulfide bond formation (Dsb) proteins that catalyze the oxidation of disulfide bonds (*123*). It was reasoned that the formation of disulfide bonds would occur in OPH variants that had been engineered to include adjacent cysteine residues once the enzymes had been exposed to oxidative conditions through cell lysis. As shown by limited proteolysis and enzymatic catalysis assays, disulfide bond oxidation did occur in these variants.

The Operational Stability of OPH is Enhanced Through Rational Design of a Novel Disulfide Bond. Several attempts were made to try to stabilize the folded enzyme structure. The first attempted to stabilize the active site and prevent the interface from disassociating. When OPH was incubated in the presence of 1 M urea or 45 ˚C, F72 was observed as a proteolytic cut site. This indicated that this region of the interface had become exposed to the protease in mild denaturing conditions. A63 is near in tertiary structure to F72 and near in primary and tertiary structure to G60, which forms part of the small pocket of the active site. Upon mutagenesis and purification, however, it was found that the A63C variant had a lower operational stability than that of the wild type enzyme (Figure 4.1). While there was an initial increase in the catalytic activity of the variant in mild denaturant conditions (similar to the wild type enzyme), it was inactivated by 3.0 M urea. The wild type enzyme, in contrast, was inactivated at approximately 6.25 M urea.

When OPH was incubated in 3 M urea, L130 was observed as a proteolytic cut site indicating that it had become exposed and mobile enough to become accessible to the protease (Chapter III). Another disulfide variant, D133C / L136C, was selected based on molecular modeling data. D133 formed a salt bridge with R139 of the opposite subunit. It was suspected that this salt bridge had a role in stabilizing the enzyme in thermal denaturing conditions and, a novel disulfide bond in this region might stabilize the enzyme in chemical denaturing conditions. Upon mutagenesis and characterization, however, it was found that this variant had less of an operational stability that either the wild type or A63C as the enzyme was inactivated at 2.0 M urea. Since these variants did not fit the goal of this study, no further attempt to characterize them was made.

Loop motions are important in the catalytic activities of TIM barrels. NMR and crystallographic studies have determined that active site loop motions are part of the natural dynamics of human triosephosphate isomerase and that the rate of motion was approximately equal to the turn over time of the substrate (*102*). Additional studies have shown that the rate of loop motion and the product release are connected and that the rate of the conformational change is subject to the identity of substrate present in the active site. Stronger binding by the substrate represented a slower conformational change. It was concluded that the rate of active site loop opening was partially rate determining in the catalysis reaction for this TIM (*101*).

Molecular modeling studies of the loop regions in OPH have determined that the dynamics of these regions are inherent properties of the enzyme and have been found to occur in the free enzyme and in the enzyme substrate complex. As previously discussed,

these motions occur in the region of the leaving group pocket of OPH. Changes between 11 and 18 angstroms (from F72 to residue L271) have been calculated to occur and the degree of motion was dependent upon the identity of the substrate present (*98*).

According to the limited proteolysis data, (Chapter III) the flexible regions (Loop 271 and Loop 309) are the first to be cleaved by thermolysin at 25 ˚C in non-denaturing conditions. Since these regions were so susceptible to the protease, it was hypothesized that joining them together with a covalent modification would stabilize the enzyme structure.

The residues forming the hydrogen bond (S267 and Y309) joining these two loop regions together were chosen for mutagenesis. Since there was already a hydrogen bond stabilizing this region, changing it to a covalent bond might improve the stability of the region while minimizing the introduction of strain. *In silico* mutagenesis also suggested that the change of these residues to cysteines would result in a placement acceptable for the formation of disulfide bonds. The activity profile as a function of denaturant concentration of S267C/Y309C::Co^{2+} (CC OPH) shows that the operational stability of this variant is increased with respect to the wild type enzyme (Figure 4.5). The activity profile of CC was similar to that of the wild type in that the activity increased to a maximum in mild denaturing conditions and then began to decline. In contrast to the activity profile of the wild type, however, the CC enzyme retained approximately 70 % of its original activity in 8.0 M urea. In 9.0 M urea, the enzyme retained approximately 2 % of its original activity. The addition of the disulfide bond has obviously increased the operational stability of the enzyme.

Guanidine HCl is a more effective denaturant than urea, and was therefore used to denature the CC enzyme to try to inactivate it. Although not as striking a difference with the activity profile as a function of urea concentration, the CC variant displayed increased operational stability when incubated in GdnHCl as compared to that of the wild type enzyme. As indicated in Figure 4.6, the CC enzyme lost its activity completely at approximately 2.0 M GdnHCl while the activity of the wild type enzyme was undetectable at approximately 1.25 M GdnHCl. The most prominent difference took place at 1.0 M GdnHCl where CC OPH retained approximately 35 % of its maximum activity while the wild type enzyme only retained 5 % of its maximum activity. The activity versus GdnHCl profiles for the single cysteine variants closely followed the activity profile of the wild type enzyme. This further suggested that the disulfide bond joining positions S267 and Y309 increased the operational stability of the enzyme.

The Reduced Flexibility of the Disulfide Variant Hinders the Enzyme's Catalytic Activity. The joining of these two regions together by a disulfide bond would be expected to increase the rigidity of this region and have an adverse impact upon the catalytic activity of the enzyme The catalytic activity (sec^{-1}) of the enzyme was hindered as compared to that of the wild type while its K_M remained virtually the same (Figure 4. 9). The decreased flexibility of the active site region imposed by the disulfide bond reduced the activity of the enzyme against both paraoxon and demeton-S (Table 4.1).

In an effort to reduce the disulfide bond so that its effects on catalytic activity could be better understood several reducers were used. TCEP does not react with divalent cations (*122*) and found not to adversely react with the enzyme in the time required for the experiments in this study. As shown in Figure 4.9A, incubation of the disulfide variant with TCEP resulted in increased activity of the disulfide variant towards paraoxon. The K_M of the disulfide enzyme against paraoxon also decreased with respect to that of the wild type K_M, which suggested the increased flexibility offered by the removal of the native hydrogen bond and novel disulfide bond increased the affinity of the enzyme for paraoxon (Figure 4.9B).

Incubation of the disulfide with TCEP reduced the disulfide bond and increased the catalytic activity of the disulfide variant against all substrates examined except for EPN (Table 4.2). TCEP did not appear to have any adverse effects on the hydrolysis of organophosphates by the wild type enzyme. Both DTT and β-mercaptoethanol were used but found to react with the divalent cations in solution so that a dark precipitate formed.

The rate limiting step for the hydrolysis of paraoxon by wild type OPH is the release of product from the active site and regeneration of free enzyme (*99*). This effect can be seen in the decrease of the activity in the hydrolysis of paraoxon by CC OPH. Additionally, the K_M for the hydrolysis of paraoxon by CC OPH increased relative to that of the wild type. The turnover number for the hydrolysis of demeton-S decreased while the K_M for both the wild type and the CC enzymes remained similar. The presence of the disulfide appeared to inhibit the flexibility of the enzyme and, although it

increased the range of the enzyme's operational stability, it decreased the enzyme's catalytic activity.

Single cysteine variants (S267C and Y309C) were also constructed and their catalytic abilities measured against paraoxon and demeton-S (Table 4.1). The turnover numbers for the hydrolysis of paraoxon and demeton-S by both S267C and Y309C were reduced compared to that of wild type OPH, while the K_M for both paraoxon and demeton-S for both of the cysteine variants were similar to those of the wild type. This suggested that the cysteine variant enzymes retained the same affinity for each of the substrates, but the loss of structure imposed by the removal of the optimal hydrogen bonding association of S267 and Y309 had a negative impact on V_{max} as the rate of product release and regeneration of free enzyme (k_5) became limiting.

Viscosity Effects Limit OPH's Catalytic Activity. The activity profiles of the wild type and CC variants were performed by incubating the enzyme in denaturant overnight and then testing the activity by initiating the reaction with substrate that did not contain urea.

To examine the effect that urea had on the catalytic activity of OPH at high denaturant concentrations, enzyme incubated in the presence of urea (0 – 8 M in 1 M increments) was tested against 1.0 mM paraoxon that also contained urea (0-8 M urea in 1 M increments). An overlay of the activity of the wild type enzyme analyzed against 1.0 mM paraoxon (with and without urea) showed that the additional denaturant did have an adverse effect on the catalytic ability of OPH (Figure 4.5). Either the enzyme

was rapidly refolding when the denaturant was diluted out or the urea was acting as a viscosogen that slowed the rate of the hydrolysis reaction.

To examine the first possibility, the wild type enzyme was incubated in the presence of 8.0 M urea overnight at 25 ˚C. At various time points, the urea-enzyme solution was diluted so that the final urea concentration in the samples was 0.8 M urea. Since the enzyme exhibits maximal activity at approximately 1.0 M urea, it was judged that these would be favorable conditions for the refolding of the enzyme. The diluted samples were then tested against paraoxon (1 mM final concentration) and the results plotted as relative paraoxonase activity as a function of dilution time (Figure 4.4). The average absorbance of paraoxon (1.0 mM) controls was used as a baseline for the activity determinations. After 2 minutes of dilution, there does not appear to be a significant change between the sample and the paraoxon control. After 30 minutes, approximately 30 % of the maximum activity had been attained. After 60 minutes of dilution approximately 40 % of the maximum activity had been attained. Although the process of refolding appears to begin to take place shortly after dilution of the denaturant, it takes a full 3 ½ hours to achieve the maximum activity or the refolded enzyme. Any refolding event that takes place over the one minute time course of the dilution of the denaturant and enzyme solution contributes a negligible amount of activity to the activity profile of OPH (Figure 4.5).

The second possibility was that urea was acting as a viscosogen which hindered the movement of substrates and products in the sample solution. When sucrose was used as a micro-viscosogen to probe the effects of solvent viscosity on the catalytic activity of

OPH, it was found that an increase in viscosity did, in fact, damper the catalytic activity of the enzyme (*99*). The sucrose solution reduced the catalytic activity of the enzyme against paraoxon by as much as three orders of magnitude. Urea and GdnHCl are also known to be viscosogens (*119*). When the relative viscosities of urea and GdnHCl were compared to those of the sucrose concentrations used in the Caldwell study (Figure 4.2), it was found that the denaturants had a large effect on the solvent viscosity. For example, a 21 % sucrose solution has a relative viscosity similar to that of a 6.5 M urea solution. Since hydrolysis of paraoxon is sensitive to solvent viscosity, it would not be unreasonable to expect that the presence of urea or GdnHCl would have a significant effect on the catalytic activity of OPH, especially in elevated concentrations.

It is therefore likely that results presented in Figure 4.5 and Figure 4.6 are accurate representations of the catalytic activities of the wild type enzyme versus the disulfide variant in increasing denaturant concentrations. Any extent of refolding that takes place in the one minute analysis time of the samples is most likely negligible. The striking differences in the activities of the wild type enzyme incubated in urea (0 – 8 M urea) tested against substrate with and without saturating urea concentrations is most likely a result of the solvent viscosity and not a refolding event (Figure 4.3).

The Disulfide Bond Does Not Provide Increased Operational Stability in Thermal Denaturing Conditions. In order to determine if the S267C / Y309C disulfide bond increased the range of activity in thermal denaturing conditions, the enzyme was incubated at increasing temperatures and its activity plotted as a function of temperature. As with the wild type enzyme, the activity of the disulfide variant increased in mildly

denaturing conditions and then began to decline. At temperatures ≥ 60 ˚C the activity of the enzyme began to rapidly decline as a white precipitate formed. The thermal denatured activity profile of the disulfide variant closely matched that of the wild type enzyme (Figure 4.7). It was concluded that the presence of the disulfide bond did not increase the operational stability of the enzyme in thermal denaturing conditions. Any unfolding event that took place and caused aggregation must do so independently of the disulfide bond and was likely not affiliated with this region of the enzyme.

In order to rule out the possibility that the overlapping activity profiles of the enzyme might have been due to a rapid refolding event upon combining temperature denatured enzyme with room temperature buffer and substrate, the substrates and the buffers used were incubated at increasing temperatures along with the enzymes. Additionally, a water controlled cuvette holder was installed in the spectrophotometer and the temperature controlled with water cycled from a water bath. This ensured that the temperature of the sample stayed as close to the desired temperatures as possible. The activity profiles of the wild type and disulfide enzymes are very similar and are compared in Figure 4.7B. Again, at temperatures ≥ 60 ˚C the activity of the enzyme began to rapidly decline as a white precipitate formed. The difference between the two experiments (Figure 4.7A and 4.7B) was the rate of increase in the relative activity detected. The experiment in which all of the reagents were incubated at increasing temperatures displayed a faster increase in the rate of activity (Figure 4.7B) than did the experiment in which only the enzyme was incubated in increasing temperatures and the other reagents held at 25 ˚C. This was most likely due to a break down in the demeton-S

or 2-TP as the temperature increased since the initial absorbance at 343 nM increased with increasing temperatures only in experiments in which all reagents were incubated at increasing temperatures. Therefore, it was concluded that the disulfide bond did not provide additional protection to the enzyme in thermal denaturing conditions that would extend its activity range past that of the inactivation of the wild type enzyme.

The Disulfide Bond Does Not Provide Added Stabilization in Low Enzyme Concentrations. Since the disulfide bond appeared to inhibit the unfolding pathway, it was hypothesized that the disulfide variant enzyme might be more stable at lower concentrations. Wild type and CC OPH::Co^{2+} were shown to have overlapping activity profiles over the range of concentrations tested. In fact both enzymes displayed a maximum in relative activity at a concentration of 4 μM. Both enzymes appeared to rapidly loose activity in lower concentrations and lost 60 % of their maximum activity in concentrations of 2 μM. The fact that the activity verses enzyme concentration profiles were overlapping indicated that the presence of the disulfide bond did not provide enhanced stability to the enzyme in lower concentrations.

The Disulfide Enzyme Is Resistant to Proteolysis by Thermolysin in Chemical and Thermal Denaturing Conditions. Protein folding (unfolding) is known to be a cooperative process. The breaking of stabilizing interactions in one part of a protein molecule has a destabilizing effect on others so that the natively folded state becomes more unstable (*124*). The disulfide bond offered resistance to the proteolysis of OPH by thermolysin. CC OPH::Co^{2+} was incubated in various concentrations of urea (0 – 6 M) for ≥ 18 hours at 25 ˚C prior to incubation with thermolysin. The presence of the

disulfide bond prevented thermolysin from cleaving OPH at the initial cut sites L271 and Y309 (Fragments U2 and U5; Table 3.2). Even when incubated in the presence of 6 M urea, thermolysin was unable to cleave OPH. Interestingly, since these flexible loop regions were not cleaved by the protease, the remaining cut sites were not observed (Figure 4.12B). The novel disulfide bond (S267C / Y309C) prevented the mobility and cleavage of Loops 271 and 309 and the subsequent regions of unfolding (characterized by F72, L66, and L130) were not allowed to unfold even in elevated urea concentrations. The absence of proteolytic fragments generated in the proteolysis of the disulfide variant enzyme further demonstrated the cooperativity of this unfolding process.

The disulfide bond was reduced by incubation with 1 mM TCEP during incubation in various concentrations of urea (0 – 6 M) for ≥ 18 hours at 25 ˚C prior to incubation with thermolysin. The resultant cut pattern (Figure 4.12A) was very similar to that of the digestion of wild type OPH by thermolysin under identical conditions (Figure 3.3B). When the progress of the digestion was followed by SDS-PAGE, the same fragments generated in the proteolysis of the wild type enzyme were observed for the disulfide enzyme. This indicated that once the disulfide bond has been reduced, the flexible loop regions became accessible to the protease and the enzyme was able to unfold via the same unfolding pathway that was previously determined (Chapter III).

In order to determine if the disulfide bond offered any protection against the effects of thermal unfolding, the limited proteolysis reaction against CC OPH::Co^{2+} was performed at 45 ˚C. This is the temperature in which the fragment T2 (F72 – 309) was observed in limited proteolysis experiments against the wild type enzyme. Over the

course of 90 minutes of incubation with thermolysin, the fragment T2 was not observed. In contrast, incubation of the wild type enzyme with thermolysin at 45 ˚C, fragment T2 was observed. This indicated that the disulfide bond offered some protection against the unfolding and proteolysis of the enzyme at 45 ˚C.

ANS Dye Binding Studies Suggest That Active Site Topology Is Maintained in CC OPH. The effect of the disulfide bond and the single cysteine mutations on the topology of the active site were measured by ANS dye binding studies. Previous studies have determined that ANS binds in the active site of OPH (*67*). The enzymes were incubated overnight in the presence of increasing concentrations of GdnHCl prior to the addition and incubation with ANS. Fluorescence emission scans (Figure 4.8) showed a maximum in ANS fluorescence intensity for each enzyme at 1.25 M GdnHCl. The emission scans for each variant overlapped and it was concluded that the active site topology, concerning ANS binding, remained the same in each of the variants. When the disulfide bond was reduced with TCEP and incubated in the presence of GdnHCl overnight, a precipitate formed and reproducible fluorescence scans were not possible.

The Wild Type and Disulfide Bond Share Similar Secondary Structure and the Structure of the Disulfide Persists Longer in Elevated Chemical Denaturing Conditions. Far-UV circular dichroism was used to determine if there were any significant changes in the secondary structure content of OPH imposed by either the removal of the hydrogen bond at position 267-309 (single cysteine variants) or the insertion on the novel disulfide bond at this position. The far-UV wave scan of each enzyme overlapped and each displayed a minimum at 208 and 222 nM, characteristic of a protein with a high

α-helical content (Figure 4.14). None of the enzymes displayed any significant changes from that of the far-UV profile of wild type and it can be concluded that the removal of the hydrogen bond or the insertion of the disulfide bond did not cause any significant changes to the overall structure of OPH.

Further wave scans were performed on wild type and CC enzymes that had been incubated in increasing concentrations of either GdnHCl or urea. The results are presented in Table 4.3. When urea was used as a denaturant, the extent of signal remained relatively constant from 0 – 3 M urea. As the urea concentration increased further, there was a more rapid decrease in the extent of secondary structure for the wild type as compared to the disulfide enzyme. When GdnHCl was used as the denaturant, however, the extent of secondary structure did not appear to vary significantly in either enzyme regardless of the increasing denaturant concentration. It appeared from this data that the disulfide bond offered more protection against unfolding in urea denaturing conditions than in GdnHCl denaturing conditions. This suggested that the novel disulfide bond has a more pronounced effect on stabilizing the hydrophobic forces than the electrostatic forces stabilizing the protein structure.

The apparent melting temperatures of each enzyme variant were measured by circular dichroism (Figure 4.15). The disulfide enzyme appeared to retain slightly more unfolded structure between 0 and 50 ˚C than the wild type enzyme, but reached its midpoint in the unfolding process sooner than wild type. The approximate T_M of the disulfide variant was calculated as 56.7 ˚C while the approximate T_M of the wild type was found to be 63.3 ˚C.

In the removal of the native disulfide bridge in human lysozyme, it was found that the melting point temperature the ΔH of denaturation for the cysteine variants was less than that of the wild type suggesting a reduction in enthalpic stabilization. Crystallography of the cysteine variants indicated similar tertiary structure to the wild type enzyme but with increased flexibility in their folded structure (*116*).
The presence of the disulfide was considered to entropically destabilize the unfolded state as well as maintain the tertiary conformation of the folded state. Similar results have been observed for the novel disulfide bond introduced into an α-amylase from *Pseudoalteromonas haloplanktis*. The disulfide enhanced the conformational stability of the enzyme while reducing the melting point of the enzyme (*111*). The authors concluded that the strain introduced into the native structure by the novel disulfide bond resulted in a reduction of the enthalpic interactions stabilizing the enzyme.

The novel disulfide bond (S267C / Y309C) inserted into OPH bridges a loop of 42 residues. According to equation 4.1 the conformational entropy contribution by this novel disulfide bond could be expected to reduce the conformational entropy of the intermediate state by 2.11 kcal/mol at 25 ˚C. The entropy change for protein unfolding has two main opposing contributions: the decrease in hydration entropy and the increase in conformational entropy (*125*).

Although there may be an unfavorable entropic contribution to the folded state structure of the enzyme, the presence of the disulfide bond appears to have inhibited the unfolding pathway (as shown by limited proteolysis and the lack of concentration dependence upon unfolding) and extended the enzyme's operational stability (as shown

by catalytic activity as a function of denaturant concentration. It can be concluded that the novel disulfide bond destabilized the inactive intermediate state in favor of the active folded state. In agreement with the Chain Entropy model, the conformational entropy of intermediate state of the disulfide variant has been reduced with respect to that of the wild type OPH indicating stabilization of the folded state through entropic destabilization of the intermediate state. This would drive the equilibrium from the dimeric intermediate towards the folded state.

In studies of barnase with novel disulfide bonds it was suggested that decreases in the entropy of denaturation are accompanied by decreases in the enthalpy of denaturation (*117*). The presence of the disulfide bond in OPH resulted in a lower apparent thermal stability of the disulfide variant as compared to the wild type. This is most likely due to a loss in favorable enthalpic interactions of the folded structure which destabilized the folded state of the variant enzyme. The van der Waals interactions resulting from the close packing of residues in the protein make a large favorable contribution to the enthalpy of protein folding (*126*). The strain likely introduced by the novel disulfide bond could be expected to have negative effect on the optimal packing of the residues in this region which would lower the enthalpic contribution to stability and cause the disulfide variant to be more temperature liable.

The Disulfide Bond Inhibits the Unfolding Pathway of OPH as Suggested by the Concentration Dependence of Equilibrium Unfolding. The equilibrium unfolding of the single cysteine variants, the disulfide, and the wild type enzymes were followed by intrinsic tryptophan fluorescence (Figure 4.16). There were no clear pre-, mid-, or post-

transitions in any of the unfolding curves which made fitting the three-state equation difficult. None of the parameters generated from the fitting of the data appeared to be reliable and so were not used in the analysis. There are common similarities between the unfolding transitions, however. Each shared a transition point around 2.0 M GdnHCl and appeared to reach the unfolded state at approximately 3.0 M urea. The wild type and Y309C unfolding curves had a much sharper transition at 2.0 M urea than do the disulfide and S267C curves which may indicate a more rapid unfolding event once that transition point had been reached.

The equilibrium unfolding of the wild type and CC in the presence of urea was followed by fluorescence and the wild type enzyme displayed the characteristic three state unfolding curve (Figure 4.17A) with the dimeric intermediate forming between 3 and 4 M urea. There was no clear midpoint in the unfolding curve for the disulfide variant (Figure 4.17B). Both enzymes reached a minimum in fluorescence by 6.5 – 7.0 M urea. Since the disulfide variant still retained activity at this urea concentration it was concluded that the enzyme must not be completely unfolded. It was hypothesized that the presence of the disulfide bond inhibited the unfolding pathway of OPH and that population of states in these elevated denaturing conditions favored the dimeric states ($N_2^* \leftrightarrow I_2$) for the disulfide variant whereas the dimeric to monomeric states were favored in the wild type ($I_2 \leftrightarrow 2U$) at these elevated urea concentrations

Since the second transition of OPH's unfolding pathway ($N_2^* \leftrightarrow I_2 \leftrightarrow 2U$) is concentration dependent (*14*) it was decided to examine the concentration dependence of unfolding of the disulfide and wild type enzymes. There was a striking difference in the

second transition of the equilibrium unfolding curves of the wild type enzyme (Figure 4.17A). As the enzyme concentration was increased from 50 μg/mL to 120 μg/mL, the midpoint of the second transition shifted to a higher urea concentration (approximately 4.5 M to 5.5 M urea, respectively). The equilibrium unfolding curves of the disulfide variant did not change significantly from 50 μg/mL to 120 μg/mL (Figure 4.17B). This suggested that dissociation of the dimeric states was not occurring and that the majority of the population of enzyme existed in dimeric form (either N_2 or I_2).

Conclusions. The unfolding pathway developed for thermal and chemical denatured OPH was used to increase the operational stability of the enzyme. The novel disulfide bond, S267C / Y309C, increased the operational stability of OPH so that it retained approximately 70 % of its original activity in 8.0 M urea whereas the wild type enzyme lost complete activity by 6.5 M urea. The disulfide activity also appeared to have an extended capability to function in higher concentrations of GdnHCl than did the wild type enzyme and it appeared to resist proteolysis in chemical and thermal denaturing conditions. This suggested that the presence of the disulfide bond bridging the two flexible loop regions together interfered with the unfolding pathway. This disulfide most likely entropically destabilized the inactive intermediate state in favor of the active native state which forced the equilibrium of states toward the folded state. The addition of TCEP reduced the disulfide bond which caused the enzyme to behave like the wild type in terms of activity and proteolytic susceptibility. The limited proteolysis data provided a useful means by which to determine the unfolding pathway of OPH and reengineer the enzyme to resist unfolding.

CHAPTER V

SUMMARY

Organophosphorus hydrolase is a remarkable enzyme with the ability to hydrolyze a variety of neurotoxic organophosphate compounds. OPH has been engineered for increased activity against selected substrates and altered stereo-selectivity (*7-12, 54, 127*). This enzyme has a lot of potential for different applications and is particularly interesting for bioremediation and nerve agent countermeasure applications.

The native *opd* from *Flavobacterium sp*. ATCC 27551 and *Pseuodomoas diminuta* were shown to be identical and encoded a 39 kDa enzyme (*28, 29*). This enzyme possessed a 29 amino acid leader sequence that was found to be post-translationally processed (*36, 41*) and X-ray crystallography later revealed that the enzyme existed as a homodimer (*2*).

OPH unfolds via a three-state unfolding pathway ($N_2^* \leftrightarrow I_2 \leftrightarrow 2U$) in chemical denaturing conditions where the active (*), native dimer (N_2) unfolds to an inactive, dimeric intermediate (I_2) before separating into its inactive, monomeric subunits (U) (*14*). OPH is a bimetallic enzyme requiring two divalent cations per active site for maximal activity. The identity of the metal ion present affects the catalytic activity and the stability of the enzyme. The cobalt substituted variant is the most active form of the enzyme (*5, 6*) and so this study is designed to determine the pathway of the unfolding transition from the active, native state to the inactive, intermediate state of the cobalt substituted form of OPH.

In an effort to determine how local regions of OPH unfolded in chemical denaturing conditions, tryptophan residues were replaced with phenylalanine residues to produce enzymes that contained only one tryptophan per subunit. Intrinsic tryptophan fluorescence could then be used to determine the localized changes in structure surround the remaining tryptophan residues upon unfolding. Unfortunately, these enzymes did not fold into active conformations, thus so any unfolding profile generated from these enzymes would not accurately reflect the unfolding pathway of the wild type enzyme. While this study could not be used to develop an accurate map of unfolding for wild type OPH, it did indicate that tryptophan residues are important in the function and folding of this enzyme.

Limited proteolysis of OPH by thermolysin was used as a sensitive probe of the unfolding profile of OPH in chemical and thermal denaturing conditions. Limited proteolysis is a powerful way to probe the unfolding profiles of enzyme as it can be used to detect subtle transitions in protein structure often before they can be detected by spectroscopic methods (*79-82*). OPH was observed to be readily susceptible to proteolysis by thermolysin at 25 ˚C and 0 M urea. Two flexible loop regions (Loop 271 and Loop 309) were identified under these conditions as being mobile and flexible enough to be accessible to the protease. Additionally, mild denaturing conditions (incubation of OPH with 1.0 M urea or at 45 ˚C) produced an initial enhancement of catalytic activity with a subsequent loss upon more aggressive denaturing treatment.

Under thermal treatment from 35 – 55 ˚C, the enzyme developed a populated and highly active intermediate (I_2*) that displayed a 28% enhancement of activity. At 45 ˚C,

limited proteolysis revealed a region of additional flexibility. The protease cut site of F72 was located in the intersubunit interface of OPH and suggested that this region of the enzyme became exposed and accessible to the protease. No additional cut sites were observed in increasing temperatures and the enzyme precipitated at temperatures greater than 60 ˚C. The resultant thermal unfolding pathway be represented as (N_2*↔ I_2* ↔ D_A).

Under mild chemical denaturing conditions (1.0 M urea) the same region of the enzyme became accessible to proteolysis. Additionally, the enzyme displayed an increase in activity over native levels under these conditions, suggesting that the increased flexibility of this region was coupled with the increase in the enzyme's catalytic abilities. Increasing the denaturant concentration to 3.0 M urea revealed the presence of two additional cut sites (L66 and L130) that were not present in the thermal denatured samples. Both of these regions are located in the intersubunit interface and adjacent to the active site of the enzyme suggesting that the appearance of these cut sites was symptomatic of this region of the interface of one subunit losing the protection from proteolysis offered by the other subunit, and this observation helps to explain the loss in activity of OPH under these chemical denaturing conditions. Two of the intersubunit salt bridges were implicated in sustaining the interface association, and thus affecting the activity, of the enzyme in thermal denaturing conditions but not chemical denaturing conditions.

The introduction of a novel disulfide bond (S267C / Y309C) into the flexible loop regions (Loop 271 and Loop309) served to bridge the loop structures together and

resulted in enhanced operational stability. This enzyme retained 70 % of its catalytic activity after prolonged incubation in 8.0 M urea; the native enzyme lost all of its activity after incubation in 6.5 M urea. The bridging of these two regions also offered protection from proteolytic degradation in both thermal and chemical denaturing conditions.

The development of an unfolding profile of OPH was used to design a new enzyme with an enhanced operational stability. Given that OPH has been engineered for enhanced activity against selected substrates and selected stereoisomers, this disulfide variant enzyme will offer a novel platform for the development of enzymes with enhanced catalytic abilities and extended operational stabilities.

REFERENCES

1. Gerlt, J. A., and Raushel, F. M. (2003) Evolution of function in (beta/alpha)8-barrel enzymes, *Curr. Opin. Chem. Biol. 2*, 252-264.

2. Benning, M. M., Kuo, J. M., Raushel, F. M., and Holden, H. M. (1994) Three-dimensional structure of phosphotriesterase: an enzyme capable of detoxifying organophosphate nerve agents, *Biochemistry 33*, 15001–15007.

3. Benning, M. M., Kuo, J. M., Raushel, F. M., and Holden, H. M. (1995) Three-dimensional structure of the binuclear metal center of phosphotriesterase, *Biochemistry* 34, 7973-7978.

4. Vanhooke, J. L., Benning M. M., Raushel, F. M., and Holden, H. M. (1996) Three-dimensional structure of the zinc-containing phosphotriesterase with the bound substrate analog diethyl 4-methylbenzylphosphonate, *Biochemistry 14*, 6020-6025.

5. Dumas, D. P. (1989) The purification and characterization of the phosphotriesterase from *Pseudomonas diminuta*, Ph.D. Dissertation, Texas A&M University, College Station.

6. Omburo, G. A., Kuo, J. M., Mullins, L. S., and Raushel, F. M. (1992) Characterization of the zinc binding site of bacterial phosphotriesterase, *J. Biol. Chem. 267,* 13278-13283.

7. diSioudi, B. D., Miller, C. E., Lai, K., Grimsley, J. K., and Wild, J. R. (1999) Rational design of organophosphorus hydrolase for altered substrate specificities, *Chem. Biol. Interact.119-120*, 211-223.

8. Rastogi, V. K., DeFrank, J. J., Cheng, T. C., and Wild, J. R. (1997) Enzymatic hydrolysis of Russian-VX by organophosphorus hydrolase, *Biochem. Biophys. Res. Commun 2*, 294-296.

9. Kuo, J. M., Chae, M. C., and Raushel, F. M. (1997) Perturbations to the active site of phosphotriesterase, *Biochemistry 36*, 1982-1988.

10. Li, W. S., Li, Y., Hill, C. M., Lum, K. T., and Raushel, F. M. (2001) Enzymatic synthesis of chiral organophosphothiolates from prochiral *precursors, J. Am. Chem. Soc. 124, 3*498-2499.

11. Benning, M. M., Hong, S., Raushel, F. M., and Holden, H. M. (2000) The binding of substrate analogs to phosphotriesterase, *J. Biol. Chem. 275*, 30556-30560

12. Gopal, S., Rastogi, V., Ashman, W., and Mulbry, W. (2000) Mutagenesis of organophosphorus hydrolase to enhance the hydrolysis of the nerve agent VX, *Biochem. Biophys. Res. Commun. 279*, 516-519.

13. Hong, S., and Raushel, F. M. (1996) Metal-substituted interactions facilitate the catalytic activity of the bacterial phosphotriesterase, *Biochemistry 35*, 10904-10912.

14. Grimsley, J. K., Scholtz, J. M., Pace, C. N., and Wild, J. R. (1997) Organophosphorus hydrolase is a remarkably stable enzyme that unfolds through a homodimeric intermediate, *Biochemistry 36*, 14366–14374.

15. McDaniel, C. S., McDaniel, J., Wales, M. E., and Wild, J. R. (2005) Biocatalytic Coatings, *Paint and Coatings Industry*, 26-33.

16. Simonian, A. L., Flounders, A. W., and Wild, J. R. (2004) FET-based biosensors for the direct detection of organophosphate neurotoxins, *Electroanalysis*, 1896-1906.

17. Rainina, E. I., Efremenco, E. N., Varfolomeyev, S. D., Simonian, A. L., and Wild, J. R. (1996) The development of a new biosensor based on recombinant *E. coli* for the direct detection of organophosphorus neurotoxins, *Biosensors and Bioelectronics 11*, 991-1000.

18. Mulchandani, A., Chen, W., Mulchandani, P., Wang, J., and Rogers, K. R. (2001) Biosensors for the direct determination of organophosphate pesticides, *Biosensors and Bioelectronics*, 225-230.

19. Petrikovics, I., Papahadjopoulos, D., Hong, K., Cheng, T. C., Baskin, S. I., Jiang, J., Jaszberenyi, J. C., Logue, B. A., Szilasi, M., McGuinn, W. D., and Way, J. L. (2004) Comparing therapeutic and prophylactic protection against the lethal effect of paraoxon, *Toxicological Sciences 77*, 258-262.

20. Saab-Rincon, G., Jarez, V. R., Osuna, J., Sanchez, F., and Soberon, X. (2001) Different strategies to recover the activity of monomeric triosephosphate isomerase by directed evolution, *Protein Eng. 14*, 149-155.

21. Borchert, T. V., Abagyan, R., Jaenicke, R., and Wierenga, R. K. (1994) Design, creation, and characterization of a stable, monomeric triosephosphate isomerase, P*roc. Natl. Acad. Sci. U.S.A. 91*, 1515-1518.

22. Hernandez-Alcantara, G., Garza-Ramos, G., Hernandez, G. M., Gomez-Puyou, A., and Perez-Montfort, R. (2002) Catalysis and stability of triosephosphate isomerase from Trypanosoma brucei with different residues at position 14 of the

dimer interface: characterization of a catalytically competent monomeric enzyme, *Biochemistry 41*, 4230–4238.

23. Beaucamp, N., Hofmann, A., Kellerer, B., and Jaenicke, R. (1997) Dissection of the gene of the bifunctional PGK-TIM fusion protein from the hyperthermophilic bacterium *Thermotoga maritima*: design and characterization of the separate triosephosphate isomerase, *Protein Sci. 6*, 2159-2165.

24. Najera, H., Costas, M., Fernandez-Velasco, D. A. (2003) Thermodynamic characterization of yeast triosephosphate isomerase refolding: insights into the interplay between function and stability as reasons for the oligomeric nature of the enzyme, *Biochem. J. 370*, 785-792.

25. Lopez-Velazquez, G., Molina-Ortiz, D., Cabrera, N., Hernandez-Alcantara, G., Peon-Peralta, J. Yepez-Mulia, L., Perez-Montfort, R., and Reyes-Vivas, H. (2004) An unusual triosephosphate isomerase from the early divergent eukaryote *Giardia lamblia*, *Proteins 55*, 824-834.

26. Mulbry W. W., K., J. S., Kearney, P. C., Nelson, J. O., McDaniel, C. S., and Wild, J. R. (1986) Identification of a plasmid-borne parathion hydrolase gene from *Flavobacterium sp*. by southern hybridization with *opd* from *Pseudomonas diminuta*, *Appl. Environ. Microbiol. 51*, 926-930.

27. McDaniel, C. S., Harper, L. L., and Wild, J.R. (1989) Cloning and sequencing of a plasmid-borne gene (*opd*) encoding a phosphotriesterase, *J. Bacteriol. 170*, 2306-2311..

28. Harper, L. L., McDaniel, C. S., Miller, C. E., and Wild, J. R. (1998) Dissimilar plasmids isolated from *Pseudomonas diminuta* MG and a *Flavobacterium sp*. (ATCC 27551) contain identical *opd* genes, *Appl. Environ. Microbiol. 54*, 1586-2589.

29. Mulbry, W. W., and Karns, J. S. (1989) Parathion hydrolase specified by the Flavobacterium opd gene: relationship between the gene and protein, *J. Bacteriol. 171*, 6740-6746.

30. Siddavattam, D., Khajamohiddin, S., Manavathi, B., Pakala, S. B., and Merrick, M. (2003) Transposon-like organization of the plasmid-borne organophosphate degradation (*opd*) gene cluster found in *Flavobacterium sp*., *Appl. Environ. Microbiol. 69*, 2533–2539.

31. Chaudhry, G. R., Ali, A. N., and Wheeler, W. B. (1988) Isolation of a methyl parathion-degrading *Pseudomonas sp*. that possesses DNA homologous to the *opd* gene from a *Flavobacterium sp., Appl. Environ. Microbiol. 54*, 288-293.

32. Steiert, J. G., Pogell, B. M., Speedie, M. K., and Laredo, J. (1989) A gene coding for a membrane-bound hydrolase is expressed as a secreted soluble enzyme in *Streptomyces lividans*, *Bio/Technology 7*, 65-68.

33. Gauger, W. K., MacDonald, J. M., Adrian, N. R., Matthees, D. P., and Walgenbach, D. D. (1986) Characterization of a Streptomycete growing on organophosphate and carbamate insecticides, *Arch. Environ. Contam. Toxicol. 15*, 137–141.

34. Brown, K. A., (1980) Phosphotriesterases of *Flavobacterium sp., Soil Biol. Biochem. 12*, 105-112.

35. Serdar, C. M., and Gibson, D. T. (1985) Enzymatic hydrolysis of organophosphates: cloning and expression of a parathion hydrolase gene from *Pseudomonas diminuta*, Bio/Technology 3, 567-571.

36. Serdar, C. M., Murdock, D.C., Rohde, M.F. (1989) Parathion hydrolase gene from *Pseudomonas diminuta* MG: subcloning, complete nucleotide sequence, and expression of the mature portion of the enzyme in *Escherichia coli*, *Bio/Technology 7*, 1151-1155.

37. von Heijne, G. (1984) How signal sequences maintain cleavage specificity, *J. Mol. Biol 173*, 243-251.

38. Mulbry, W. W., and Karns, J. S. (1989) Purification and characterization of three parathion hydrolases from gram-negative bacterial strains, *Appl. Environ. Microbiol. 55*, 289–293.

39. Rowland, S. S., Zultry, J. J., Sathyamoorthy, M., Pogell, B. M., Speedie, and M. K. (1992) The effect of signal sequences on the efficiency of secretion of a heterologous phosphotrieseterase by *Streptomyces lividans*, *Appl. Microbiol. Biotechnol. 38*, 94-100.

40. Sathyamoorthy, M., Stemke, D., and Speedie, M.K. (1996) Native and heterologous protein secretion by *Streptomyces lividans*, *Appl Microbiol Biotechnol 46*, 347-352.

41. Dave, K. I., Phillips, L., Luckow, V. A., and Wild, J. R. (1994) Expression and post-translational processing of a broad-spectrum organophosphorus-neurotoxin-degrading enzyme in insect tissue culture, *Biotechnol. Appl. Biochem. 19*, 271-284.

42. Sathyamoorthy, M., and Speedie, M. K. (1995) Monitoring transport of a recombinant phosphotriesterase in *Streptomyces lividans* using a pulse-chase system, *Appl. Microbiol. Biotechnol. 43*, 493-497.

43. Miller, C. E. (1992) Structure/function studies on the signal sequence of organophosphorus hydrolase of *Pseudomonas diminuta*, Ph.D. Dissertation, Texas A&M University, College Station.

44. Derman, A. I., and Beckwith, J. (1991) *Escherichia coli* alkaline phosphatase fails to acquire disulfide bonds when retained in the cytoplasm, *J. Bacteriol. 173*, 7719-7722.

45. von Heijne, G. (1983) Patterns of amino acids near signal-sequence cleavage sites, *Eur. J. Biochem. 133*, 17-21.

46. Berks, B. C. (1996) A common export pathway for proteins binding complex redox cofactors?, *Mol. Microbiol. 22*, 393-404.

47. Bronstein, P., Marrichi, M., and DeLisa, M. P. (2004) Dissecting the twin-arginine translocation pathway using genome-wide analysis, *Res. Microbiol. 155*, 803-810.

48. DeLisa, M. P., Tullman, D., and Georgiou, G. (1990) Folding quality control in the export of proteins by the bacterial twin-arginine translocation pathway, *Proc. Natl. Acad. Sci. U.S.A. 100*, 6115-6120.

49. Bogsch, E., Brink, S., and Robinson, C. (1997) Pathway specificity for a ΔpH-dependent precursor thylakoid lumen protein is governed by a 'sec-avoidance' motif in the transfer peptide and a 'sec-incompatible' mature protein, *EMBO J. 16*, 3851-3859.

50. Brock, I. W., Mills, J. D., Robinson, D., and Robinson, C. (1995) The ΔpH-driven, ATP-independent protein translocation mechanism in the chloroplast thylakoid membrane, *J. Biol. Chem. 270*, 1657-1662.

51. Alder, N. N., and Theg, S. M. (2003) Energetics of protein transport across biological membranes: a study of the thylakoid ΔpH-Dependent/cpTat Pathway, *Cell 112*, 231-242.

52. Horne, I., Sutherland, T.D., Harcourt, R.L., Russell, R.J., and Oakeshott, J.G. (2002) Identification of an *opd* (organophosphate degradation) gene in an *Agrobacterium* isolate, *Appl. Environ. Microbiol. 68*, 3371-3376.

53. Horne, I., Qiu, X., Russell, R.J., and Oakeshott, J.G. (2003) The phosphotriesterase gene *opdA* in *Agrobacterium radiobacter* P230 is transposable, *FEMS Microbiol. Lett. 222*, 1-8.

54. diSioudi, B., Grimsley, J. K., Lai, K., and Wild, J. R. (1999) Modification of near active site residues in organophosphorus hydrolase reduces metal stoichiometry and alters substrate specificity, *Biochemistry 38*, 2866-2872.

55. Jackson, C., Kim, H. K., Carr, P. D., Liu, J. W., and Ollis, D. L. (2005) The structure of an enzyme-product complex reveals the critical role of a terminal hydroxide nucleophile in the bacterial phosphotriesterase mechanism, *Biochim. Biophys. Acta 1752*, 56-64.

56. Royer, C. A., Mann, C. J., and Matthews, C. R. (1993) Resolution of the fluorescence equilibrium unfolding profile of trp aporepressor using single tryptophan mutants, *Protein Sci. 2*, 1844–1852.

57. Chanez-Cardenas, M. E., Fernandez-Velasco, D. A., Vazquez-Contreras, E. V., Coria, R., Saab-Rincon, G., and Perez-Montfort, R. (2002) Unfolding of triosephosphate isomerase from *Trypanosoma brucei*: identification of intermediates and insight into the denaturation pathway using tryptophan mutants, *Arch. Biochem. Biophys. 399*, 117-129.

58. Smith, C. J., Clarke, A. R., Chia, W. N., Irons, L. I., Atknson, T., and Holbrook, J. J. (1991) Detection and characterization of intermediates in the folding of large proteins by the use of genetically inserted tryptophan probes, *Biochemistry 30*, 1028-1036.

59. Mann, C. J., Royer, C. A., and Matthews, C. R. (1993) Tryptophan replacements in the *trp* aporepressor from *Escherichia coli*: probing the equilibrium and kinetic folding models, *Protein Sci. 2*, 1853-1861.

60. Gibbons, D. L., Hixson, J. D., Hay, N., Lund, P., Gorovits, B. M., Ybarra, J., and Horowitz, P. M. (1996) Intrinsic fluorescence studies of the chaperonin GroEL containing single tyr to trp replacements reveal ligand-induced conformational changes, *J. Biol. Chem. 271*, 31989–31995.

61. Shao, X., and Matthews, C. R. (1998) Single-tryptophan mutants of monomeric tryptophan repressor: optical spectroscopy reveals nonnative structure in a model for an early folding intermediate, *Biochemistry 37*, 7850-7858.

62. Vivian, J. T., and Callis, P. R. (2001) Mechanisms of tryptophan fluorescence shifts in proteins, *Biophys. J . 80*, 2093-2109.

63. Lakowicz, J. R. (1999) *Principles of Fluorescence Spectroscopy, 2nd ed*., pp 446–456, Kluwer Academic / Plenum Publishers, New York.

64. Chen, Y., and Barkley, M. D. (1998) Toward understanding tryptophan fluorescence in proteins, *Biochemistry 37*, 9976-9982.

65. Chen-Goodspeed, M., Sogorb, M. A., Wu, F., Hong, S. B., and Raushel, F. M. (2001) Structural determinants of the substrate and stereochemical specificity of phosphotriesterase, *Biochemistry 40*, 1325-1331.

66. Kuo, J. M., and Raushel, F. M. (1994) Identification of the histidine ligands to the binuclear metal center of phosphotriesterase by site-directed mutagenesis, *Biochemistry 33*, 4265-4272.

67. Reeves, T. E. (2006) Rational design of organophosphorus hydrolase for the degradation and detection of neurotoxic pesticides and chemical warfare agents, Ph.D. Dissertation, Texas A&M University, College Station.

68. Grimsley, J. K., Calamini, B., Wild, J. R., and Mesecar, A. D. (2005) Structural and mutational studies of organophosphorus hydrolase reveal a cryptic and functional allosteric-binding site, *Arch. Biochem. Biophys. 442*, 169-179.

69. Lai, K., Dave, K. I., and Wild, J. R. (1994) Bimetallic binding motifs in organophosphorus hydrolase are important for catalysis and structural organization, *J. Biol. Chem. 269*, 16579-16584.

70. Pace, C. N., Vajdos, F., Fee, L., Grimsley, G., and Gray, T. (1995) How to measure and predict the molar absorption coefficient of a protein, *Protein Sci. 4*, 2411-2423.

71. Pace, C. N., and Scholtz, J. M. (1997) Measuring the conformational stability of a protein, *Protein Structure: A Practical Approach,* 2nd Edition, Oxford University Press.

72. Myers, J. K., Pace, C. N., and Scholtz, J. M. (1995) Denaturant *m* values and heat capacity changes: relation to changes in accessible surface areas of protein unfolding, *Protein Sci. 4*, 2138–2148.

73. Schliebs, W., Thanki, N., Eritja, R., and Wierenga, R. (1996) Active site properties of monomeric triosephosphate isomerase (monoTIM) as deduced from mutational and structural studies, *Protein Sci. 5*, 229-239.

74. Aubert, S. D., Li, Y., and Raushel, F. M. (2004) Mechanism for the hydrolysis of organophosphates by the bacterial phosphotriesterase, *Biochemistry 18*, 5707-5715.

75. Chedad, A., Van Dael, H., Vanhooren, A., and Hanssens, I. (2005) Influence of trp mutation on native, intermediate, and transition states of goat alpha-lactalbumin: an equilibrium and kinetic study, *Biochemistry 44*, 15129-15138.

76. Cai, K., and Schirch, V. (1996) Structural studies on folding intermediates of serine hydroxymethyltransferase using single tryptophan mutants, *J. Biol. Chem. 271*, 2987-2994. .

77. Chakraborty, S., Ittah, V., Bai, P., Luo, L., Haas, E., and Peng, Z. (2001) Structure and dynamics of the α-lactalbumin molten globule: fluorescence studies using proteins containing a single tryptophan residue, *Biochemistry 40*, 728-7238.

78. Steer, B. A., and Merrill, A. R. (1995) Guanidine hydrochloride-induced denaturation of the colicin E1 channel peptide: unfolding of local segments using genetically substituted tryptophan residues, *Biochemistry 34*, 7225-7233.

79. Tsou, C. L. (1995) Inactivation precedes overall molecular conformation changes during enzyme denaturation, *Biochim Biophys Acta 1253*, 151-162.

80. Arnold, U., Ulbrich-Hofmann, R. (2000) Differences in the denaturation behavior of ribonuclease A induced by temperature and guanidine hydrochloride, *J. Protein Chem. 19*, 345-352.

81. Arnold, U., Ulbrich-Hofmann, R. (2001) Proteolytic degradation of ribonuclease A in the pretransition region of thermally and urea-induced unfolding, *Eur. J. Biochem. 268*, 93-97.

82. Koditz, J., Arnold, U., Ulbrich-Hofmann, R. (2002) Dissecting the effect of trifluoroethanol on ribonucease A; subtle structural changes detected by nonspecific proteases, *Eur. J. Biochem. 269*, 3821-3837.

83. Hubbard, S. J., Eisenmenger, F., and Thornton, J. M. (1994) Modeling studies of the change in conformation required for cleavage of limited proteolytic sites, *Protein Sci. 3*, 757-768.

84. Hubbard, S. J., Beynon, R. J., and Thornton, J. M. (1998) Assessment of conformational parameters as predictors of limited proteolytic sites in native protein structures, *Protein Eng. 11*, 239-359.

85. Hubbard, S. J., Beynon, R. J., and Thornton, J. M. (1998) The structural aspects of limited proteolysis of native proteins, *Biochim Biophys Acta 1382*, 191-206.

86. Rochu, D., Beaufet, N., Renault, F., Viguie, N., and Masson, P. (2002) The wild type bacterial Co2+/Co2+-phosphotriesterase shows a middle-range thermostability, *Biochim. Biophys. Acta 1594*, 207-218.

87. Heinrikson, R. L. (1997) Applications of thermolysin in protein structural analysis, *Methods Enzymol. 47*, 175-189.

88. Rogers, S., Wells, R., and Rechsteiner, M. (1986) Amino acid sequences common to rapidly degraded proteins: the PEST hypothesis, *Science 234*, 364-368.

89. Rechsteiner, M., and Rogers, S. W. (1986) PEST sequences and regulation by proteolysis, *TIBS 21*, 267-271.

90. Hou, X., Maser, R. L., Magenheimer, B. S., and Calvet, J. P. (1996) A mouse kidney- and liver- expressed cDNA having homology with a prokaryotic parathion hydrolase (phosphotriesterase)-encoding gene: abnormal expression in injured and polycystic kidneys, *Gene 168*, 157-163.

91. Hooft, R. W. W., Sander, C., and Vriend, G. (1996) Positioning hydrogen atoms by optimizing hydrogen-bond networks in protein structures, *Proteins 26*, 363-376.

92. Picotti, P., Marabotti, A., Negro, A., Musi, V., Spolaore, B., Zambonin, M., Fontana, A. (2004) Modulation of the structural integrity of helix F in apomyoglobin by single amino acid replacements, *Protein Sci. 13*, 1572-1585.

93. Heinrikson, R. L. (1977) Applications of thermolysin in protein structural analysis, *Methods Enzymol. 47*, 175-189.

94. Mainfroid, V., Terpstra, P., Beauregard, M., Frere, J. M., Mande, S. C., Hol, W. G. J., Martial, J. A., and Goraj, K. (1996) Three hTIM mutants that provide new insights on why TIM is a dimer, *J. Mol. Biol. 257*, 441-456.

95. Schliebs, W., Thanki, N., Jaenicke, R., and Wierenga, R. K. (1997) A double mutation at the tip of the dimer interface loop of triosephosphate isomerase generates active monomers with reduced stability, *Biochemistry 36*, 9655-9662.

96. Rietveld, A. W. M., and Ferreira, S. T. (1998) Kinetics and energetics of subunit dissociation/unfolding of TIM: the importance of oligomerization for the conformational persistence and chemical stability of proteins, *Biochemistry 37*, 933-937.

97. Wierenga, R. K., Nobel, M. E. M, and Davenport, R. C. (1992) Comparison of the refined crystal structures of liganded and unliganded chicken, yeast and trypanosomal triosephosphate isomerase, *J. Mol. Biol. 224*, 1115-1145.

98. Koca, J., Zhan, C. G., Rittenhouse, R. C., and Ornstein, R. L. (2001) Mobility of the active site bound paraoxon and sarin in zinc-phosphotriesterase by molecular dynamics simulation and quantum chemical calculation, *J. Am. Chem. Soc. 123*, 817-826.

99. Caldwell, S. R., Newcomb, J. R., Schlecht, K. A., and Raushel, F. M. (1991) Limits of diffusion in the hydrolysis of substrates by the phosphotriesterase from *Pseudomonas diminuta*, *Biochemistry 30*, 7438-7444.

100. Eisenmesser, E. Z., Millet, O., Labeikovsky, W., Korzhnev, D. M., Wolf-Watz, M., Bosco, D. A., Skalicky, J. J., Kay, L. E., and Kern, D. (2005) Intrinsic dynamics of an enzyme underlies catalysis, *Nature 438*, 117–121.

101. Rozovsky, S., Jogl, G., Tong, L, and McKermott, A. E. (2001) Solution-state NMR investigations of triosephosphate isomerase active site loop motion: ligand release in relation to active site loop dynamics., *J. Mol. Biol. 310*, 271-280.

102. Williams, J. C., and McDermott, A. E. (1995) Dynamics of the flexible loop of triosephosphate isomerase: the loop motion is not ligand gated, *Biochemistry 34*, 8309–8319.

103. Elcock, A. H. (1998) The stability of salt bridges at high temperatures: implications for hyperthermophilic proteins, *J. Mol. Biol. 284*, 489-502.

104. Shortle, D., and Ackerman, M. S. (2001) Persistence of native-like topology in a denatured protein in 8 M urea, *Science 293*, 487-489.

105. Dill, K. A., and Shortle, D. (1991) Denatured states of proteins, *Annu. Rev. Biochem 60*, 795–825.

106. Shortle, D., Simons, K. T., and Baker, D. (1998) Clustering of low-energy conformations near the native structures of small proteins, *Proc. Natl. Acad. Sci. U.S.A. 95*, 11158–11162.

107. Smith, J. S., and Scholtz, J. M. (1996) Guanidine hydrochloride unfolding of peptide helices: separation of denaturant and salt effects, *Biochemistry 35*, 7292-7297.

108. Monera, O. D., Kay, C. M., and Hodges, R. S. (1994) Protein denaturation with guanidine hydrochloride or urea provides a different estimate of stability depending on the contributions of electrostatic interactions, *Protein Sci. 3*, 1984-1991.

109. Akhtar, M. S., Ahmad, A., and Bhakuni, V. (2002) Guanidinium chloride- and urea-induced unfolding of the dimeric enzyme glucose oxidase, *Biochemistry 41*, 3819-3827.

110. Doig, A. J., and Williams, D. H. (1991) Is the hydrophobic effect stabilizing or destabilizing in proteins?, *J. Mol. Biol. 217*, 389–398.

111. D'Amico, S., Gerday, C., and Feller, G. (2002) Dual effects of an extra disulfide bond on the activity and stability of a cold-adapted α-amylase, *J. Biol. Chem. 277*, 46110-46115.

112. Pace, C. N., Grimsley, G. R., Thomson, J. A., and Barnett, B. J. (1988) Conformational stability and activity of ribonuclease T_1 with zero, one, and two intact disulfide bonds, *J. Biol. Chem 263*, 11820-11825.

113. Matsumura, M., Becktel, W.J., Levitt, M., and Matthews, B. W. (1986) Stabilization of phage T4 lysozyme by engineered disulfide bonds. *Proc. Natl. Acad. Sci. U.S.A. 86*, 6562-6566.

114. Katz, B. A., and Kossiakoff, A. (1986) The cystallographically determined structures of atypical strained disulfides engineered into subtilisin, *J. Biol. Chem. 261*, 15480-15485.

115. Guzzi, R., Andolfi, L., Cannistraro, S., Verbeet, M. P., Canters, G. W., and Sportelli, L. (2004) Thermal stability of wild type and disulfide bridge containing mutant of poplar plastocyanin, *Biophys. Chem. 112*, 35-43.

116. Kuroki, R., Inaka, K., Taniyama, Y., Kidokoro, S., Matsushima, M., Kikuchi, M., and Yutani, K. (1992) Enthalpic destabilization of a mutant human lysozyme lacking a disulfide bridge between cysteine-77 and cysteine-95, *Biochemistry 31*, 8323-8328.

117. Johnson, C. M., Oliveberg, M., Clarke, J., and Fersht, A. R. (1997) Thermodynamics of denaturation of mutants of barnase with disulfide crosslinks, *J. Mol. Biol. 268*, 198-208.

118. Zavodszky, M., Chen, C. W., Huang, J. K., Zolkiewski, M., Wen, L., Krishnamoorthi, R. (2001) Disulfide bond effects on protein stability: designed variants of *Cucurbita maxima* trypsin inhibitor-V, *Protein Sci. 10*, 149-160.

119. Kawahara, K., and Tanford, C. (1966) Viscosity and density of aqueous solutions of urea and guanidine hydrochloride, *J. Biol. Chem. 241*, 3228-3232.

120. Neto, L. E. S., and Stadtman, E. R. (1996) The iron-catalyzed oxidation of dithiothreitol is a biphasic process: hydrogen peroxide is involved in the initiation of a free radical chain of reactions, *Arch. Biochem. Biophys. 333*, 233-242.

121. Lambeth, D. O., Gwen, R. E., Yorek, M. A., and Ray, P. D. (1986) Implications for in vitro studies of the auto oxidation of ferrous ion and the iron-catalyzed auto oxidation of dithiothreitol, *Biochim. Biophys. Acta 719*, 501-508.

122. Burmeister Getz, E., Xiao, M., Chakrabarty, T., Cooke, R., and Selvin, P. R. (1999) A comparison between the sulfhydryl reductants tris(2-carboxyethyl)phosphine and dithiothreitol for use in protein biochemistry, *Anal. Biochem. 273*, 73–80.

123. Raina, S. (1997) Making and breaking disulfide bonds, *Annu. Rev. Microbiol. 51*, 179-202.

124. Creighton, T. E. (1990) Protein folding, *Biochem. J. 270*, 1-16.

125. Vaz, D. C., Rodrigues, J. R., Sebald, W., Dobson, C. M., and Brito, R. M. M. (2006) Ethalpic and entropic contributions mediate the role of disulfide bonds on the conformational stability of interleukin-4, *Protein Sci. 15*, 33-44.

126. Pace, C. N. (2001) Polar group burial contributes more to protein stability than nonpolar group burial, *Biochemistry 40*, 310-313.

127. Li, W., Lum, K. T., Chen-Goodspeed, M., Sorgorb, M. A., and Raushel, F. M. (2001) Stereoselective detoxification of chiral sarin and soman analogues by phosphotriesterase, *Bioorg. Med. Chem. 9*, 2083-2091.

VITA

Name:	Charles David Armstrong
Address:	MS 2128 Biochemistry Biophysics, Texas A&M University, College Station, Texas 77843
Email Address:	cdarmstrong@gmail.com
Education:	B.S., Biochemistry, Texas A&M University, 1997 M.S., Environmental Management, University of Houston at Clear Lake, 2000